12-2007

Novel Numerical Approaches for the Resolution of Direct and Inverse Heat Transfer Problems

Gregory Evan Osborne

University of Tennessee - Knoxville

To the Graduate Council:

I am submitting herewith a dissertation written by Gregory Evan Osborne entitled "Novel Numerical Approaches for the Resolution of Direct and Inverse Heat Transfer Problems." I have examined the final electronic copy of this dissertation for form and content and recommend that it be accepted in partial fulfillment of the requirements for the degree of Doctor of Philosophy, with a major in Mechanical Engineering.

J. I. Frankel, Major Professor

We have read this dissertation and recommend its acceptance:

M. Keyhani, R. V. Arimilli, J. Wu

Accepted for the Council:
Carolyn R. Hodges

Vice Provost and Dean of the Graduate School

(Original signatures are on file with official student records.)

To the Graduate Council:

I am submitting herewith a dissertation written by Gregory Evan Osborne entitled "Novel Numerical Approaches for the Resolution of Direct and Inverse Heat Transfer Problems." I have examined the final electronic copy of this dissertation for form and content and recommend that it be accepted in partial fulfillment of the requirements for the degree of Doctor of Philosophy, with a major in Mechanical Engineering.

Dr. J. I. Frankel, Major Professor

We have read this dissertation
and recommend its acceptance:

Dr. M. Keyhani

Dr. R. V. Arimilli

Dr. J. Wu

Accepted for the Council:

Carolyn R. Hodges, Vice Provost
and Dean of the Graduate School

(Original signatures are on file with official student records.)

Novel Numerical Approaches for the Resolution of Direct and Inverse Heat Transfer Problems

A Dissertation Presented for the
Doctor of Philosophy Degree
The University of Tennessee, Knoxville

Gregory Evan Osborne

December 2007

Dedication

This dissertation is dedicated to my father, Dr. C. Edward Osborne and my mother Columba V. Osborne whose love and support have always been immeasurable.

"Nel mezzo del cammin di nostra vita
mi ritrovai per una selva oscura
chè la diritta via era smarrita."
—Dante Alighieri, *La Divina Commedia – Inferno* (Canto I, vv. 1–3)

"Inferna tetigit, posset ut supera assequi."
—Seneca, *Hercules Furens* [Megara. Act I, vv. 423]

"A witty saying proves nothing."
—Voltaire, *Le Dîner du Comte de Boulainvilliers*

Acknowledgments

I would like to thank my major professor Dr. Jay I. Frankel for his advice and suggestions which have made this dissertation a better document. I am particularly thankful for his help and encouragement in guiding me through the final stages of this process. I would also like to thank the other members of my dissertation committee, Profs. Majid Keyhani, Rao V. Arimilli and Jayne Wu for their contributions as well as their time and patience.

I would be remiss if I did not acknowledge that the research presented in this dissertation was supported under grants from the U.S. National Science Foundation, contract CTS-9619192 and the U.S. Department of Energy, Assistant Secretary for Energy Efficiency and Renewable Energy, Industrial Technologies Program, Materials for the Future (IMF), contract DE-AC05-00OR22725 (with UT-Battelle, LLC).

Lastly, although definitely not least, I would like to express sincere gratitude to my family and friends. I would especially like to thank my mother and father for their unwavering support and encouragement at all times and in all things. "Thank you" hardly seems sufficient. *Mille grazie* and *diolch yn fawr*.

Abstract

This dissertation describes an innovative and robust global time approach which has been developed for the resolution of direct and inverse problems, specifically in the disciplines of radiation and conduction heat transfer.

Direct problems are generally well-posed and readily lend themselves to standard and well-defined mathematical solution techniques. Inverse problems differ in the fact that they tend to be ill-posed in the sense of Hadamard, i.e., small perturbations in the input data can produce large variations and instabilities in the output. The stability problem is exacerbated by the use of discrete experimental data which may be subject to substantial measurement error. This tendency towards ill-posedness is the main difficulty in developing a suitable prediction algorithm for most inverse problems. Previous attempts to overcome the inherent instability have involved the utilization of smoothing techniques such as Tikhonov regularization and sequential function estimation (Beck's future information method).

As alternatives to the existing methodologies, two novel mathematical schemes are proposed. They are the Global Time Method (GTM) and the Function Decomposition Method (FDM). Both schemes are capable of rendering time and space in a global fashion thus resolving the temporal and spatial domains simultaneously. This process effectively treats time elliptically or as a fourth spatial dimension. A Weighted Residuals Method (WRM) is utilized in the mathematical formulation wherein the

unknown function is approximated in terms of a finite series expansion. Regularization of the solution is achieved by retention of expansion terms as opposed to smoothing in the classical Tikhonov sense.

In order to demonstrate the merit and flexibility of these approaches, the GTM and FDM have been applied to representative problems of direct and inverse heat transfer. Those chosen are a direct problem of radiative transport, a parameter estimation problem found in Differential Scanning Calorimetry (DSC) and an inverse heat conduction problem (IHCP). The IHCP is resolved for the cases of diagnostic deduction (discrete temperature data at the boundary) and thermal design (prescribed functional data at the boundary). Both methods are shown to provide excellent results for the conditions under which they were tested. Finally, a number of suggestions for future work are offered.

Contents

List of Figures

List of Tables

Chapter 1

Introduction

Inverse analysis has rapidly become an important tool for the study of a wide assortment of thermal problems. Often, extremely harsh surface environments preclude the use of surface probes. Such is the case, for example, when material ablation or excessively high temperatures are involved. It is, however, critical to these physical applications that accurate surface information be available for analysis. Hence, embedded sensors that are safely located away from the extreme conditions must somehow be used to predict the surface temperature and heat flux. This prediction requires that the collected data from an interior site be mathematically projected to the surface in a stable and accurate manner. These problems must therefore be resolved using an inverse methodology.

There are numerous applications within the field of thermal science which experience the extreme conditions described above. Practical issues such as space vehicle reentry, material casting and solidification, turbomachinery operation, direct-energy impingement, and the determination of hypersonic flow characteristics fall into this category. Furthermore, controlled experiments which expose materials to extremely high heating rates for short periods of time (i.e., arcjet testing to simulate reentry conditions) are becoming prevalent. Likewise, inverse methods are employed in other fields of science and technology, for example, image reconstruction and tomography. Hence, inverse analysis represents an important topic of research.

1.1 Introduction to Inverse Analysis

Problems of mathematical physics can be broadly classified as either direct or inverse. Most scientists and engineers are well acquainted with direct problems and the analytical and numerical methods used to solve them. Such is usually not the case with the inverse counterpart which often combines experimental data directly into the mathematics and numerics. These data can be utilized in the projection leading to the surface temperature and heat flux or for determining thermophysical properties.

Figure 1.1 * illustrates two forms of traditional direct analysis in a simple schematic form. The first diagram represents the most basic well-posed problem, i.e., a known system with known and well-specified input that contains no uncertainty. The second diagram illustrates a somewhat more complicated (and realistic) problem but one which remains well-posed. This problem is often referred to as state estimation and requires the resolution of a fully specified system where one or more of the auxiliary conditions is given in terms of discrete, measured data. While the data contain measurement uncertainty, numerical stability is retained.

In contrast, three basic types of inverse problem are shown in Fig. 1.2. Part (a) illustrates what is generally known as parameter estimation. In this case, there is adequate input available, but the governing system is not fully specified. Part (b) describes function reconstruction (or function estimation) which requires the prediction of surface conditions based on discrete measurements gathered at an embedded

*all figures may be found in Appendix I

location. Finally, part (c) qualitatively shows the thermal design problem wherein it is desired to predict, say a boundary condition that will assure a predefined outcome.

Inverse problems are mathematically classified as ill-posed [1–6] whereas direct problems are considered well-posed. Hadamard originally introduced the concept, stating that a well-posed problem must have a solution which satisfies three criteria [2]:

- The solution must exist;
- The solution must be unique;
- The solution must be stable under small changes to the input data.

One can logically infer that a solution exists for any particular inverse heat transfer problem by physical reasoning [7]. Any observed effect on a physical system must have a cause. The issue of uniqueness has only been proven for a few special cases [1, 4]. Still, the main difficulty in resolving inverse heat transfer problems lies in Hadamard's third condition, i.e, small perturbations of the input data can produce randomly large variations in the solution. In order to demonstrate this difficulty, a simple example is now presented [8].

Baumeister [9] illustrates the ill-posed nature of a function reconstruction problem by examining the governing second-order ordinary differential equation which can be used to describe a basic dynamic system. This initial-value problem is given by

$$\frac{d^2y}{dt^2}(t) \;+\; y(t) \;=\; f(t), \quad t \geq 0, \tag{1.1a}$$

subject to the initial conditions

$$y(0) \;=\; y_0, \tag{1.1b}$$

and

$$\frac{dy}{dt}(0) \;=\; \dot{y}_0. \tag{1.1c}$$

The problem given by Eq. (1.1a–c) is typical of a mass–spring dynamic system where the function $y(t)$ represents displacement. For the direct problem, one would seek a solution for $y(t)$ based on the well-specified initial conditions shown in Eq. (1.1b,c) and known forcing function $f(t)$. One can also propose an inverse analog in which $y(t)$ is known in some form and it is incumbent to reconstruct the presumed unknown forcing function $f(t)$. The ill-posed nature of such a reconstruction problem can readily be demonstrated. As example, consider the case where $y(t)$ is given as e^{-t}. Here, by necessity, the forcing function $f(t)$ is $2e^{-t}$ and the initial conditions $y(0) = y_0 = 1$ and $\frac{dy}{dt}(0) = \dot{y}_0 = -1$. Now, assume that $y(t)$ is given in terms of the perturbed input function $\hat{y}(t) = y(t) + a\sin(\omega t)$, where a represents the amplitude of the perturbation and ω can be viewed as the frequency of change. Substitution of $\hat{y}(t)$ into Eq. (1.1a) produces the perturbed forcing function $\hat{f}(t) = f(t) + a(1-\omega^2)\sin(\omega t)$. Even if the amplitude $''a''$ is presumed small, it is evident that $\hat{f}(t)$ changes considerably as the frequency of variation ω increases. Hence, even a small perturbation in the input can cause a significantly large change in the reconstruction. It is interesting to note, however, that if one could measure $\ddot{y}(t)$, which would realistically contain random error with the assumption that bias, if it exists, has been removed, then $f(t)$ could be readily reconstructed. This observation leads to a subtle issue on the choice of sensor in the data collection process. In other words, the problem itself can provide a valuable clue with regard to the optimal choice of data space.

Returning specifically to inverse heat transfer, the mathematically ill-posed nature of such problems can be traced back to their physics [10]. When considering a direct problem, it is apparent that fluctuations in surface temperature and heat flux become diminished or damped as the surface is penetrated. Furthermore, the higher frequency components of the boundary conditions experience this damping effect at a higher rate than do the lower frequency components. Unfortunately, the opposite holds true for inverse problems. Higher frequency fluctuations in internal measurements become amplified as they are projected to the surface which is analogous to the example given above. Because of this tendency, predictions for the unknown surface conditions can become meaningless due to excessive noise magnification.

1.2 Inverse Problems of Heat Transfer

Interest in inverse heat transfer problems as well as advancements in solution techniques began to grow in the 1950's with the advent of the aerospace industry and space exploration programs [6]. Development of faster and more powerful digital computers aided these studies [10]. The measurement of surface temperatures of the thermal shields on space vehicles during atmospheric reentry was (and still is) a problem which garnered particular attention. In this case, the aerodynamic heating is so intense that it would be impossible to place sensors at the heat shield surface. These sensors would most likely be unable to withstand the thermal conditions created by atmospheric friction or maintain reliability. Thus, measurement devices must be installed at a safe location beneath the surface and the gathered data used to project or estimate outer conditions. Inverse analysis is required to accomplish this task.

Many other practical examples of the need for inverse analysis in heat transfer processes exist. One of the most basic types of inverse problem is parameter estimation. Here, one or more system parameters must be determined from known input in order to fully specify the governing equations. As related to thermal problems, these unknown parameters are usually system coefficients such as thermal conductivity, specific heat and/or thermal diffusivity but may also include the location of internal heat sources, if they are present [5, 6, 10]. Generally speaking, parameter estimation problems are considered to be only mildly ill-posed. Their resolution can become more complicated, however, when numerous parameters must be recovered or when model complexity results in instability.

Another area of great interest for many thermal science disciplines is the inverse heat conduction problem (IHCP). In this class of problem, the surface heat flux of an opaque solid is estimated based on known conditions (e.g., an insulated back wall and measured transient temperature history) at a specified location. A second example can be given by the measurement of temperature at two embedded locations. Because the region between the two probes is properly specified at its boundaries, resolution of the temperature profile within this region would be considered a direct problem. The solution of the direct problem leads to knowledge of heat fluxes at the probe locations. Hence, overspecific conditions are developed which can then be used to project temperature and heat flux information outside the region contained by the probes. Heat shield temperature estimation under opaque conditions during atmospheric reentry, mentioned above, falls into the IHCP category. Inverse heat conduction problems are ill-posed and, depending upon the complexity of the particular system, can require considerable computational effort to resolve.

Besides determining the conditions on the outer surfaces of space vehicles during reentry, inverse analysis can be applied to numerous areas of contemporary study in thermal science and engineering. Such applications include but are not limited to monitoring the surface conditions of rocket or jet engines, tracking the motion of a projectile over a gun barrel surface, melting and ablation, material heat treating and quenching processes, solidification and casting processes, indirect calorimetry for laboratory use, and optimal systems design [4–6, 10]. Recently, topics such as health management and thermal protection systems for platforms which experience extreme thermal stress have also become important fields of study which benefit from improved inverse analysis techniques.

1.3 Existing Methodologies

Inverse problems are usually solved through the minimization of an objective function with the incorporation of some stabilizing or regularizing technique [1, 3, 4, 6, 10, 11]. Under these circumstances, the objective function that provides minimum variance estimates is the ordinary least-squares norm. Methods which utilize this philosophy require the solution of the corresponding direct problem based on previous estimates for the unknown quantities or boundary conditions. They are by necessity iterative in nature and require educated initial guesses to begin the process.

Much of the work done in this area is based on the future information technique of Beck *et al.* [4]. While multiple variations exist, this method is basically a time-marching scheme which, for the case of the inverse heat conduction problem, begins with an assumed estimate of surface heat flux at each step. The solution obtained from this estimate is then marched through a chosen number of future time steps. The calculated temperature field that results from this process is compared with known temperature data and, using a minimizing algorithm, the corrected surface heat flux value is generated. The process is repeated until satisfactory convergence is achieved. Regularization is based on the number of future time steps chosen. In effect, smoothing (i.e., reduction of high frequency content) is achieved by increasing the number of future time steps.

Also utilized for resolving inverse problems in heat transfer is the Tikhonov regularization method [12–15]. This procedure modifies the standard least-squares approach by adding smoothing factors which influence the stability of the solution as the minimization is performed. The sum of the smoothing parameters is multiplied by a regularization parameter that is greater than zero. As this regularization parameter approaches zero, the solution may oscillate and become unstable; however, if it is chosen to be too large, the solution will become damped and deviate from the exact solution [6]. It is therefore necessary to employ a means of balancing the trade-off between stability and solution accuracy. One means of choosing an optimal regularization parameter is Morozov's Discrepancy Principle [11, 16] which estimates the regularization parameter by comparing the residual (or discrepancy) and the assumed bound for the noise level. Another regularization parameter selection scheme is based on the L-Curve Method [11, 17, 18]. Here, a log-log plot between the squared norm of the solution and the squared norm of the residual is generated over a range of regularization parameter values. The resulting plot usually resembles the letter "L" (although it is not guaranteed [11]), and the optimal value is assumed to correspond to the corner.

Other existing methods include the Levenberg-Marquardt Method [5, 19–22] and the Conjugate Gradient Method with the Adjoint Problem [1, 7, 23, 24]. The former is used primarily for solving linear and nonlinear parameter estimation problems. The latter is employed for problems of function estimation when there is no *a priori* information available for the functional form of the unknown quantity [6]. Both are iterative techniques which can require significant computational effort for complex problems.

1.4 Motivation, Scope and Document Organization

A general drawback to the existing methods used to resolve inverse heat transfer problems is that greater stability in the solution comes at the expense of resolving power [6]. In order to address overall stability and other practical issues, two innovative mathematical schemes which are capable of treating both time and space in a global fashion are proposed for the resolution of problems in direct and inverse heat conduction and radiation. These schemes are known as the Global Time Method (GTM) and the Function Decomposition Method (FDM). These unique approaches represent new thinking in an important area of heat transfer research and add significantly to the body of knowledge in the subject. For example, in contrast to Beck's method, these techniques add higher frequencies back into the prediction as additional expansion terms are retained.

This dissertation is organized in the following manner. First, a brief review of the pertinent literature in the areas discussed is presented in Chapter 2. Chapter 3 gives an overview of the basic proposed analytic/numeric methodologies. These techniques are illustrated more fully in the three chapters that follow. Chapter 4 demonstrates the application of the Global Time Method on a direct nonlinear problem of radiative heat transport. Chapter 5 describes a parameter estimation problem in calorimetry that is resolved using the Function Decomposition Method. Chapter 6 describes an inverse heat conduction problem that is resolved utilizing both the GTM and FDM. Finally, Chapter 7 presents some conclusions and recommendations for future work.

Chapter 2

Literature Review

In historical terms, the use of inverse analysis to solve problems in mathematics and mathematical physics is relatively new. It began in earnest in the late-middle part of the twentieth century. The concept of inverse analysis, however, is quite old. Groetsch [25] has cleverly pointed out that over two thousand years ago Plato [26] posed a philosophical inverse problem with his allegory of the cave. In this instance, Plato was contemplating the implications of reconstructing 'reality' based on interpretations of shadows cast on the wall. This allegory provides a good analogy to the difficulties faced when attempting to resolve inverse problems. As with shadows cast on a wall, it is easier to determine effect when given cause than *vice versa*. Moreover, few inverse problems of physical significance can be solved analytically and instead require advanced numerical techniques; hence, many applications had to remain speculative until computational science caught up with theoretical mathematics. This chapter provides a brief review of early work as well as a more extensive compendium of existing and current inverse applications and methodologies. It concludes with a statement of motivation for the work presented in this dissertation.

2.1 Historical Perspective

As noted earlier, Hadamard [2] is credited as being the first to give a concise definition for well-posedness and so no discussion of inverse analysis can begin without his mention. The aspect of Hadamard's conditions which most exacerbates the ill-posed nature of inverse problems is their sensitivity to small changes in the input data. Because it was thought at the time that any violation of the conditions for well-posedness would render a problem unsolvable or its resolution meaningless, only minimal research was attempted in areas where inverse analysis would be necessary [1,6]. This situation changed when the high-temperature, harsh environment applications of space exploration and hypersonic aircraft operation became priorities [4,6]. Interest was further spurred by advancements in digital computing [10].

While interest was piqued, the problem of obtaining stable and meaningful predictions remained. One of the earliest works that discusses inverse heat conduction is given by Giedt [27] whose 1955 paper investigated heat transfer processes in the inner chamber of a gun barrel. At approximately the same time (1957), a paper by Shumakov [28] concerning the inverse heat conduction problem (IHCP) was translated from the original Russian text. Another important early publication (1960) is attributed to Stolz [29] who developed a procedure for the calculation of heat transfer rates of simply shaped bodies during quenching by using internal temperature measurements. His method involved the inversion of a convolution integral, i.e., the numerical solution of a first kind Volterra integral equation. Unfortunately, the time-marching algorithm required relatively large time steps to retain stability. A modification of the Stolz method was later offered by Beck [30] wherein he was able to maintain stability using time increments that were as small as one sixth the size of those used by Stolz. Through the progression of his work [30–32], Beck was able to develop an algorithm [33] which became the one of the standard computational schemes of its time [4].

Likewise during the 1950's and 1960's (perhaps earlier), Soviet mathematicians and physicists were conducting similar research regarding the stability issues of inverse thermal analysis. Tikhonov [15] published on the subject as early as 1943. More importantly, in 1963 he introduced a new procedure known as Tikhonov regularization [3, 12–14, 34]. His method was able to reduce sensitivity to input error by adding smoothing terms, modified by a regularization parameter, to the least-squares minimization equation. This smoothing effect required a judicious choice of regularization parameter since too much smoothing could lead to a loss of the physics of the problem. As a result, iterative schemes, such as Alifanov's iterative regularization technique [1, 24] were developed in order to produce more accurate resolutions. These algorithms generate a sequential improvement of the prediction until an appropriate stopping criterion is reached. Other methods of determining the optimal regularization parameter are available including Morozov's Discrepancy Principle (MDP) [11, 16] and the L-curve Method [11, 17, 18].

2.2 Developed Methodologies and Recent Work

By the early 1980's, the body of research in thermal inverse analysis had grown considerably and a number of potential solution techniques had been introduced. In his 1979 paper, Beck [35] gave a series of sixteen criteria for choosing the best solution method for the IHCP. He applied these criteria to his own method as example but also briefly considered older work including that of Stolz [29] and Tikhonov [12]. He concluded that time steps must increase in size for accuracy and stability to be maintained as input error becomes larger. Many other monographs which either compare or discuss multiple algorithms are also available. Elden [36] investigated the IHCP in a half-space domain ($t \geq 0, x \geq 0$) and considered the application of truncated singular-value decomposition (TSVD), Tikhonov regularization, Fourier transform analysis, space-marching schemes and Beck's method, to name a few. Lamm [37] reviewed regularization schemes, both classical and newer, and suggested that local regularization methods may be preferable to generic Tikhanov based schemes because of their reduced computational effort and cost. Mera *et al.* [38] also compared regularization methods for the resolution of an anisotropic heat conduction problem. Using a Boundary Element Method (BEM) to discretize the Cauchy problem, they investigated TSVD, Tikhonov regularization, the Conjugate Gradient Method and an alternating iterative algorithm as means of regularization. They concluded that while all four methods produce stable results, the alternating iterative algorithm is the most accurate.

There are also many books available that cover the subject of inverse and ill-posed problems [1, 3–6, 9–11, 16, 25, 39–41], and it is beyond the scope of this dissertation to do more than give them mention. At this point, however, it is useful to examine a few of the existing techniques and corresponding representative work.

2.2.1 Sequential Function Specification (Beck's Method)

The development of Beck's sequential function specification method has been briefly detailed above. A complete explanation of this method as it relates to the IHCP can be found in Beck *et al.* [4]. It is important to note that the solution is regularized by the number of future time steps incorporated into the algorithm. Beck's algorithm has been widely used as a starting point for inverse heat transfer investigations. Osman and Beck [42,43] used the technique to predict the time history of transient heat transfer coefficients during quenching with mixed results. They reported that predictions of early transient results are substantially higher than those given by empirical correlations for free convection, but later transient results are in good agreement. Beck *et al.* [44] employed experimental data for the comparison of function specification with classical Tikhonov regularization and iterative regularization. They found that both function specification and iterative regularization produce good results without undue computational effort and concluded that function specification is conceptually simpler. Other published accounts include Osman *et al.* [45] wherein the method is extended to a general two-dimensional IHCP and Blanc *et al.* [46] which includes a time-variable number of future temperatures in the solution scheme. More recently, Lin *et al.* [47] proposed a modified form of the algorithm which they claim reduces the leading error caused by addition of future time information in the preliminary estimation process. Behbahani-nia and Kowsary [48] introduced a scheme based on a dual reciprocity BEM which is used in conjunction with sequential function specification. They reported good results for the two-dimensional IHCP in the presence of noisy data as long as thermocouples are placed close to the active surface. Additionally, a hybrid scheme which combines the use of future temperature information with past flux history has been offered by Ling *et al.* [49].

2.2.2 Tikhonov Regularization

The explanation and application of classical Tikhonov regularization as a means of stabilizing inverse problems can be found in many sources [1, 3, 4, 10–12, 25, 40]. It is therefore the purpose of this part of the literature review to inspect the algorithms developed to determine the optimal value for the Tikhonov regularization parameter. One of the best known is Morozov's Discrepancy Principle (MDP) [11, 16]. This method has been used with general success for linear ill-posed problems. For instance, Nair [50] demonstrated that for an ill-posed linear operator equation, Tikhonov regularization generates an order-optimal algorithm when MDP is utilized. Likewise, Muniz *et al.* [51] were able to obtain positive results using MDP in the resolution of an IHCP. It should be noted, however, that MPD is less useful for nonlinear ill-posed problems as shown by Scherzer *et al.* [52]. Consequently, Scherzer and his colleagues proposed a modification to Morozov's technique which allows for optimal convergence and parameter choice given a nonlinear equation operator [52, 53]. Other modifications have been proposed by Qi-nian [54] and more recently by Lu *et al.* [55] who have developed a choice rule which operates only with the elements of the minimizing sequence.

An alternative to MDP is the L-curve method [11, 17, 18]. Initially advocated by Hansen [17, 18], this method relies upon the log-log plot of the squared norm of the approximate solution versus the squared norm of the residual for a range of regularization parameters. The optimal parameter choice is assumed to correspond with the corner of the L-shaped figure that is generated. Successful utilization of the L-curve method has been reported by Reginska [56], Lesnic *et al.* [57] and Mera [58], among others. Algorithms based on the L-curve have also been used with regularization techniques other than Tikhonov. For instance, Rodriquez and Theis [59] coupled the method with TSVD and introduced a geometrical approach for finding the corner. Likewise, Belge *et al.* [60] have extended the concept to find more than one regularization parameter for multiple-dimensional problems. The L-curve method does have potential drawbacks, as illustrated by Vogel [61] and Hanke [62]. The basic limitation arises from the difficulty in accurately determining the corner point. Vogel [61] demonstrated the the L-curve approach generated regularized solutions that failed to converge for certain types of problem. Hanke [62] postulated a similar failure in convergence when the exact solution of the problem is smooth.

A number of other techniques have been proposed for determining an optimal regularization parameter. Among these are the Maximum Likelihood Method (ML) [11] and the Generalized Cross-Validation Method (GVC) of Grace Wahba [40, 63].

2.2.3 Conjugate Gradient Method

The Conjugate Gradient Method with the Adjoint Problem (CGM) has also been in general usage for resolving inverse problems in heat transfer. For instance, Jarny *et al.* [64] utilized the CGM to investigate a multi-dimensional IHCP. Quite recently, Reinhardt and Frohne [65] also reported success in solving a multi-dimensional IHCP with the CGM and Tikhonov regularization. Similar methodology was introduced by Hong and Baek [66] for the consideration of two-phase laminar flow in a parallel plate channel. Hao [67] has proposed use of the CGM with an optimal-order stopping criteria for inverse problems in heat conduction, while Huang *et al.* [68] employed the CGM in their investigations of contact conductance during casting processes. A Fourier analysis of the implementation of the CGM for IHCPs was conducted by Prud'homme and Nguyen [69]. They determined that the convergence speed of the algorithm slows as frequency increases. As a final example, a novel approach was put forward by Narayanan and Zabaras [70] where they incorporated a CGM scheme with uncertainty techniques.

2.2.4 Space Marching

Finite difference, space-marching schemes have been offered by some researchers as a means of solving inverse heat transfer problems. An early investigation is described by Carasso [71]. In this work, he demonstrated a method based on Tikhonov regularization which utilized space marching to solve a one-dimensional IHCP in the half space. In a later paper, Carasso [72] detailed eighteen different finite difference, space-marching algorithms which could be employed on nonlinear IHCPs whose solutions have negligible high frequency content. An extension of this work can be found in [73]. Space marching combined with data mollification has been studied extensively by Murio and his colleagues [74–77]. The mollification method introduced by Murio [39, 78, 79] employs a Gaussian functional which strongly damps out the high frequency components of the surface heat flux in Fourier space. The concept of data filtering is one with great merit and is discussed again in the future work section at the end of this dissertation.

2.2.5 The Levenberg-Marquardt Method

The Levenberg-Marquardt Method (LMM) [5, 19–22] has been used extensively to resolve problems of parameter estimation. For instance, Sawaf *et al.* [80] used the LMM to determine temperature dependent thermal properties of an orthotropic solid. Vozar and Sramkova [81] compared the LMM with a basic least-squares technique to estimate thermal diffusivity from step-heating measurements. They found that the LMM generated comparable results but could require an excessive number of iterations under certain circumstances. Dantas *et al.* [82] were able to extract most of the desired parameters for a heat and mass transfer problem in a capillary porous medium using the LMM. However, they were unsuccessful in obtaining parameters whose sensitivity coefficients were of small magnitude. Other applications can be found in Ou and Wu [83], Murphy *et al.* [84] and Feng *et al.* [85].

2.2.6 Other Thermal Inverse Applications

The papers discussed above relate mostly to the IHCP or parameter estimation. However, these problems are not the only ones of interest to thermal scientists and engineers. One example is the inverse problem in radiative transport. Important foundational work in this concentration has been performed by Siewert [86–88]. In his two monographs [87,88], he demonstrated the use of a spherical-harmonics method to estimate the source term in a plane-parallel medium with anisotropic scattering given specified angular distributions of radiation emitted from the two surfaces. At about the same time, Li and Ozisik [89] solved a similar problem using the Conjugate Gradient Method with the Adjoint problem. Likewise, Subramaniam and Menguc [90] predicted the profile of the single scattering albedo in an inhomogeneous, anisotropic medium using a Monte Carlo technique. They also considered a homogeneous, anisotropically scattering slab wherein the single scattering albedo and asymmetry factor were recovered. Recent investigations of inverse radiation problems can be found in Park and Lee [91] and Kim and Baek [92].

Another field of study which is of significant importance to the casting and treatment of metals is the use of inverse analysis for solidification processes. Here, it is important to control the solidification velocity as well as the temperature gradient on the liquid side of the solidification front to obtain the desired casting morphology [93]. Much of the published literature with respect to inverse solidification analysis is attributable to Zabaras and his colleagues [94–100]. In an early study, Zabaras *et al.* [94] utilized an integral method in conjunction with the sensitivity analysis proposed by Beck *et al.* [4] to resolve an inverse solidification problem for which the exact analytical solution was known, achieving good agreement. Other investigations have employed Beck's sequential function specification in a finite element algorithm [95–97] and adjoint methods [100]. Nevertheless, it has been noted by Hale *et al.* [101] that none of these studies address the issue of independent control of both the solidification front velocity and liquid-side interfacial temperature gradient. They offered an algorithm based on the elliptic treatment of time as outlined by Frankel and Keyhani [102] which generated excellent performance.

2.3 Proposed Methodology

All inverse problems require some form of regularization to promote and maintain stability in the prediction. For the existing methods, this regularization is primarily accomplished by the incorporation of a smoothing function which, in effect, successively removes high frequency content from the solution until acceptable stability and accuracy are achieved. However, diffusion is known to be a low frequency phenomenon [10], i.e., the high frequency content of an applied surface heat flux is rapidly damped out as it penetrates the interior of a material. It therefore makes sense to instead formulate a scheme which starts with the fundamental frequencies and successively adds higher frequency content to the solution.

The proposed Global Time Method and Function Decomposition Method accomplish this alternative concept by representing the unknown function as an approximate series expansion in a global sense for both space and time coordinates. Regularization is achieved by retaining terms in the finite expansion which corresponds to adding higher frequency content back to the solution. As such, these techniques fill a void in the present research and offer insight into future advancements in problem resolution and data gathering platforms.

Chapter 3

Generalized Overview of Proposed Methodologies

Two novel and robust techniques are proposed as means of resolving direct and inverse problems, particularly those of radiative and conductive heat transfer. The Global Time Method (GTM) and the Function Decomposition Method (FDM) both make use of Weighted Residuals Methods and are thus able to treat time elliptically and produce solutions in a non-marching fashion. As a means of introducing both algorithms, a general overview of the Weighted Residuals Method (WRM) is presented followed by a qualitative discussion of the GTM and FDM.

3.1 Weighted Residuals Method

In order to achieve problem resolution, GTM and FDM incorporate the Weighted Residuals Method [103, 104] to develop an approximate solution for the unknown function. With this technique, the unknown function is represented as a finite series expansion in terms of known, well-defined and linearly independent basis functions which have corresponding unknown expansion coefficients. The functional representation can be modified by the inclusion of auxiliary conditions into the expansion, thus providing exactness at the boundaries when boundary conditions are linear. Substitution of the approximate series expansion, i.e., truncated form of the infinite series, into the governing equation for the physical problem produces a residual function. Subsequently, the unknown expansion coefficients can be determined by minimizing the residual function in some manner. Possible minimization techniques, often called projection methods [105], include orthogonal collocation, Bubnov-Galerkin and continuous least squares. The result is a closed system of linear or nonlinear equations for the unknown expansion coefficients. Resolution of this system allows for the final reconstruction of the desired unknown variable.

At this point, it is useful to examine the process in general terms. Following the presentation of Frankel [8], consider the simple second-order, linear ordinary differential equation in operator form

$$L[\theta(x)] = -f(x), \quad x \in [0,1], \tag{3.1a}$$

subject to the general boundary conditions

$$B_0[\theta(x_0)] = g_0, \quad x_0 \in [0,1], \tag{3.1b}$$

$$B_1[\theta(x_1)] = g_1, \quad x_1 \in [0,1]. \tag{3.1c}$$

Here, L is a second-order, linear differential operator acting on the unknown function $\theta(x)$, $f(x)$ is the prescribed forcing function, and B_0 and B_1 are general linear operators acting on $\theta(x)$ at the presumed boundaries x_0 and x_1 to give the prescribed boundary conditions g_0 and g_1, respectively. Application of the Weighted Residuals

Method begins with the expression of the unknown function $\theta(x)$ in Eq. (3.1a) in terms of an infinite series expansion

$$\theta(x) \;=\; \sum_{m=0}^{\infty} a_m \varphi_m(x), \quad x \in (0,1), \tag{3.2}$$

where $\{\varphi_m(x)\}_{m=0}^{\infty}$ is a set of linearly independent global basis functions which have a corresponding set of unknown expansion coefficients given by $\{a_m\}_{m=0}^{\infty}$. In practice, it is not possible to retain an infinite number of expansion terms, thus it is necessary to truncate the series at say $N+2$ terms which leads to the approximation

$$\theta(x) \;\approx\; \Theta_{N+1}(x) \;=\; \sum_{m=0}^{N+1} a_m^{N+1} \varphi_m(x), \quad x \in (0,1), \tag{3.3}$$

where $a_m \approx a_m^{N+1}$ for each m when $N+1$ is sufficiently large. The finite series expansion given by Eq. (3.3) can be made to explicitly satisfy the known boundary conditions which leads to the new form

$$\theta(x) \;\approx\; \theta_N(x) \;=\; \hat{\Psi}(x) + \sum_{m=1}^{N} c_m^N \Psi_m(x), \quad x \in [0,1]. \tag{3.4}$$

The new approximation, renamed $\theta_N(x)$, retains N unknown expansion coefficients (two coefficients having been determined by the inclusion of the boundary conditions) which are now represented by the set $\{c_m\}_{m=1}^{N}$. Likewise, because $\theta_N(x)$ is now exact at the boundaries, it is defined by a new set of trial functions, $\{\Psi_m(x)\}_{m=1}^{N}$, which is somewhat different from the initial proposed basis set, $\{\varphi_m(x)\}_{m=0}^{N+1}$. Furthermore, it should be noted that $\hat{\Psi}(x)$ satisfies the nonhomogeneous boundary conditions, i.e., $B_0[\hat{\Psi}(x_0)] = g_0$ and $B_1[\hat{\Psi}(x_1)] = g_1$ while the set $\{\Psi_m(x)\}_{m=1}^{N}$ satisfies the associate set of homogeneous boundary conditions, i.e., $B_0[\Psi_k(x_0)] = 0$ and $B_1[\Psi_k(x_1)] = 0$ for $k = 1, 2, \ldots, N$.

The general approximation presented in Eq. (3.4) must now be introduced back into the governing equation. Substitution leads to

$$R_N(\theta_N(x)) + L[\theta_N(x)] \;=\; -\,f(x), \quad x \in [0,1], \tag{3.5}$$

where $R_N(\theta_N(x))$ is the residual function which must be present due to the approximate nature of $\theta_N(x)$. In order to obtain the best possible resolution of the unknown function, this residual function must be minimized in some sense which will return an optimal set of expansion coefficients. There are a number of ways to accomplish the minimization, a few of which will be briefly discussed below. For the sake of clarity, it is necessary to introduce some basic concepts of functional analysis. First, the inner product of two real functions $f_1(x)$ and $f_2(x)$ can be defined as [106]

$$\langle f_1(x), f_2(x)\rangle_{w(x)} \;\triangleq\; \int_{x\in\Omega} w(x)\, f_1(x)\, f_2(x)\, dx, \quad w(x) \;\geq\; 0, \tag{3.6a}$$

where $w(x)$ is a real, positive integrable weight function and Ω represents a finite domain. Similarly, the corresponding norm can be defined as [106]

$$\|f_1(x)\|^2_{w(x)} \;\triangleq\; \int_{x\in\Omega} w(x)\, f_1^2(x)\, dx, \quad w(x) \;\geq\; 0. \tag{3.6b}$$

As noted above, the overall goal is to determine the unknown expansion coefficients such that some measure of the residual function $R_N(\theta_N(x))$ is required to be small. This goal can be achieved by enforcing the orthogonality condition

$$\langle R_N(\theta_N(x)), \psi_k(x)\rangle_{w(x)} \;=\; 0, \quad k = 1, 2, \ldots, N, \tag{3.7}$$

where $\psi_k(x)$ represents the test function by which a particular weighted-residuals technique is defined. In words, Eq. (3.7) requires that the residual function $R_N(\theta_N(x))$ and the test function $\psi_k(x)$ be orthogonal with respect to the weight function $w(x)$ on the given interval. Substitution of Eq. (3.5) into Eq. (3.7) yields

$$\langle L[\theta_N(x)], \psi_k(x)\rangle_{w(x)} = -\langle f(x), \psi_k(x)\rangle_{w(x)}, \quad k = 1, 2, \ldots, N. \tag{3.8}$$

Equation (3.8) can be adapted for use in any number of weighted-residuals techniques depending on the choice of test and weight functions. The three most popular approaches – orthogonal collocation, Bubnov-Galerkin and continuous least squares – will now be introduced.

3.1.1 Orthogonal Collocation

The first approach to be discussed is that of orthogonal collocation. This systematic procedure is sometimes referred to as a pseudospectral method; however, the term pseudospectral is only applied if collocation is used in conjunction with a global basis set [107]. As its name implies, the collocation method relies upon a pre-defined set of locations within the domain of the independent variable (or variables for multi-dimensional problems). It is required that the residual function be identically zero at the collocation points. Given Eq. (3.4), it can be seen that N unknown expansion coefficients will be needed to resolve $\theta_N(x)$ and therefore a set of N collocation points, denoted as $\{x_j\}_{j=1}^N$, will also be needed for the determination of these coefficients. It is important to give careful consideration to the choice of $\{x_j\}_{j=1}^N$ since this choice can affect the conditioning of the system of algebraic equations as well as the convergence of the solution. Often, the basis set upon which the trial functions are derived will provide a good indication of how collocation points should be chosen. Using the Dirac delta function as the test function, i.e., $\phi_k(x) = \delta(x - x_j), j = 1, 2, \ldots, N$ and setting the weight function equal to unity, i.e., $w(x) = 1$, the orthogonality condition found in Eq. (3.7) produces

$$\langle R_N(\theta_N(x)), \delta(x - x_k)\rangle_1 \;=\; 0, \quad k = 1, 2, \ldots, N. \tag{3.9}$$

The Dirac delta function used in Eq. (3.9) can be formally defined as

$$\delta(x) \;=\; \begin{cases} \infty, & \text{if } x = 0; \\ 0, & \text{if } x \neq 0. \end{cases} \tag{3.10}$$

Hence, $\delta(x)$ is a shorthand notation and not a function in the strictest sense [108]. It takes on meaning, however, from the important defining characteristic

$$\int_{x=-\infty}^{\infty} f(x)\delta(x)dx \;=\; f(0), \tag{3.11}$$

where $f(x)$ is an appropriate test function. It can thus be seen that a beneficial sifting property is associated with the Dirac delta function when the singularity is located at an arbitrary point x and not at zero [108]

$$\int_{x=-\infty}^{\infty} f(x')\delta(x' - x)dx' \;=\; f(x). \tag{3.12}$$

Using the definition of the inner product from Eq. (3.6a) and noting Eq. (3.12), the minimization statement for orthogonal collocation can be given by

$$R_N(\theta_N(x_k)) \;=\; 0, \quad k = 1, 2, \ldots, N. \tag{3.13}$$

Equation (3.13) produces a closed system of N algebraic equations which are used to calculate the N unknown expansion coefficients.

3.1.2 Bubnov–Galerkin

Conventional development of the Bubnov–Galerkin method is similar to that of orthogonal collocation with the exception that the expansion trial function is used as the test function instead of $\delta(x)$. The weight function is still assumed to be unity. Here, the residual function is forced to be zero by making it orthogonal to every member of a complete set [8]. A basis set is considered complete for a particular class of functions if all functions within the class can be expressed as a sum of a sufficiently large number of basis functions [107]. Given these conditions, the Galerkin method will yield $R_N(\theta_N) \to 0$ as $N \to \infty$ [103].

Substituting $\psi_k(x) = \Psi_k(x), k = 1, 2, \ldots, N$ and $w(x) = 1$ into Eq. (3.7), orthogonality requires

$$\langle R_N(\theta_N(x)), \Psi_k(x) \rangle_1 \;=\; 0, \quad k = 1, 2, \ldots, N, \tag{3.14}$$

or

$$\langle L[R_N(\theta_N(x))], \Psi_k(x) \rangle_1 \;=\; -\langle f(x), \Psi_k(x) \rangle_1, \quad k = 1, 2, \ldots, N. \tag{3.15}$$

Galerkin techniques have proven to be quite effective for the computational resolution of integral equations [106].

3.1.3 Least Squares

Finally, the least-squares approach is introduced. In this case, the L_2–norm of the real-valued residual function is directly minimized. Recalling the definition in Eq. (3.6b), the L_2–norm is given by

$$\|R_N(\theta_N(x))\|_2^2 \;=\; \langle R_N(\theta_N(x)), R_N(\theta_N(x))\rangle_1 \;=\; \int_{x=0}^{1} R_N^2(\theta_N(x))dx. \tag{3.16}$$

In order to determine the N unknown expansion coefficients, it is necessary to minimize the integral in Eq. (3.16) with respect to each individual expansion coefficient, i.e.,

$$\frac{\partial\|R_N(\theta_N(x))\|_2^2}{\partial c_k^N} \;=\; 2\int_{x=0}^{1} \frac{\partial R_N(\theta_N(x))}{\partial c_k^N} R_N(\theta_N(x))dx \;=\; 0, \quad k = 1, 2, \ldots, N. \tag{3.17}$$

From a comparison of Eq. (3.6a) and Eq. (3.17) it can be seen that

$$\psi_k(x) \;=\; \frac{\partial R_N(\theta_N(x))}{\partial c_k^N}, \quad k = 1, 2, \ldots, N, \tag{3.18a}$$

and

$$w(x) \;=\; 1, \quad k = 1, 2, \ldots, N. \tag{3.18b}$$

Using

$$\int_{x=0}^{1} \frac{\partial R_N(\theta_N(x))}{\partial c_k^N} R_N(\theta_N(x))dx \;=\; 0, \quad k = 1, 2, \ldots, N, \tag{3.19a}$$

the least-squares method produces

$$\int_{x=0}^{1} \left(\frac{\partial}{\partial c_k^N} L[\theta_N(x)]\right) L[\theta_N(x)]dx \;=\; -\int_{x=0}^{1} \left(\frac{\partial}{\partial c_k^N} L[\theta_N(x)]\right) f(x)dx,$$

$$k = 1, 2, \ldots, N. \tag{3.19b}$$

The closed system of equations given by Eq. (3.19b) can be solved for the set of expansion coefficients $\{c_k^N\}_{k=1}^N$.

3.2 Global Time Method

The generalized example given in the previous section is based on a simple boundary-value problem and only the spatial domain is considered. Indeed, Weighted Residuals Methods are most often associated with boundary-value problems [103,104] and Fredholm integral equations [105]. Classical analysis has generally focused on the use of time-marching schemes for initial-value problems and for physical systems that are governed by parabolic partial differential equations. The Global Time Method is unique in that both space and time are represented by spectral basis sets. Thus, the spatial and temporal domains are resolved simultaneously and, in effect, time is treated elliptically or as a fourth spatial dimension. Hence it makes mathematical and computational sense.

Because the GTM is a spectral method, appropriate basis sets must be chosen for each independent variable. Each dimension can be constructed using different basis sets. For the purposes of this investigation, Chebyshev polynomials of the first kind are used [106, 107, 109, 110]. This particular basis set has many advantageous characteristics [107]. Notably, it has been shown that series expansions employing Chebyshev polynomials converge faster than those using any other set of Gegenbauer polynomials [111]. Likewise, they promote considerably faster convergence than standard power series [112]. Generally, Chebyshev polynomials of the first kind are given by [106]

$$T_m(z) \;=\; \cos\left[m(\cos^{-1} z)\right], \quad m = 0, 1, \ldots, \tag{3.20}$$

where it is apparent that z is restricted to the domain $[-1, 1]$. As such, it is usually necessary to perform a coordinate transformation.

Once the problem is recast, the expansion for the unknown variable is constructed with any linear boundary or initial conditions incorporated to retain exactness in the solution representation. The approximate expression, consisting of known basis functions with unknown expansion coefficients, is then substituted into the governing equation for the physical problem to produce a residual function which must be minimized in some sense. Minimization is most often achieved through orthogonal collocation or least squares.

The Global Time Method has proven itself capable of producing accurate and stable results for inverse problems using the original mathematical formulation. The approximation process is advantageous in that it promotes stability without the need for specification of an external Tikhonov regularization parameter. This technique also profits from a reduction of matrix size needed for the resolution of the unknown function.

3.3 Function Decomposition Method

The Function Decomposition Method (FDM) is, like the GTM, a global method; however, instead of using the original mathematical formulation, the FDM recasts the inverse problem into a series of direct problems. This approach is predicated by the assumption of a functional representation for either the unknown surface temperature or heat flux and, if necessary, is followed by the application of Bellman's quasilinearization technique. The dependent variable is then decomposed into a finite sum of functions defined in terms of a baseline function and a finite set of sensitivity functions. The decomposition results in a series of concurrent, well-posed partial differential equations which can be resolved by the Weighted Residuals Method using a spectral basis set for both space and time. The choice of a Chebyshev polynomial of the first kind basis set again necessitates a coordinate transformation as previously noted. Once the sensitivity and baseline functions have been determined, the sensitivity coefficients required for reconstruction of the assumed boundary condition and the original dependent variable can be obtained by an additional application of the Weighted Residuals Method. In this case, a least-squares method is used at the surface where boundary data are available. Knowledge of the sensitivity coefficients completes the problem resolution.

As with the Global Time Method, the Function Decomposition Method yields accurate and stable results without the need for an external Tikhonov regularization parameter. Another beneficial aspect of this method is its unique design as a unified numerical treatment for the solution of both inverse and direct problems. The formulation is only somewhat changed depending on the nature of the data available or applied at the boundary, i.e., discrete input data requires the use of a discrete least-squares method to determine sensitivity coefficients while an applied continuous function at the boundary needs the use of a continuous least-squares method. Finally, the FDM exhibits some favorable computational advantages [113].

Chapter 4

Direct Heat Transfer Problem - Radiative Transport in an Absorbing Medium

As previously stated, standard direct heat transfer problems benefit from having fully specified governing systems and auxiliary conditions and, as such, are considered to be well-posed based on the criteria given by Hadamard [2]. However, the well-posed nature of these problems does not guarantee numerical stability for any given solution technique. The presence of characteristics such as stiffness or singularities in the governing system can produce unreliable results if care is not taken in the implementation of the chosen solution method. For example, explicit finite difference methods, while simple to implement, suffer greater numerical instability than do implicit techniques [22]. As a result, explicit routines may require prohibitively small time steps. Hence, the necessary precautions can lead to an undue amount of computational effort and complexity. When stiffness is involved, even implicit algorithms require strict stability considerations [114]. It would thus be advantageous to employ a methodology which can retain stability without the need for substantial modification when ill-conditioning effects occur. The formalism offered in this chapter illustrates the effectiveness with which a globalized space-time routine can be applied to potentially unstable and stiff direct problems.

4.1 Introduction

The accurate numerical treatment of the type of nonlinear, weakly singular partial integro-differential equations which appears in transient radiative (and conductive) heat transfer problems has often posed a formidable challenge to researchers. Algebraic and exponential nonlinearities, and singular kernels arise in applications involving transient, one-dimensional [115–121] and multi-dimensional [122–124] heat transfer in participating media. Physical applications involving combustion [125], thermal ignition [126], radiating gas jets [127], heat transfer in ceramic diesel liners [128], and insulating materials [129] contain such mathematical characteristics. Typically, it is necessary to rely upon numerical techniques to recover the unknown dependent variables of interest. In most previous studies, finite difference or finite element methods have been applied.

Kumar and Sloan [130] developed a formulation for one-dimensional Hammerstein integral equations that permits efficient computation by a collocation method. Several other works have followed which discuss this concept [131–133]. Frankel and Choudhury [134] indicated the merit of introducing 'cumulative' variables when investigating the logistic equation with heredity. Frankel [117–119] integrated the concepts of 'cumulative' variables and the method of Kumar and Sloan [130] to develop encouraging numerical results in transient cooling in radiative heat transfer studies. In these investigations [117–119], a time-marching numerical method was implemented. In particular, explicit [117,118] and implicit [119] Runge-Kutta methods were used to resolve the temporal variable. Prasad and Hering [115] reported that ill-conditioning effects occurred in some cases for their developed numerical method. It is well known that explicit time-marching methods suffer from stability constraints. Owing to this dilemma, Frankel [119] implemented an implicit Runge-Kutta method in order to overcome situations where stability constraints can cause unreasonably small steps to be required.

Frankel and Keyhani [102] made the observation that time collocation removed the effect of numerical ill-conditioning in the context of solving an inverse solidification design problem. With the success of this study in mind, an approach which employs collocation in both space and time is developed for the aforementioned problem in radiative heat transport. This methodology resolves all space and time simultaneously and is therefore fully implicit in nature. As will be shown, the use of time-collocation in place of time-marching produces accurate numerical results with a minimal amount of computational effort.

4.2 Cumulative Variable Formulation

Prasad and Hering [115], and Frankel [117] considered the problem of transient, one-dimensional heat transport in an absorbing, purely radiating, non-scattering gray medium bounded by black surfaces. A simple representation of the physical problem can be found in Fig. 4.1. The distance between the parallel black surfaces is x_1. The lower black boundary ($x = 0$) is maintained at the time-varying temperature $T_0(t)$ while the upper black boundary temperature is given by $T_1(t)$. Following the formulation of Prasad and Hering [115], conservation of energy requires

$$\rho c_v \frac{\partial T}{\partial t} \;=\; -\frac{\partial \Phi}{\partial x}, \quad x \in [0, x_1], \quad t \;>\; 0, \tag{4.1a}$$

where T is the local absolute temperature, Φ is the local radiative heat flux, and ρ and c_v denote the mass density and constant volume specific heat of the medium, respectively. For black boundaries separated by a distance x_1, the local radiative heat flux can be given by

$$\begin{aligned} \Phi(x^*, t) \;=\; & 2\sigma[T_0^4(t)E_3(x^*) \;-\; T_1^4(t)E_3(L - x^*) \\ & + \int_{y=0}^{L} T^4(y,t)E_2(|y - x^*|)\mathrm{sign}(x^* - y)dy], \end{aligned} \tag{4.1b}$$

where the spatial coordinate has been nondimensionalized such that

$$x^* \;=\; \kappa_\nu x, \quad x \in [0, x_1], \tag{4.1c}$$

with

$$L \;=\; \kappa_\nu x_1. \tag{4.1d}$$

In Eq. (4.1b), σ is the Stefan-Boltzmann constant, while in Eqs. (4.1c) and (4.1d) κ_ν is the radiation absorption coefficient such that $x^* = \kappa_\nu x$ is designated the optical distance measured from the lower boundary and $L = \kappa_\nu x_1$ represents the optical depth of the medium. Lastly, $E_n(z)$ is the exponential integral function which is defined by the expression [135]

$$E_n(z) \;=\; \int_{\tau=1}^{\infty} \frac{e^{-z\tau}}{\tau^n} d\tau \quad n \;=\; 0, 1, 2, \ldots; \quad \Re z \;>\; 0, \tag{4.2a}$$

with its derivative expressible as [135]

$$\frac{dE_n(z)}{dz} \;=\; -\,E_{n-1}(z) \quad n \;=\; 1, 2, 3, \ldots. \tag{4.2b}$$

Differentiation of Eq. (4.1b) with respect to x and substitution of the results into Eq. (4.1a) yields

$$\rho c_v \frac{\partial T}{\partial t}(x^*, t) \;=\; 2\kappa_\nu \sigma [T_0^4(t) E_2(x^*) \;+\; T_1^4(t) E_2(L - x^*) \;-\; 2T^4(x^*, t)$$

$$+ \int_{y=0}^{L} T^4(y, t) E_2(|y - x^*|) dy], \quad x^* \in [0, L], \quad t > 0. \tag{4.3}$$

For the purposes of this study, the radiating medium is considered to be at uniform temperature T_1 when the lower boundary undergoes a step change to the constant temperature T_0. As a result, the medium experiences a transient temperature variation which eventually approaches a new steady-state value. Based on this condition, nondimensionalization of Eq. (4.3) leads to the generalized governing system

$$\frac{\partial \bar{\theta}}{\partial t^*}(x^*, t^*) \;=\; \bar{g}(x^*) \;-\; \bar{\theta}^4(x^*, t^*) \;+\; \lambda \int_{y=0}^{L} \bar{\theta}^4(y, t^*) E_1(|y - x^*|) dy,$$

$$x^* \in [0, L], \quad t^* \;>\; 0, \tag{4.4a}$$

subject to the initial condition

$$\bar{\theta}(x^*, 0) \;=\; \theta_1, \quad x^* \in [0, L], \tag{4.4b}$$

where

$$\bar{g}(x^*) \;=\; \lambda \left[E_2(x^*) \;+\; \theta_1^4 E_2(L - x^*) \right], \tag{4.4c}$$

and

$$\lambda = \frac{1}{2}. \tag{4.4d}$$

The nondimensional temperature is represented by $\bar{\theta}(x^*, t^*)$ in Eq. (4.4a). The dimensionless variables introduced in Eq. (4.4) are defined as

$$\bar{\theta} = \frac{T}{T_0}, \tag{4.4e}$$

$$\theta_1 = \frac{T_1}{T_0}, \tag{4.4f}$$

$$t^* = \frac{4\kappa_\nu \sigma T_0^3}{\rho c_v} t. \tag{4.4g}$$

It should be noted that $E_1(z)$, defined as the first exponential integral function, contains a logarithmic singularity as $z \to 0$.

To accommodate the Weighted Residuals Method and anticipated choice of basis function to be used with the global time approach, the equations and conditions given by Eq. (4.4) are recast to fit a square domain such that $x^* \in [0, L] \to \eta \in [-1, 1]$ and $t^* \in [0, t_{max}] \to \xi \in [-1, 1]$, i.e.,

$$x^* = \alpha(1 + \eta), \quad x^* \in [0, L], \quad \eta \in [-1, 1], \tag{4.5a}$$

and

$$t^* = \beta(1 + \xi), \quad t^* \in [0, t_{max}], \quad \xi \in [-1, 1], \tag{4.5b}$$

with $\alpha = L/2$ and $\beta = t_{max}/2$ where t_{max} represents the maximum time of interest. Application of this square-domain mapping produces the new set of governing equations

$$\frac{1}{\beta}\frac{\partial\theta}{\partial\xi}(\eta,\xi) \;=\; g(\eta) \;-\; \theta^4(\eta,\xi) \;+\; \lambda\alpha\int_{\eta_0=-1}^{1}\theta^4(\eta_0,\xi)E_1(\alpha|\eta-\eta_0|)d\eta_0,$$

$$(\eta,\xi)\in[-1,1], \quad (4.6a)$$

subject to the initial condition

$$\theta(\eta,-1) \;=\; \theta_1, \quad \eta\in[-1,1], \tag{4.6b}$$

with

$$g(\eta) \;=\; \lambda\left[E_2(\alpha(1+\eta)) \;+\; \theta_1^4 E_2(\alpha(1-\eta))\right], \tag{4.6c}$$

and where $\theta(\eta,\xi) \;=\; \bar{\theta}(\alpha(1+\eta),\beta(1+\xi))$.

Using the cumulative variable technique introduced by Frankel and Choudhury [134] and further adapted to the collocation method of Kumar and Sloan [130] by Frankel [117–119], Eq. (4.6a) is integrated with respect to the temporal variable ξ. Formally interchanging orders of integration yields

$$\theta(\eta,\xi) \;=\; h(\eta,\xi) \;-\; \beta\Psi(\eta,\xi) \;+\; \lambda\alpha\beta\int_{\eta_0=-1}^{1}\Psi(\eta_0,\xi)E_1(\alpha|\eta-\eta_0|)d\eta_0,$$

$$(\eta,\xi)\in[-1,1], \quad (4.7a)$$

where the nonlinear term has been isolated and renamed such that

$$\Psi(\eta,\xi) \;=\; \int_{\xi_0=-1}^{\xi}\theta^4(\eta,\xi_0)d\xi_0, \tag{4.7b}$$

and with

$$h(\eta, \xi) \;=\; \theta_1 \;+\; \beta g(\eta)(\xi \;+\; 1). \tag{4.7c}$$

The function $\Psi(\eta, \xi)$ denotes the cumulative variable. Equation (4.7a) represents an integral transform back to the original physical variable $\theta(\eta, \xi)$. This powerful technique is not limited to a single nonlinearity but can also be applied to multiple nonlinear forms in an analogous fashion with good results as shown by Frankel [136]. Furthermore, it should be noted that the term 'cumulative' is not applied without meaning, as it can be seen from Eq. (4.7b) that $\Psi(\eta, \xi)$ is an accumulation in time of $\theta^4(\eta, \xi)$. It is then clear that

$$\frac{\partial \Psi}{\partial \xi} \;=\; \theta^4(\eta, \xi), \tag{4.8}$$

and thus substituting Eq. (4.7a) into Eq. (4.8) produces a new nonlinear, partial integro-differential equation in terms of the cumulative variable $\Psi(\eta, \xi)$

$$\frac{\partial \Psi}{\partial \xi}(\eta, \xi) \;=\; \left[h(\eta, \xi) \;-\; \beta \Psi(\eta, \xi) \;+\; \lambda \alpha \beta \int_{\eta_o=-1}^{1} \Psi(\eta_o, \xi) E_1(\alpha |\eta - \eta_o|) d\eta_o \right]^4,$$

$$(\eta, \xi) \;\in\; [-1, 1], \tag{4.9a}$$

subject to the initial condition

$$\Psi(\eta, -1) \;=\; 0, \quad \eta \;\in\; [-1, 1], \tag{4.9b}$$

which results from the definition given by Eq. (4.7b).

An important observation is that the original algebraic nonlinearity has been relocated from within the integral operator shown in Eq. (4.6a) to a new location outside the integral operator as illustrated in Eq. (4.9a). This advantageous new form permits the implementation of a collocation method in a highly efficient manner. Once satisfactory resolution of $\Psi(\eta, \xi)$ is achieved, the desired function $\theta(\eta, \xi)$ may be reconstructed by means of the integral transform given in Eq. (4.7a) or through the relation in Eq. (4.8).

4.3 Solution by Orthogonal Collocation

The problem given by Eq. (4.9) may be resolved by finding an approximation for $\Psi(\eta, \xi)$ in terms of a series expansion. For this purpose, a Weighted Residuals Method based on orthogonal collocation is employed. First, let the unknown function $\Psi(\eta, \xi)$ be represented as

$$\Psi(\eta, \xi) = \sum_{m=0}^{\infty} a_m(\xi) T_m(\eta), \tag{4.10}$$

where $\{T_m(\eta)\}_{m=0}^{\infty}$ represents the set of Chebyshev polynomials of the first kind [109]. While other basis sets may be chosen for the expansion, Chebyshev polynomials have numerous well-known properties and have successfully been applied to problems involving fluid mechanics [137], solid mechanics [138], radiative transport [117–119, 139], and many other problems in mathematical physics [107]. Here, $\{a_m(\xi)\}_{m=0}^{\infty}$ is the unknown set of time-varying expansion coefficients which correspond to the known basis set. The Chebyshev polynomials of the first kind are given by [106]

$$T_m(\eta) \;=\; \cos[m(\cos^{-1}\eta)], \quad m \;=\; 0, 1, \ldots. \tag{4.11}$$

In practice, the infinite series expansion displayed in Eq. (4.10) must be truncated after a finite number of terms, say at $N + 1$, and so Eq. (4.10) becomes

$$\Psi(\eta, \xi) \approx \Psi_N(\eta, \xi) = \sum_{m=0}^{N} a_m^N(\xi) T_m(\eta), \tag{4.12}$$

where $a_m^N(\xi) \approx a_m(\xi),\ m = 0, 1, \ldots, N$, for sufficiently large N.

At this point in the analysis, the concept of treating time globally by use of the Global Time Method (GTM) is introduced in lieu of a time-marching scheme. This strategy is suggested by previous findings [117–119] wherein the quantification of the mathematical character of similar expansion coefficients leads to the conclusion that these time-varying expansion coefficients can easily be approximated by polynomials. For instance, the problem treated by Frankel [118], which includes both conductive and radiative transport effects in the transient analysis, indicates that the time-varying expansion coefficients tend to behave as linear functions of time. Likewise, it can be seen that this problem may exhibit stiffness under the proper circumstances. As a result, a fully-implicit, nonmarching scheme appears to be advantageous.

The approximate, time-varying expansion coefficients can be expressed in terms of the finite series

$$a_m^N(\xi) = \sum_{n=0}^{P_m} b_n^m T_n(\xi), \quad \xi \in [-1, 1], \tag{4.13}$$

where $\{b_n^m\}, n = 0, 1, \ldots, P_m; m = 0, 1, \ldots, N$ denote the unknown expansion coefficients. The expansion for $\Psi_N(\eta, \xi)$ now becomes

$$\Psi(\eta, \xi) \approx \Psi_N(\eta, \xi) = \sum_{m=0}^{N} \sum_{n=0}^{P_m} b_n^m T_n(\xi) T_m(\eta), \quad (\eta, \xi) \in [-1, 1]. \tag{4.14}$$

The expansion shown in Eq. (4.13) can be modified to satisfy the initial condition displayed in Eq. (4.9b). Incorporation of the auxiliary conditions, such as boundary and initial conditions, to form a trial set is often possible [102] and removes the necessity of forming auxiliary residual statements which must be appended to the solution algorithm. By evaluating Eq. (4.14) at $\xi = -1$ and using the initial condition found in Eq. (4.9b), it can be seen that

$$\sum_{m=0}^{N} b_0^m T_m(\eta) \;=\; -\; \sum_{m=0}^{N}\sum_{n=0}^{P_m} b_n^m (-1)^n T_m(\eta), \tag{4.15}$$

since $T_n(-1) = (-1)^n$ [109]. Next, releasing the leading term, i.e., $n = 0$ in the expansion for $\Psi_N(\eta, \xi)$ as shown in Eq. (4.14) and substituting in the result of Eq. (4.15), we find

$$\Psi_N(\eta,\xi) \;=\; \sum_{m=0}^{N}\sum_{n=1}^{P_m} b_n^m T_m(\eta)[T_n(\xi) + (-1)^{n+1}], \quad (\eta,\xi) \;\in\; [-1,1], \tag{4.16}$$

where Eq. (4.16) automatically satisfies the initial condition given in Eq. (4.9b).

Because the expansion for the solution is given by a finite series and is therefore in approximate form, substituting $\Psi_N(\eta, \xi)$ into the nonlinear integro-differential equation shown in Eq. (4.9a) produces a residual equation; namely,

$$R_N(\eta,\xi) \;+\; \frac{\partial \Psi_N}{\partial \xi}(\eta,\xi) \;=\; \Big[h(\eta,\xi) \;-\; \beta\Psi_N(\eta,\xi) \;+$$

$$\lambda\alpha\beta \int_{\eta_o=-1}^{1} \Psi_N(\eta_o,\xi) E_1(\alpha|\eta \;-\; \eta_o|) d\eta_o\Big]^4, \quad (\eta,\xi) \;\in\; [-1,1]. \tag{4.17}$$

Substitution of the expansion for $\Psi_N(\eta,\xi)$, as shown in Eq. (4.16), into Eq. (4.17) yields

$$R_N(\eta,\xi) = - \sum_{m=0}^{N}\sum_{n=1}^{P_m} b_n^m T_m(\eta)\frac{dT_n}{d\xi}(\xi) + \Big[h(\eta,\xi) - \beta\sum_{m=0}^{N}\sum_{n=1}^{P_m} b_n^m T_m(\eta)[T_n(\xi)+(-1)^{n+1}] + \lambda\alpha\beta\sum_{m=0}^{N}\sum_{n=1}^{P_m} b_n^m A_m(\eta)[T_n(\xi)+(-1)^{n+1}]\Big]^4, \quad (\eta,\xi) \in [-1,1], \tag{4.18a}$$

where $A_m(\eta)$ is defined as

$$A_m(\eta) = \int_{\eta_o=-1}^{1} T_m(\eta_o)E_1(\alpha|\eta-\eta_o|)d\eta_o, \quad m = 0,1,\ldots,N, \tag{4.18b}$$

which analytically integrates to [117]

$$A_m(\eta) = -\sum_{i=0}^{m}\frac{1}{\alpha^{i+1}}[(-1)^k T_m^{(i)}(-1)E_{i+2}[\alpha(1+\eta)] + T_m^{(i)}(1)E_{i+2}[\alpha(1-\eta)]] + 2\sum_{i=0}^{m/2}\frac{1}{\alpha^{2i+1}}T_m^{(2i)}(\eta)E_{2i+2}(0), \quad m = 0,1,\ldots,N, \tag{4.18c}$$

where $T_m^{(i)}(\eta)$ represents the i^{th} derivative of the m^{th} Chebyshev polynomial of the first kind. Here, $[m/2]$ is interpreted as the integer result of $(m/2)$. The function $R_N(\eta,\xi)$ is the local and instantaneous residual function and as stated earlier must be introduced in order to properly display the equal sign shown in Eq. (4.18a). The exponential integral function, $E_n(z)$, in Eq. (4.18c) can be obtained by way of the general recurrence relation [135]

$$E_{n+1}(z) \;=\; \frac{1}{n}[e^{-z} \;-\; zE_n(z)], \quad n = 1, 2, 3, \ldots. \tag{4.19}$$

The higher derivatives for the Chebyshev polynomials, $T_m^{(i)}(\eta)$, can be determined using various established methods. One means [107] is to make use of the elementary trigonometric identity

$$\frac{d}{d\eta} \;\longleftrightarrow\; \Big[-\frac{1}{\sin(u)}\Big]\frac{d}{du}, \tag{4.20a}$$

where

$$\eta \;=\; \cos(u) \;\longleftrightarrow\; u \;=\; \cos^{-1}(\eta), \quad \eta \;\in\; [-1,1], \quad u \;\in\; [0,\pi], \tag{4.20b}$$

where u is a real function. It is now possible to develop a recurrence relation. Differentiation of the Chebyshev polynomial as defined in Eq. (4.11) yields

$$\frac{dT_m}{d\eta}(\eta) \;=\; \Big[-\frac{1}{\sin(u)}\Big]\frac{d}{du}(\cos mu) \;=\; \frac{m\sin mu}{\sin u}. \tag{4.20c}$$

Application of trigonometrical formulae leads to the relation

$$\frac{T_{m+1}^{(1)}(\eta)}{m+1} \;-\; \frac{T_{m-1}^{(1)}(\eta)}{m-1} \;=\; 2T_{m-1}(\eta), \quad \eta \;\in\; [-1,1], \quad m \;>\; 1, \tag{4.20d}$$

which can be used to build similar relations for higher derivatives by successive differentiations of Eq. (4.20d). A full description of this and other methods can be found in [107]. It should be noted that higher-order differentiation of Chebyshev polynomials is mildly ill-conditioned [107].

Unless the exact solution to $\Psi_N(\eta,\xi)$, at any instant in time $\xi \in [-1,1]$ and position $\eta \in [-1,1]$, is a linear combination of the trial functions shown in Eq. (4.16), it is not possible to obtain the set of expansion coefficients $\{b_n^m\}$, $n = 1, 2, \ldots, P_m$; $m = 0, 1, \ldots, N$ which make the residual function, $R_N(\eta, \xi)$, vanish for all $(\eta, \xi) \in [-1, 1]$.

Defining the inner product of two real-valued functions $g_1(u)$ and $g_2(u)$ as [106]

$$\big\langle g_1, g_2 \big\rangle_1 \triangleq \int_{u=-1}^{1} g_1(u) g_2(u) du, \tag{4.21}$$

permits a straightforward definition for the collocation method to be developed. For the collocation method, it is required that

$$\big\langle R_N(\eta, \xi), \delta(\eta - \eta_j)\delta(\xi - \xi_k) \big\rangle_1 = 0, \quad k = 1, 2, \ldots, P_j; \quad j = 0, 1, \ldots, N. \tag{4.22}$$

Plainly stated, Eq. (4.22) indicates that the residual function must be orthogonal to the test functions, given by the Dirac delta functions, at the specified spatial and temporal collocation points. In this case, the temporal collocation points are given by the open rule [106]

$$\xi_k = cos\Big(\frac{(2k-1)\pi}{2P_j}\Big), \quad k = 1, 2, \ldots, P_j. \tag{4.23}$$

The reasoning for this particular choice of collocation points is understood when one considers the problem at hand. The open rule given by Eq. (4.23) indicates that there will be no collocation point corresponding to $\xi = -1$, i.e., $t = 0$. It has already been established, however, that the initial condition has been incorporated into the approximate functional expansion. Hence, at $\xi = -1$ the solution is exact, the residual vanishes, and no collocation point is needed. Similarly, the global treatment of time allows for the arbitrary choice of t_{max} (corresponding to $\xi = 1$) and does not require exactness at this endpoint. Should an additional constraint be required at a specific

t_{max}, it can easily be incorporated into the solution in the same manner used for the initial condition. The spatial collocation points are expressed by the closed rule [106]

$$\eta_j \ = \ cos\Big(\frac{\pi j}{N}\Big), \quad j \ = \ 0, 1, \ldots, N. \tag{4.24}$$

Here, collocation points are established at the endpoints.

Upon substituting Eq. (4.18a) into Eq. (4.22), a closed set of nonlinear algebraic equations is obtained for the unknown expansion coefficients $\{b_n^m\}, n = 0, 1, \ldots, P_m$; $m = 0, 1, \ldots, N$, namely

$$-\sum_{m=0}^{N}\sum_{n=1}^{P_m} b_n^m T_m(\eta_j)\frac{dT_n}{d\xi}(\xi_k) \ + \ \Big[h(\eta_j, \xi_k) \ - \ \beta\sum_{m=0}^{N}\sum_{n=1}^{P_m} b_n^m[T_n(\xi_k) + (-1)^{n+1}]$$

$$\times \ [T_m(\eta_j) - \lambda\alpha A_m(\eta_j)\Big]^4 \ = \ 0, \quad k \ = \ 1, 2, \ldots, P_j; \quad j \ = \ 0, 1, \ldots, N, \tag{4.25}$$

where the collocation points are defined in Eq. (4.23) and Eq. (4.24). This form is readily adaptive to a Newton-Raphson procedure. Reconstruction of the original dependent variable $\theta(\eta, \xi)$ is obtained from the inversion formula displayed in Eq. (4.7a), in the approximate sense, namely

$$\theta(\eta, \xi) \ \approx \ \theta_N(\eta, \xi) \ = \ h(\eta, \xi) \ - \ \beta\Psi_N(\eta, \xi)$$

$$+ \ \lambda\alpha\beta\int_{\eta_0=-1}^{1}\Psi_N(\eta_0, \xi)E_1(\alpha \mid \eta - \eta_0 \mid)d\eta_0, \quad (\eta, \xi) \ \in \ [-1, 1], \tag{4.26a}$$

or

$$\theta_N(\eta,\xi) \;=\; h(\eta,\xi) \;-\; \beta\sum_{m=0}^{N}\sum_{n=1}^{P_m} b_n^m\big(T_m(\eta)-\lambda\alpha A_m(\eta)\big)\big(T_n(\xi)+(-1)^{n+1}\big),$$

$$(\eta,\xi)\in[-1,1], \tag{4.26b}$$

or through Eq. (4.8).

4.4 Steady-State Analysis and Error Estimations

At steady-state conditions, Eq. (4.6a) can be written as

$$\hat{\theta}^4(\eta) \;=\; \lambda\alpha\int_{\eta_0=-1}^{1}\hat{\theta}^4(\eta_0)E_1(\alpha\mid\eta-\eta_0\mid)d\eta_0 \;+\; g(\eta), \quad \eta\in[-1,1], \tag{4.27a}$$

where

$$\hat{\theta}(\eta) \;=\; \lim_{t\to\infty,\xi=1}\theta(\eta,\xi). \tag{4.27b}$$

Equation (4.27a) is a linear, weakly-singular Fredholm integral equation of the second kind for the unknown variable $\hat{\theta}^4(\eta)$. It is possible to develop *a posteriori* error estimates for Eq. (4.27a) through the use of classical analysis [106]. To demonstrate this process, a series expansion can be constructed for $\hat{\theta}^4(\eta)$, i.e.,

$$\hat{\theta}^4(\eta) \;=\; \sum_{m=0}^{\infty}c_mT_m(\eta), \quad \eta\in[-1,1], \tag{4.28a}$$

where the N^{th} order approximation to the above representation is

$$\hat{\theta}^4(\eta) \;\approx\; \hat{\theta}_N^4(\eta) \;=\; \sum_{m=0}^{N}c_m^NT_m(\eta), \quad \eta\in[-1,1], \tag{4.28b}$$

with $T_m(\eta)$ being the first kind Chebyshev polynomials defined in Eq. (4.11). Following a procedure similar to the one described in the previous section, a residual equation can be obtained in the form

$$\hat{R}_N(\eta) \;+\; \hat{\theta}_N^4(\eta) \;=\; \lambda\alpha \int_{\eta_0=-1}^{1} \hat{\theta}_N^4(\eta_0) E_1(\alpha \mid \eta - \eta_0 \mid) d\eta_0 \;+\; g(\eta),$$

$$\eta \in [-1, 1]. \tag{4.29}$$

Substitution of Eq. (4.28b) into Eq. (4.29), noting that the expansion coefficients are now time invariant, and implementation of the collocation method yields

$$\sum_{m=0}^{N} c_m^N [T_m(\eta_j) - \lambda\alpha A_m(\eta_j)] \;=\; g(\eta_j), \quad j \;=\; 0, 1, \ldots, N, \tag{4.30}$$

which represents a closed system of linear algebraic equations for the unknown expansion coefficients $\{c_m^N\}_{m=0}^N$. Here, the identical spatial collocation points are chosen as in the case of the transient problem.

At this point, it is possible to establish *a posteriori* error bounds for $\hat{\theta}_N^4(\eta)$. While an examination of the residual can give a sense of the local behavior of the numerical scheme, the error bounds provide an assessment of the overall accuracy of the approximate solution which would otherwise be unavailable without a known exact solution. The local, steady-state N^{th} degree error, $\hat{\epsilon}_N(\eta)$, is defined as

$$\hat{\epsilon}_N(\eta) \;=\; \hat{\theta}^4(\eta) \;-\; \hat{\theta}_N^4(\eta), \quad \eta \in [-1, 1]. \tag{4.31}$$

Subtracting Eq. (4.29) from Eq. (4.27a) and making use of the error definition found in Eq. (4.31) yields

$$-\hat{R}_N(\eta) \ + \ \hat{\epsilon}_N(\eta) \ = \ \lambda\alpha \int_{\eta_0=-1}^{1} \hat{\epsilon}_N(\eta_0) E_1(\alpha \mid \eta - \eta_0 \mid) d\eta_0, \quad \eta \in [-1, 1], \tag{4.32a}$$

or in operator form

$$-\hat{R}_N \ + \ \hat{\epsilon}_N \ = \ \lambda\alpha\kappa\hat{\epsilon}_N, \tag{4.32b}$$

where the integral operator, κ, is defined through

$$\kappa g \ = \ \int_{\eta_0=-1}^{1} E_1(\alpha \mid \eta - \eta_0 \mid) g(\eta_0) d\eta_0, \tag{4.32c}$$

with $g(\eta)$ being some real function. Noting that the infinity norm of some function $\Gamma(\eta)$ can be defined as [106]

$$\|\Gamma\|_\infty \ = \ \sup_{\eta\in[-1,1]} \mid \Gamma(\eta) \mid, \tag{4.33a}$$

while the infinity norm of the integral operator in Eq. (4.32c) can be given by [106]

$$\|\kappa\|_\infty \ = \ \sup_{\eta\in[-1,1]} \int_{\eta_0=-1}^{1} \mid E_1(\alpha \mid \eta - \eta_0 \mid) \mid d\eta_0, \tag{4.33b}$$

then it is possible to develop the error bounds based on functional analysis as

$$\frac{\|\hat{R}_N\|_\infty}{1+ \mid \lambda\alpha \mid \|\kappa\|_\infty} \ \leq \ \|\hat{\epsilon}_N\|_\infty \ \leq \ \frac{\|\hat{R}_N\|_\infty}{1- \mid \lambda\alpha \mid \|\kappa\|_\infty}, \tag{4.34}$$

when $1- \mid \lambda\alpha \mid \|\kappa\|_\infty > 0$.

The development of the error bounds in Eq. (4.34) presents an opportunity for an interesting aside which foreshadows the difficulties one can encounter in the resolution of inverse problems. It can easily be established that Eq. (4.32) gives the error, $\hat{\epsilon}_N$, in the form of a second kind Fredholm integral equation. For this case, it can be seen from Eq. (4.34) that an acceptable amount of error in the approximation is maintained as long as the residual is small. Typically, however, the inverse problems found in heat conduction produce Volterra integral equations of the first kind which are ill-posed [41]. Frankel [140] illustrated this characteristic as related to the basic inverse heat conduction problem by performing an error analysis similar to the one above. Following [140] for the sake of demonstration, consider the residual equation in operator form

$$R_N = \mathbf{K}\hat{\epsilon}_N, \tag{4.35a}$$

where $\mathbf{K}$ represents the linear integral operator and $\hat{\epsilon}_N$ is again the actual error in the approximate solution. Classical analysis reveals

$$\frac{\|\hat{R}_N\|_\infty}{\|\mathbf{K}\|_\infty} \leq \|\hat{\epsilon}_N\|_\infty, \tag{4.35b}$$

which produces only a lower bound for the error. Hence, a small residual does not guarantee the error in the approximate solution will likewise be small. In other words, the integral operator is unbounded [41]. This exercise provides added insight into why the numerical resolution of inverse problems requires special attention.

4.5 Transient Analysis

From viewing the steady-state formulation, and taking into account the possible effect of using a polynomial expansion raised to the fourth power to determine the approximation $\theta_N^4(\eta,\xi)$, it can be worthwhile to express this physical quantity in terms of a separate expansion, i.e.,

$$\theta_N^4(\eta,\xi) \;=\; \sum_{m=0}^{N} d_m^N(\xi)T_m(\eta), \quad (\eta,\xi) \in [-1,1], \tag{4.36}$$

which reduces the order of the polynomial representation for $\theta_N^4(\eta,\xi)$. In order to produce an accurate resolution for this function at non-collocation points, the time-varying expansion coefficients $\{d_m^N(\xi)\}_{m=0}^N$ can be determined at any instant in time ξ through

$$\theta_N^4(\eta_j,\xi) \;=\; \sum_{m=0}^{N} d_m^N(\xi)T_m(\eta_j), \quad j=0,1,\ldots,N, \quad \xi \in [-1,1], \tag{4.37}$$

where results using the inversion formula shown in Eq. (4.26b) are substituted into the left-hand side of Eq. (4.37) at a desired time ξ. With these definitions, it is expected that as $t_{max} \to \infty$

$$\lim_{\xi\to 1} d_m^N(\xi) \;=\; c_m^N, \quad m=0,1,\ldots,N, \tag{4.38}$$

if the induced transient errors are zero. An alternative approach for obtaining $\theta_N^4(\eta_j,\xi)$ can be developed using the definition for the cumulative variable found in Eq. (4.8).

4.6 Numerical Results

The accuracy and merit of the proposed global time approach as applied to the present example of a direct radiative transport problem can be demonstrated by an examination of numerical and graphical findings. In order to compare the present results with earlier works [115, 116], the following dimensionless variables are introduced

$$f_N^4(\eta,\xi) \;=\; \frac{\theta_N^4(\eta,\xi)-\theta_1^4}{1-\theta_1^4}, \quad (\eta,\xi)\in[-1,1], \tag{4.39a}$$

and

$$\hat{f}_N^4(\eta) \;=\; \frac{\hat{\theta}_N^4(\eta)-\theta_1^4}{1-\theta_1^4}, \quad \eta\in[-1,1], \tag{4.39b}$$

which are used for transient and steady-state analyses, respectively. With these definitions, the steady-state error estimate given in Eq. (4.34) becomes

$$\frac{\|\hat{R}_N\|_\infty/(1-\theta_1^4)}{1+\mid\lambda\alpha\mid\|\kappa\|_\infty} \;\le\; \|\hat{\Gamma}_N\|_\infty \;\le\; \frac{\|\hat{R}_N\|_\infty/(1-\theta_1^4)}{1-\mid\lambda\alpha\mid\|\kappa\|_\infty}, \tag{4.40a}$$

when $1-\mid\lambda\alpha\mid\|\kappa\|_\infty>0$ and where

$$\hat{\Gamma}_N(\eta) \;=\; \hat{f}^4(\eta) \;-\; \hat{f}_N^4(\eta). \tag{4.40b}$$

Numerical results are achieved by means of a computational scheme coded in ANSI standard Fortran. A flowchart displaying the basic logic for the algorithm can be found in Fig. 4.2. The major task involves determining the expansion coefficients $\{b_n^m\}, n=1,2,\ldots,P_m; m=0,1,\ldots,N$. The Newton-Raphson method, which is iterative, is used to recover these expansion coefficients. Convergence in the iterative procedure is established following the guideline given by the absolute error, namely, $\mid\epsilon_{n,m}^{i+1}\mid=\mid(b_n^m)^{i+1}-(b_n^m)^i\mid, n=1,2,\ldots,P; m=0,1,\ldots,N$ where i is the i^{th} iterate. When $\mid\epsilon_{n,m}^{i+1}\mid< tol$ for all (m,n), where tol is a chosen tolerance value, then convergence for fixed N,P is established. A converged solution is declared when comparison among runs in which the values for N and P are varied produces no substantial change in the solution.

The Newton-Raphson procedure requires an initial guess for the desired expansion coefficients. If zeros are used as this initial guess, convergence typically requires 15 to 18 iterations for a system with adequate spatial and temporal collocation points. The necessary number of iterations as well as overall computational load can be reduced, however, if the process begins with a relatively crude approximation based on the resolution of a much smaller system, say $N = 3, P = 4$. Such an approximation can be accomplished with a negligible amount of computational effort since it only requires the inversion of a 16×16 coefficient matrix. The crude leading order coefficients can then be padded with zeros to form a better initial guess for the larger system. This tactic generally reduces convergence effort to 5 or 6 iterations which produces a substantial reduction of total CPU time for a particular run.

Tables 4.1–4.3 * present a comparison of steady-state results using $\hat{f}_N^4(\eta)$ as defined by Eq. (4.39b) for cases of optical depth $L = 0.1$, $L = 1$ and $L = 10$, respectively. The comparisons are made between the published results of Prasad and Hering [115], Heaslet and Warming [141] and the proposed GTM. As can be seen, the GTM generates excellent agreement with established results for all three cases.

Figures 4.3–4.8 show typical numerical results for the dimensionless temperature $\theta_N(\eta, \xi)$ as a function of space (for increasing times) given the cases of (i) $L = 1$ and (ii) $L = 5$. For each case, three different values of t_{max} have been chosen to demonstrate transient and steady-state behavior; $t_{max} = 2$, $t_{max} = 45$ and $t_{max} = 90$. It should be noted that the value of t_{max} can be chosen arbitrarily depending upon the demands of the particular simulation. In other words, if a detailed inspection of early transient behavior is desired, then a small value for t_{max} can and should be chosen. Convergence of the solution can be established regardless of the numerical choice for t_{max}.

*all tables may be found in Appendix II

Likewise, Figs. 4.9–4.14 show typical numerical results for the dimensionless temperature $\theta_N(\eta, \xi)$ as a function of the mapped temporal coordinate at five equidistant spatial locations for the same cases (i) $L = 1$ and (ii) $L = 5$. As before, values of $t_{max} = 2$, $t_{max} = 45$ and $t_{max} = 90$ have been chosen. Here, steep ascents are present in the early transient, especially for case (i), followed by transition to steady state. The GTM algorithm is able to accommodate the rapid transient without difficulty. Again, solutions for all cases are converged.

Chapter 5

Parameter Estimation Heat Transfer Problem - Thermal Lags and Resistances in a Heat-Flux Differential Scanning Calorimeter (DSC)

Parameter estimation represents a class of inverse problems which is of practical importance. Such problems are characterized by complete knowledge of the input, i.e., the source function and all auxiliary conditions, but an incomplete specification of the governing system. Furthermore, input data are gathered for the dependent variable (or variables) and are likely to contain some degree of uncertainty [4]. Therefore, it is incumbent to recover or estimate the parameters that are unspecified in the governing system. These parameters are often valuable quantities such as physical properties.

Generally speaking, parameter estimation problems are considered to be mildly ill-posed in the sense of Hadamard [2]. As such, care must be taken in the development of solution techniques to account for the potential difficulties associated with uncertainty. These difficulties can become magnified as the number of unknown parameters increases. This chapter illustrates the resolution of a practical parameter estimation problem using the Function Decomposition Method (FDM). The nature of the physical system and significant number of unknown parameters provide an excellent test for the methodology.

5.1 Introduction

An example of a complex parameter estimation problem may be found in Differential Scanning Calorimetry (DSC), which is often used to characterize thermophysical properties associated with phase transformation of metals and alloys [142]. These properties include specific heat and melting and solidification characteristics such as the onset temperatures of phase transformation, the enthalpy of fusion, and the solid fraction as a function of temperature [143–147]. In such devices, the practical design of the instrument does not allow for direct temperature measurements of the sample material. As a result, the contact conductances and radiative interactions among system components yield thermal lags between the collected temperature data and sample temperature [148]. As a result, any simplified attempt to attach the recorded thermocouple reading to the sample site may lead to erroneous results. It is imperative, therefore, to develop a mathematical model that correctly accounts for the heat transfer mechanisms in the DSC chamber where the sample is placed. Results from such a simulation provide an accurate depiction of the sample temperature by incorporating thermal lags into the modeled system.

It is possible to construct such a model based on lumped heat transfer analysis of the key DSC components. This approach requires the determination of numerous parameters which are represented as time constants that correspond to the resistances between individual components in the system. These time constants are determined by means of an iterative algorithm based on the FDM to achieve resolution. The governing system of initial-value problems is first linearized by quasilinearization. Each dependent variable is then decomposed into a series of baseline and sensitivity functions with corresponding sensitivity coefficients which represent the unknown parameters. At each iterative step, the baseline and sensitivity functions are numerically calculated with an explicit fourth-order Runge-Kutta scheme, and a discrete least-squares minimization method is introduced using the collected data streams to determine the updated values for the unknown parameters. The numerical process is continued until convergence takes place for all system parameters.

5.2 Analytical Model

A generalized physical model for the heat-flux DSC of interest may be described by the schematic diagram shown in Fig. 5.1. The model consists of two cylindrical containers (or pans) resting on disk-shaped plates. One combination of container and plate is associated with the sample whose thermophysical properties are unknown, while the other combination is defined as a known reference. For the purpose of this investigation, the sample and reference containers and plates are considered to be symmetric. The supporting plates are, in turn, connected by thin wires to a larger container holder which is attached to a disk holder. The entire apparatus is surrounded by a uniform heating surface or furnace whose temperature is known as a function of time. Thermocouples embedded in the bottom surfaces of the sample and reference plates are utilized to obtain temperature data for both components.

Heat flow analysis of a similar heat flux DSC model has shown that the temperature gradients within a particular component are negligible when compared to the differences which occur at the boundaries between two separate regions of the calorimeter [149]. Therefore, it is possible to represent each component as a region possessing a spatially uniform temperature at any instant during the heating or cooling process. Heat transfer within the calorimeter may then be assumed to take place between the individual regions in the form of thermal resistances as suggested by [150] and [142].

Neglecting the effects of convection, which are small when compared with the other modes of heat transfer in the high temperature regime of interest, a heat balance between the components of a generalized physical model for the instrument produces the system of governing equations for nondimensionalized temperature in the form [151]

$$c_1 \frac{d\theta_1}{dt} = \frac{\theta_3 - \theta_1}{\tau_{c1}} + \frac{\theta_3^4 - \theta_1^4}{\tau_{r1}} + \frac{\theta_4 - \theta_1}{\tau_{c3}} + \frac{\theta_6^4 - \theta_1^4}{\tau_{r4}}, \tag{5.1a}$$

$$c_2 \frac{d\theta_2}{dt} = \frac{\theta_{32} - \theta_2}{\tau_{c2}} + \frac{\theta_{32}^4 - \theta_2^4}{\tau_{r1}} f_1 + \frac{\theta_5 - \theta_2}{\tau_{c4}} + \frac{\theta_6^4 - \theta_2^4}{\tau_{r4}} f_1, \tag{5.1b}$$

$$c_3 \frac{d\theta_3}{dt} = \frac{\theta_1 - \theta_3}{\tau_{c1}} f_2 + \frac{\theta_2 - \theta_3}{\tau_{c2}} \frac{f_2}{f_1} + \frac{\theta_0^4 - \theta_3^4}{\tau_{r2}} + \frac{\theta_6^4 - \theta_3^4}{\tau_{r5}}, \tag{5.1c}$$

$$c_4 \frac{d\theta_4}{dt} = \frac{\theta_1 - \theta_4}{\tau_{c3}} f_3 + \frac{\theta_0^4 - \theta_4^4}{\tau_{r3}}, \tag{5.1d}$$

$$c_5 \frac{d\theta_5}{dt} = \frac{\theta_2 - \theta_5}{\tau_{c4}} f_4 + \frac{\theta_0^4 - \theta_5^4}{\tau_{r3}} f_5, \tag{5.1e}$$

$$c_6 \frac{d\theta_6}{dt} = \frac{\theta_3^4 - \theta_6^4}{\tau_{r5}} f_6 + \frac{\theta_0^4 - \theta_6^4}{\tau_{r6}}, \qquad t \geq 0, \tag{5.1f}$$

where $\theta_k(t) = T_k(t)/T_o$ is the dimensionless temperature function, T_o is the uniform initial temperature, $c_k = C_k(\theta_k)/C_k(1)$ is the dimensionless specific heat capacity for components $k = 1, 2, \ldots, 6$ and $C_k(1)$ is the initial specific heat capacity for component k. It should also be noted that the term θ_{32} in Eq. (5.1b) has been included to accommodate possible asymmetry in the system due to uneven heating from the furnace wall. This term is discussed in greater detail later in this section. As illustrated in Fig. 5.1, the association between $\theta_k(t)$ and physical component can be given by

$\theta_1(t) \quad \longleftrightarrow \quad$ Reference Plate Temperature,

$\theta_2(t) \quad \longleftrightarrow \quad$ Sample Plate Temperature,

$\theta_3(t) \quad \longleftrightarrow \quad$ Container Holder Temperature,

$\theta_4(t) \quad \longleftrightarrow \quad$ Reference Container Temperature,

$\theta_5(t) \quad \longleftrightarrow \quad$ Sample Container Temperature,

$\theta_6(t) \quad \longleftrightarrow \quad$ Disk Holder Temperature.

Likewise, $\theta_0(t) = T_f(t)/T_o$ represents the dimensionless furnace temperature where $T_f(t)$ is the programmed DSC furnace temperature function. The factors f_i, $i =$

$1, 2, \ldots, 6$ are obtained through the normalization process and are defined as

$$f_1 = \frac{m_1}{m_2}, \tag{5.2a}$$

$$f_2 = \frac{m_1}{m_3}, \tag{5.2b}$$

$$f_3 = \frac{m_1 C_1(1)}{m_4 C_4(1)}, \tag{5.2c}$$

$$f_4 = \frac{m_2 C_2(1)}{m_5 C_5(1)}, \tag{5.2d}$$

$$f_5 = \frac{m_4}{m_5}, \tag{5.2e}$$

$$f_6 = \frac{m_3 C_3(1)}{m_6 C_6(1)}. \tag{5.2f}$$

Thermal resistances between components are represented by the time constants, τ given in seconds, where $\tau_{ci}, i = 1, \ldots, 4$ correspond to conductive resistances and $\tau_{ri}, i = 1, \ldots, 6$ correspond to radiative resistances. Explicitly, these time constants can be given by

$$\tau_{c1} = \frac{m_1 C_1(1)}{h_{c1}}, \tag{5.3a}$$

$$\tau_{c2} = \frac{m_2 C_2(1)}{h_{c2}}, \tag{5.3b}$$

$$\tau_{c3} = \frac{m_1 C_1(1)}{h_{c3}}, \tag{5.3c}$$

$$\tau_{c4} = \frac{m_2 C_2(1)}{h_{c4}}, \tag{5.3d}$$

$$\tau_{r1} = \frac{m_1 C_1(1)}{T_o^3\, h_{r1}}, \tag{5.3e}$$

$$\tau_{r2} = \frac{m_3 C_3(1)}{T_o^3\, h_{r2}}, \tag{5.3f}$$

$$\tau_{r3} = \frac{m_4 C_4(1)}{T_o^3\, h_{r3}}, \tag{5.3g}$$

$$\tau_{r4} = \frac{m_1 C_1(1)}{T_o^3\, h_{r4}}, \tag{5.3h}$$

$$\tau_{r5} = \frac{m_3 C_3(1)}{T_o^3\, h_{r5}}, \tag{5.3i}$$

$$\tau_{r6} = \frac{m_6 C_6(1)}{T_o^3\, h_{r6}}, \tag{5.3j}$$

where $h_{ci}, i = 1, \ldots, 4$ and $h_{rj}, j = 1, \ldots, 6$ correspond to conduction and radiation heat transfer coefficients, respectively. These heat transfer coefficients incorporate all necessary parameters in order to describe heat flow between the appropriate components. Generally speaking, $h_{ci}, i = 1, \ldots, 4$ can be described as the product of the contact area between components and the corresponding conduction heat transfer coefficient, k. Likewise, $h_{rj}, j = 1, \ldots, 6$ is a product of the appropriate radiating area, shape factor and emissivity, as well as the Stefan-Boltzmann constant. Since the problem does not specifically require knowledge of the individual parameters of which h_{ci} and h_{rj} are constructed, and because these parameters are difficult to measure with accuracy and repeatability, it is advantageous to combine them into time constants. Such time constants have the added benefit of providing physical meaning by representing the thermal lags in the system.

This simplified model has been constructed based on the following assumptions:

- All of the DSC components are maintained at the initial temperature T_o when heating begins.
- The material and reference containers are considered empty.
- Contact resistances between the sample/reference plates and their respectively attached thermocouples are neglected.
- Component heat transfer interactions which are comparatively small are neglected.
- Potential heat losses down the head stem are neglected.

These assumptions can be justified by the scope of the study which is to develop a simple means of estimating the basic thermal lags that are characteristic to individual instruments. Inclusion of thermocouple contact resistances and heat losses down the head stem would be excellent refinements for future study.

Given that the DSC is lumped at the initial temperature T_o when heating begins, Eqs. (5.1a – f) are subject to the initial conditions

$$\theta_k(0) = 1, \qquad k = 1, 2, \ldots, 6. \tag{5.4}$$

The model is driven by the furnace wall temperature, θ_0 which can be constructed as

$$\theta_0 \;=\; 1 + \alpha t - \alpha\tau_f\big(1 - e^{-\frac{t}{\tau_f}}\big), \qquad t \geq 0, \tag{5.5a}$$

where α is given by

$$\alpha = \frac{R}{T_o}, \tag{5.5b}$$

and corresponds to the programmed furnace heating rate R in Kelvins per second. Furthermore, τ_f is a time constant that represents the thermal lag in the furnace response. This particular thermal lag can be determined empirically and so τ_f is considered known.

Finally, it is assumed that temperature data are available at both the reference plate and sample plate, i.e.,

$$\{\theta_{1,i}\}_{i=0}^{M} \quad \longrightarrow \quad \theta_1(t_i) = \theta_{1,i}, \quad i = 0, 1, \ldots, M, \tag{5.6a}$$

$$\{\theta_{2,i}\}_{i=0}^{M} \quad \longrightarrow \quad \theta_2(t_i) = \theta_{2,i}, \quad i = 0, 1, \ldots, M, \tag{5.6b}$$

where $M + 1$ data points are collected at equidistant time intervals, i.e.

$$t_i = i\,\Delta t = i\,\frac{t_{max}}{M}. \tag{5.6c}$$

In theory, the DSC furnace wall should provide even heating over all instrument components throughout the temperature regime of interest. In practice, however, characteristic flaws in individual instruments will result in slight eccentricities. It is therefore necessary to account for the potential of uneven heating in some manner. One possible means of correction is to introduce an asymmetry term which can allow a degree of flexibility within the governing system. This term, θ_{32}, is incorporated into Eq. (5.1b) and is defined as

$$\theta_{32} = \theta_3 + \epsilon_{32}, \tag{5.7a}$$

where

$$c_3 \frac{d\epsilon_{32}}{dt} = \frac{(\theta_0 + \epsilon_0)^4 - \theta_0^4 + \theta_3^4 - (\theta_3 + \epsilon_{32})^4}{\tau_{r2}}, \tag{5.7b}$$

subject to the initial condition

$$\epsilon_{32}(0) = 0, \tag{5.7c}$$

and the definition

$$\epsilon_0 = K_0(\theta_0 - 1), \qquad t \geq 0, \tag{5.7d}$$

where K_0 is an unknown parameter which represents the amount of asymmetry in heat flow from the furnace wall to the different sides of the container holder. The introduction of Eq. (5.7a–d) anticipates that the radiative heat flow from the container holder to the sample plate will be somewhat different from its radiative heat flow to the reference plate. As a result, Eq. (5.7b) is added to the governing system leading to a model which requires the calculation of seven unknown variables and the resolution of eleven unknown parameters.

5.3 Mathematical Formulation

This section gives a general outline for the analytical procedure used to resolve the unknown system parameters. Osborne *et al.* [152, 153] contains a detailed account as applied to a simpler model.

5.3.1 Quasilinearization

In order to apply FDM to the set of simultaneous nonlinear ordinary differential equations which govern the system, it is first necessary to employ Bellman's quasilinearization technique [154]. Based in part upon the Newton–Raphson method, quasilinearization provides a powerful and rapidly converging means for solving nonlinear equations. As an initial step, Eq. (5.1a–f) may be recast in the general form

$$\Psi_k = c_k \frac{d\theta_k}{dt} - g_k(\theta) = 0, \qquad k = 1, 2, \ldots, 7, \qquad t \geq 0, \tag{5.8}$$

where $g_k(\theta)$ represents the right-hand side of the k^{th} governing equation and $\{\Psi_k\}_{k=1}^{7}$ is considered to be functionally dependent on all unknown variables and parameters, i.e.,

$$\{\Psi_k\}_{k=1}^{7} = f(\vec{x_1}, \vec{x_2}, \vec{x_3}), \tag{5.9a}$$

with

$$\begin{aligned}
\vec{x}_1 &= \left\{ \frac{d\theta_1}{dt}, \frac{d\theta_2}{dt}, \frac{d\theta_3}{dt}, \frac{d\theta_4}{dt}, \frac{d\theta_5}{dt}, \frac{d\theta_6}{dt}, \frac{d\epsilon_{32}}{dt} \right\}, \\
\vec{x}_2 &= \{\theta_1, \theta_2, \theta_3, \theta_4, \theta_5, \theta_6, \epsilon_{32}\}, \\
\vec{x}_3 &= \{\tau_{c1}, \tau_{c2}, \tau_{c3}, \tau_{c4}, \tau_{r1}, \tau_{r2}, \tau_{r3}\tau_{r4}, \tau_{r5}, \tau_{r6}\}.
\end{aligned} \tag{5.9b}$$

Developing a multivariable Taylor series about iterate p, a recurrence relation between iterates p and $p+1$ may be obtained in the form

$$\begin{aligned}
\Psi_k^{(p+1)} = \Psi_k^{(p)} &+ \left.\frac{\partial \Psi_k}{\partial \vec{x}_1}\right)_p \left(\vec{x}_1^{(p+1)} - \vec{x}_1^{(p)}\right) + \left.\frac{\partial \Psi_k}{\partial \vec{x}_2}\right)_p \left(\vec{x}_2^{(p+1)} - \vec{x}_2^{(p)}\right) \\
&+ \left.\frac{\partial \Psi_k}{\partial \vec{x}_3}\right)_p \left(\vec{x}_3^{(p+1)} - \vec{x}_3^{(p)}\right) + H.O.T., \qquad k = 1, ..., 7,
\end{aligned} \tag{5.10}$$

where $H.O.T.$ represents higher-order terms. For convenience, the label for iterate p can be dropped while variables and parameters at iterate $p+1$ can be expressed with an overbar. Evaluating the required partial derivatives, enforcing the condition $\bar{\Psi}_k = \Psi_k = 0, k = 1, 2, \ldots, 7$, and truncating higher-order terms in Eq. (5.10) yields the system of equations

$$
\begin{aligned}
0 \;=\;\; & 0 \quad + c_1 \left(\frac{d\bar{\theta}_1}{dt} - \frac{d\theta_1}{dt} \right) + \left[\frac{1}{\tau_{c1}} + \frac{1}{\tau_{c3}} + 4\Big(\frac{1}{\tau_{r1}} + \frac{1}{\tau_{r4}} \Big) \theta_1^3 \right] (\bar{\theta}_1 - \theta_1) \\
- \;\; & \left[\frac{1}{\tau_{c1}} + \frac{4}{\tau_{r1}} \theta_3^3 \right] (\bar{\theta}_3 - \theta_3) - \frac{1}{\tau_{c3}} (\bar{\theta}_4 - \theta_4) - \frac{4}{\tau_{r4}} \theta_6^3 (\bar{\theta}_6 - \theta_6) \\
- \;\; & [\theta_3 - \theta_1] \left(\frac{1}{\bar{\tau}_{c1}} - \frac{1}{\tau_{c1}} \right) - [\theta_4 - \theta_1] \left(\frac{1}{\bar{\tau}_{c3}} - \frac{1}{\tau_{c3}} \right) \\
- \;\; & [\theta_3^4 - \theta_1^4] \left(\frac{1}{\bar{\tau}_{r1}} - \frac{1}{\tau_{r1}} \right) - [\theta_6^4 - \theta_1^4] \left(\frac{1}{\bar{\tau}_{r4}} - \frac{1}{\tau_{r4}} \right),
\end{aligned}
\tag{5.11a}
$$

$$
\begin{aligned}
0 \;=\;\; & 0 \quad + c_2 \left(\frac{d\bar{\theta}_2}{dt} \; - \; \frac{d\theta_2}{dt} \right) + \left[\frac{1}{\tau_{c2}} + \frac{1}{\tau_{c4}} + 4 f_1 \Big(\frac{1}{\tau_{r1}} + \frac{1}{\tau_{r4}} \Big) \theta_2^3 \right] (\bar{\theta}_2 - \theta_2) \\
- \;\; & \left[\frac{1}{\tau_{c2}} + 4 f_1 \frac{1}{\tau_{r1}} (\theta_3 + \epsilon_{32})^3 \right] (\bar{\theta}_3 - \theta_3) - \frac{1}{\tau_{c4}} (\bar{\theta}_5 - \theta_5) \\
- \;\; & \left[4 f_1 \frac{1}{\tau_{r4}} \theta_6^3 \right] (\bar{\theta}_6 - \theta_6) - \left[\frac{1}{\tau_{c2}} + 4 f_1 \frac{1}{\tau_{r1}} (\theta_3 + \epsilon_{32})^3 \right] (\bar{\epsilon}_{32} - \epsilon_{32}) \\
- \;\; & [(\theta_3 + \epsilon_{32}) - \theta_2] \left(\frac{1}{\bar{\tau}_{c2}} - \frac{1}{\tau_{c2}} \right) - [\theta_5 - \theta_2] \left(\frac{1}{\bar{\tau}_{c4}} - \frac{1}{\tau_{c4}} \right) \\
- \;\; & f_1 [(\theta_3 + \epsilon_{32})^4 - \theta_2^4] \left(\frac{1}{\bar{\tau}_{r1}} - \frac{1}{\tau_{r1}} \right) - f_1 [\theta_6^4 - \theta_2^4] \left(\frac{1}{\bar{\tau}_{r4}} - \frac{1}{\tau_{r4}} \right),
\end{aligned}
\tag{5.11b}
$$

$$
\begin{aligned}
0 \;=\; 0 \; &+ c_3\left(\frac{d\bar{\theta}_3}{dt} \;-\; \frac{d\theta_3}{dt}\right) + \left[f_2\frac{1}{\tau_{c1}} + \frac{f_1}{f_2}\frac{1}{\tau_{c2}} + 4\Big(\frac{1}{\tau_{r2}} + \frac{1}{\tau_{r5}}\Big)\theta_3^3\right](\bar{\theta}_3 - \theta_3) \\
&- \; f_2\frac{1}{\tau_{c1}}(\bar{\theta}_1 - \theta_1) - \frac{f_1}{f_2}\frac{1}{\tau_{c2}}(\bar{\theta}_2 - \theta_2) - \frac{4}{\tau_{r5}}\theta_6^3(\bar{\theta}_6 - \theta_6) \\
&- \; f_2[\theta_1 - \theta_3]\left(\frac{1}{\bar{\tau}_{c1}} - \frac{1}{\tau_{c1}}\right) - \frac{f_2}{f_1}[\theta_2 - \theta_3]\left(\frac{1}{\bar{\tau}_{c2}} - \frac{1}{\tau_{c2}}\right) \\
&- \; [\theta_0^4 - \theta_3^4]\left(\frac{1}{\bar{\tau}_{r2}} - \frac{1}{\tau_{r2}}\right) - [\theta_6^4 - \theta_3^4]\left(\frac{1}{\bar{\tau}_{r5}} - \frac{1}{\tau_{r5}}\right), \qquad (5.11\text{c})
\end{aligned}
$$

$$
\begin{aligned}
0 \;=\; 0 \; &+ c_4\left(\frac{d\bar{\theta}_4}{dt} \;-\; \frac{d\theta_4}{dt}\right) + \left[f_3\frac{1}{\tau_{c3}} + \frac{4}{\tau_{r3}}\theta_4^3\right](\bar{\theta}_4 - \theta_4) \\
&- \; f_3\frac{1}{\tau_{c3}}(\bar{\theta}_1 - \theta_1) - f_3[\theta_1 - \theta_4]\left(\frac{1}{\bar{\tau}_{c3}} - \frac{1}{\tau_{c3}}\right) \\
&- \; [\theta_0^4 - \theta_4^4]\left(\frac{1}{\bar{\tau}_{r3}} - \frac{1}{\tau_{r3}}\right), \qquad (5.11\text{d})
\end{aligned}
$$

$$
\begin{aligned}
0 \;=\; 0 \; &+ c_5\left(\frac{d\bar{\theta}_5}{dt} \;-\; \frac{d\theta_5}{dt}\right) + \left[f_4\frac{1}{\tau_{c4}} + 4f_5\frac{1}{\tau_{r3}}\theta_5^3\right](\bar{\theta}_5 - \theta_5) \\
&- \; f_4\frac{1}{\tau_{c4}}(\bar{\theta}_2 - \theta_2) - f_4[\theta_2 - \theta_5]\left(\frac{1}{\bar{\tau}_{c4}} - \frac{1}{\tau_{c4}}\right) \\
&- \; f_5[\theta_0^4 - \theta_5^4]\left(\frac{1}{\bar{\tau}_{r3}} - \frac{1}{\tau_{r3}}\right), \qquad (5.11\text{e})
\end{aligned}
$$

$$
\begin{aligned}
0 \;=\; & 0 \quad + c_6\left(\frac{d\bar{\theta}_6}{dt} \;-\; \frac{d\theta_6}{dt}\right) + \left[4\left(f_6\frac{1}{\tau_{r5}} + \frac{1}{\tau_{r6}}\right)\theta_6^3\right](\bar{\theta}_6 - \theta_6) \\
& - \;\; 4f_6\frac{1}{\tau_{r5}}\theta_3^3(\bar{\theta}_3 - \theta_3) - f_6[\theta_3^4 - \theta_6^4]\left(\frac{1}{\bar{\tau}_{r5}} - \frac{1}{\tau_{r5}}\right) \\
& - \;\; [\theta_0^4 - \theta_6^4]\left(\frac{1}{\bar{\tau}_{r6}} - \frac{1}{\tau_{r6}}\right),
\end{aligned} \tag{5.11f}
$$

$$
\begin{aligned}
0 \;=\; & 0 \quad + c_3\left(\frac{d\bar{\epsilon}_{32}}{dt} \;-\; \frac{d\epsilon_{32}}{dt}\right) + \left[\frac{4}{\tau_{r2}}(\theta_3 + \epsilon_{32})^3\right](\bar{\epsilon}_{32} - \epsilon_{32}) \\
& - \;\; \frac{4}{\tau_{r2}}\left[\theta_3^3 - (\theta_3 + \epsilon_{32})^3\right](\bar{\theta}_3 - \theta_3) \\
& - \;\; \frac{4}{\tau_{r2}}(\theta_0 - 1)\left[\theta_0 + K_0(\theta_0 - 1)\right]^3(\bar{K}_0 - K_0) \\
& - \;\; \left[[\theta_0 + K_0(\theta_0 - 1)]^4 - \theta_0^4 + \theta_3^4 - (\theta_3 + \epsilon_{32})^4\right]\left(\frac{1}{\bar{\tau}_{r2}} - \frac{1}{\tau_{r2}}\right),
\end{aligned}
$$

$$
t \;\geq\; 0. \tag{5.11g}
$$

The expressions in Eq. (5.11a–g) can be further simplified by algebraic manipulation and recognition that some terms associated with iterate p can be combined to form

$\Psi_k = 0, k = 1, 2, \ldots, 7$. Hence, the equations are reduced to

$$c_1 \frac{d\bar{\theta}_1}{dt} + \left[\frac{1}{\tau_{c1}} + \frac{1}{\tau_{c3}} + 4\left(\frac{1}{\tau_{r1}} + \frac{1}{\tau_{r4}}\right)\theta_1^3\right]\bar{\theta}_1$$

$$- \left[\frac{1}{\tau_{c1}} + \frac{4}{\tau_{r1}}\theta_3^3\right]\bar{\theta}_3 - \frac{1}{\tau_{c3}}\bar{\theta}_4 - \left[\frac{4}{\tau_{r4}}\theta_6^3\right]\bar{\theta}_6$$

$$= \left[\frac{1}{\tau_{c1}} + \frac{1}{\tau_{c3}}\right]\theta_1 + 4\left(\frac{1}{\tau_{r1}} + \frac{1}{\tau_{r4}}\right)\theta_1^4$$

$$- \frac{1}{\tau_{c1}}\theta_3 - \frac{4}{\tau_{r1}}\theta_3^4 - \frac{1}{\tau_{c3}}\theta_4 - \frac{4}{\tau_{r4}}\theta_6^4 + (\theta_3 - \theta_1)\frac{1}{\bar{\tau}_{c1}}$$

$$+ (\theta_4 - \theta_1)\frac{1}{\bar{\tau}_{c3}} + (\theta_3^4 - \theta_1^4)\frac{1}{\bar{\tau}_{r1}} + (\theta_6^4 - \theta_1^4)\frac{1}{\bar{\tau}_{r4}}, \tag{5.12a}$$

$$
\begin{aligned}
c_2\frac{d\bar{\theta}_2}{dt} &+ \left[\frac{1}{\tau_{c2}} + \frac{1}{\tau_{c4}} + 4f_1\left(\frac{1}{\tau_{r1}} + \frac{1}{\tau_{r4}}\right)\theta_2^3\right]\bar{\theta}_2 - \left[\frac{1}{\tau_{c2}} + 4f_1\frac{1}{\tau_{r1}}(\theta_3+\epsilon_{32})^3\right]\bar{\theta}_3 \\
&- \frac{1}{\tau_{c4}}\bar{\theta}_5 - \left[4f_1\frac{1}{\tau_{r4}}\theta_6^3\right]\bar{\theta}_6 - \left[\frac{1}{\tau_{c2}} + 4f_1\frac{1}{\tau_{r1}}(\theta_3+\epsilon_{32})^3\right]\bar{\epsilon}_{32} \\
= \;& \left[\frac{1}{\tau_{c2}} + \frac{1}{\tau_{c4}}\right]\theta_2 + 4f_1\left(\frac{1}{\tau_{r1}} + \frac{1}{\tau_{r4}}\right)\theta_2^4 - \frac{1}{\tau_{c2}}(\theta_3+\epsilon_{32}) \\
&- 4f_1\frac{1}{\tau_{r1}}(\theta_3+\epsilon_{32})^4 - \frac{1}{\tau_{c4}}\theta_5 - 4f_1\frac{1}{\tau_{r4}}\theta_6^4 \\
&+ \left[(\theta_3+\epsilon_{32}) - \theta_2\right]\frac{1}{\bar{\tau}_{c2}} + [\theta_5-\theta_2]\frac{1}{\bar{\tau}_{c4}} \\
&+ f_1\left[(\theta_3+\epsilon_{32})^4 - \theta_2^4\right]\frac{1}{\bar{\tau}_{r1}} + f_1[\theta_6^4-\theta_2^4]\frac{1}{\bar{\tau}_{r4}}, \qquad (5.12b)
\end{aligned}
$$

$$
\begin{aligned}
c_3\frac{d\bar{\theta}_3}{dt} &+ \left[f_2\frac{1}{\tau_{c1}} + \frac{f_1}{f_2}\frac{1}{\tau_{c2}} + 4\left(\frac{1}{\tau_{r2}} + \frac{1}{\tau_{r5}}\right)\theta_3^3\right]\bar{\theta}_3 - \left[f_2\frac{1}{\tau_{c1}}\right]\bar{\theta}_1 \\
&- \left[\frac{f_1}{f_2}\frac{1}{\tau_{c2}}\right]\bar{\theta}_2 - \left[\frac{4}{\tau_{r5}}\theta_6^3\right]\bar{\theta}_6 \\
= &\left[f_2\frac{1}{\tau_{c1}} + \frac{f_1}{f_2}\frac{1}{\tau_{c2}}\right]\theta_3 + 4\left[\frac{1}{\tau_{r2}} + \frac{1}{\tau_{r5}}\right]\theta_3^4 - \left[f_2\frac{1}{\tau_{c1}}\right]\theta_1 \\
&- \left[\frac{f_1}{f_2}\frac{1}{\tau_{c2}}\right]\theta_2 - \left[\frac{4}{\tau_{r5}}\right]\theta_6^4 + f_2[\theta_1 - \theta_3]\frac{1}{\bar{\tau}_{c1}} \\
&+ \frac{f_1}{f_2}[\theta_2 - \theta_3]\frac{1}{\bar{\tau}_{c2}} + [\theta_0^4 - \theta_3^4]\frac{1}{\bar{\tau}_{r2}} + [\theta_6^4 - \theta_3^4]\frac{1}{\bar{\tau}_{r5}},
\end{aligned}
\tag{5.12c}
$$

$$
\begin{aligned}
c_4\frac{d\bar{\theta}_4}{dt} &+ \left[f_3\frac{1}{\tau_{c3}} + \frac{4}{\tau_{r3}}\theta_4^3\right]\bar{\theta}_4 - f_3\frac{1}{\tau_{c3}}\bar{\theta}_1 \\
= &\left[f_3\frac{1}{\tau_{c3}}\right]\theta_4 + \left[\frac{4}{\tau_{r3}}\right]\theta_4^4 - \left[f_3\frac{1}{\tau_{c3}}\right]\theta_1 \\
&+ f_3[\theta_1 - \theta_4]\frac{1}{\bar{\tau}_{c3}} + [\theta_0^4 - \theta_4^4]\frac{1}{\bar{\tau}_{r3}},
\end{aligned}
\tag{5.12d}
$$

$$
\begin{aligned}
c_5\frac{d\bar{\theta}_5}{dt} + \left[f_4\frac{1}{\tau_{c4}} + 4f_5\frac{1}{\tau_{r3}}\theta_5^3\right]\bar{\theta}_5 - f_4\frac{1}{\tau_{c4}}\bar{\theta}_2 & \\
= \ & \left[f_4\frac{1}{\tau_{c4}}\right]\theta_5 + \left[4f_5\frac{1}{\tau_{r3}}\right]\theta_5^4 - \left[f_4\frac{1}{\tau_{c4}}\right]\theta_2 \\
& + f_4[\theta_2 - \theta_5]\frac{1}{\bar{\tau}_{c4}} + f_5[\theta_0^4 - \theta_5^4]\frac{1}{\bar{\tau}_{r3}},
\end{aligned}
\tag{5.12e}
$$

$$
\begin{aligned}
c_6\frac{d\bar{\theta}_6}{dt} + \left[4\left(f_6\frac{1}{\tau_{r5}} + \frac{1}{\tau_{r6}}\right)\theta_6^3\right]\bar{\theta}_6 - \left[4f_6\frac{1}{\tau_{r5}}\theta_3^3\right]\bar{\theta}_3 & \\
= \ & 4\left[f_6\frac{1}{\tau_{r5}} + \frac{1}{\tau_{r6}}\right]\theta_6^4 - 4\left[f_6\frac{1}{\tau_{r5}}\right]\theta_3^4 \\
& + f_6[\theta_3^4 - \theta_6^4]\frac{1}{\bar{\tau}_{r5}} + [\theta_0^4 - \theta_6^4]\frac{1}{\bar{\tau}_{r6}},
\end{aligned}
\tag{5.12f}
$$

$$c_3 \frac{d\bar{\epsilon}_{32}}{dt} + \left[\frac{4}{\tau_{r2}} (\theta_3 + \epsilon_{32})^3 \right] \bar{\epsilon}_{32} - \frac{4}{\tau_{r2}} \left[\theta_3^3 - (\theta_3 + \epsilon_{32})^3 \right] \bar{\theta}_3$$

$$= \left[\frac{4}{\tau_{r2}} \right] (\theta_3 + \epsilon_{32})^4 - \left[\frac{4}{\tau_{r2}} \right] \theta_3^4$$

$$+ \frac{4}{\tau_{r2}} (\theta_0 - 1) \left[\theta_0 + K_0(\theta_0 - 1) \right]^3 \bar{K}_0$$

$$- \frac{4}{\tau_{r2}} (\theta_0 - 1) \left[\theta_0 + K_0(\theta_0 - 1) \right]^3 K_0$$

$$+ \left[[\theta_0 + K_0(\theta_0 - 1)]^4 - \theta_0^4 + \theta_3^4 - (\theta_3 + \epsilon_{32})^4 \right] \frac{1}{\bar{\tau}_{r2}},$$

$$t \geq 0. \tag{5.12g}$$

The final form of the system generated by Eq. (5.10) can be confirmed by checking the limit as $p \to \infty$, in which case the governing equations are returned.

5.3.2 Function Decomposition

With the iterative, linearized recurrence relations defined, functional decomposition of the unknown temperature variables may now be applied. The process begins by expressing these variables at iterate $p + 1$ as functional expansions of the form

$$\bar{\theta}_i(t) = z_0^{(i)}(t) + \sum_{m=1}^{NP} \bar{b}_m z_m^{(i)}(t), \quad i = 1, ..., NV, \tag{5.13}$$

where $z_0^{(i)}(t)$ is the baseline function for $\bar{\theta}_i(t)$, $\left\{z_m^{(i)}(t)\right\}_{m=1}^{NP}$ is the set of sensitivity functions for $\bar{\theta}_i(t)$, $\left\{\bar{b}_m\right\}_{m=1}^{NP}$ is the set of unknown system parameters and coefficients, NP is the number of unknown system parameters, and NV is the number of unknown variables. For the model described above, there are seven unknown variables and eleven unknown system parameters. Hence, the expansions for the unknown variables can be given explicitly by

$$\bar{\theta}_1(t) = z_0^{(1)}(t) \;+ \sum_{m=1}^{11} \bar{b}_m z_m^{(1)}(t), \tag{5.14a}$$

$$\bar{\theta}_2(t) = z_0^{(2)}(t) \;+ \sum_{m=1}^{11} \bar{b}_m z_m^{(2)}(t), \tag{5.14b}$$

$$\bar{\theta}_3(t) = z_0^{(3)}(t) \;+ \sum_{m=1}^{11} \bar{b}_m z_m^{(3)}(t), \tag{5.14c}$$

$$\bar{\theta}_4(t) = z_0^{(4)}(t) \;+ \sum_{m=1}^{11} \bar{b}_m z_m^{(4)}(t), \tag{5.14d}$$

$$\bar{\theta}_5(t) = z_0^{(5)}(t) \;+ \sum_{m=1}^{11} \bar{b}_m z_m^{(5)}(t), \tag{5.14e}$$

$$\bar{\theta}_6(t) = z_0^{(6)}(t) \;+ \sum_{m=1}^{11} \bar{b}_m z_m^{(6)}(t), \tag{5.14f}$$

$$\bar{\epsilon}_{32}(t) = z_0^{(7)}(t) \;+ \sum_{m=1}^{11} \bar{b}_m z_m^{(7)}(t), \quad t \geq 0, \tag{5.14g}$$

where

$$\{\bar{b}_m\}_{m=1}^{11} = \left\{\frac{1}{\bar{\tau}_{c1}}, \frac{1}{\bar{\tau}_{c2}}, \frac{1}{\bar{\tau}_{c3}}, \frac{1}{\bar{\tau}_{c4}}, \frac{1}{\bar{\tau}_{r1}}, \frac{1}{\bar{\tau}_{r2}}, \frac{1}{\bar{\tau}_{r3}}, \frac{1}{\bar{\tau}_{r4}}, \frac{1}{\bar{\tau}_{r5}}, \frac{1}{\bar{\tau}_{r6}}, \bar{K}_0\right\}. \tag{5.14h}$$

Substituting Eq. (5.14a–g) into the recurrence relations and equating terms containing like coefficients from the set $\{1, \bar{b}_1, \ldots, \bar{b}_{NP}\}$ yields a new linear system of ordinary differential equations for the baseline and sensitivity functions. Therefore, for example, the baseline functions are given by

$$\begin{aligned}
c_1 \frac{dz_0^{(1)}}{dt} &+ \left[\frac{1}{\tau_{c1}} + \frac{1}{\tau_{c3}} + 4\left(\frac{1}{\tau_{r1}} + \frac{1}{\tau_{r4}}\right)\theta_1^3\right] z_0^{(1)} \\
&- \left[\frac{1}{\tau_{c1}} + \frac{4}{\tau_{r1}}\theta_3^3\right] z_0^{(3)} - \frac{1}{\tau_{c3}} z_0^{(4)} - \left[\frac{4}{\tau_{r4}}\theta_6^3\right] z_0^{(6)} \\
&= \left[\frac{1}{\tau_{c1}} + \frac{1}{\tau_{c3}}\right]\theta_1 + 4\left(\frac{1}{\tau_{r1}} + \frac{1}{\tau_{r4}}\right)\theta_1^4 \\
&- \frac{1}{\tau_{c1}}\theta_3 - \frac{4}{\tau_{r1}}\theta_3^4 - \frac{1}{\tau_{c3}}\theta_4 - \frac{4}{\tau_{r4}}\theta_6^4,
\end{aligned} \tag{5.15a}$$

$$
\begin{aligned}
c_2\frac{dz_0^{(2)}}{dt} &+ \left[\frac{1}{\tau_{c2}}+\frac{1}{\tau_{c4}}+4f_1\Big(\frac{1}{\tau_{r1}}+\frac{1}{\tau_{r4}}\Big)\theta_2^3\right]z_0^{(2)} - \left[\frac{1}{\tau_{c2}}+4f_1\frac{1}{\tau_{r1}}(\theta_3+\epsilon_{32})^3\right]z_0^{(3)} \\
&- \frac{1}{\tau_{c4}}z_0^{(5)} - \left[4f_1\frac{1}{\tau_{r4}}\theta_6^3\right]z_0^{(6)} - \left[\frac{1}{\tau_{c2}}+4f_1\frac{1}{\tau_{r1}}(\theta_3+\epsilon_{32})^3\right]z_0^{(7)} \\
= &\left[\frac{1}{\tau_{c2}}+\frac{1}{\tau_{c4}}\right]\theta_2 + 4f_1\Big(\frac{1}{\tau_{r1}}+\frac{1}{\tau_{r4}}\Big)\theta_2^4 - \frac{1}{\tau_{c2}}(\theta_3+\epsilon_{32}) \\
&- 4f_1\frac{1}{\tau_{r1}}(\theta_3+\epsilon_{32})^4 - \frac{1}{\tau_{c4}}\theta_5 - 4f_1\frac{1}{\tau_{r4}}\theta_6^4, \qquad (5.15b)
\end{aligned}
$$

$$
\begin{aligned}
c_3\frac{dz_0^{(3)}}{dt} &+ \left[f_2\frac{1}{\tau_{c1}}+\frac{f_1}{f_2}\frac{1}{\tau_{c2}}+4\Big(\frac{1}{\tau_{r2}}+\frac{1}{\tau_{r5}}\Big)\theta_3^3\right]z_0^{(3)} \\
&- \left[f_2\frac{1}{\tau_{c1}}\right]z_0^{(1)} - \left[\frac{f_1}{f_2}\frac{1}{\tau_{c2}}\right]z_0^{(2)} - \left[\frac{4}{\tau_{r5}}\theta_6^3\right]z_0^{(6)} \\
= &\left[f_2\frac{1}{\tau_{c1}}+\frac{f_1}{f_2}\frac{1}{\tau_{c2}}\right]\theta_3 + 4\left[\frac{1}{\tau_{r2}}+\frac{1}{\tau_{r5}}\right]\theta_3^4 \\
&- \left[f_2\frac{1}{\tau_{c1}}\right]\theta_1 - \left[\frac{f_1}{f_2}\frac{1}{\tau_{c2}}\right]\theta_2 - \left[\frac{4}{\tau_{r5}}\right]\theta_6^4, \qquad (5.15c)
\end{aligned}
$$

$$c_4 \frac{dz_0^{(4)}}{dt} + \left[f_3 \frac{1}{\tau_{c3}} + \frac{4}{\tau_{r3}} \theta_4^3 \right] z_0^{(4)} - f_3 \frac{1}{\tau_{c3}} z_0^{(1)}$$

$$= \left[f_3 \frac{1}{\tau_{c3}} \right] \theta_4 + \left[\frac{4}{\tau_{r3}} \right] \theta_4^4 - \left[f_3 \frac{1}{\tau_{c3}} \right] \theta_1, \tag{5.15d}$$

$$c_5 \frac{dz_0^{(5)}}{dt} + \left[f_4 \frac{1}{\tau_{c4}} + 4 f_5 \frac{1}{\tau_{r3}} \theta_5^3 \right] z_0^{(5)} - f_4 \frac{1}{\tau_{c4}} z_0^{(2)}$$

$$= \left[f_4 \frac{1}{\tau_{c4}} \right] \theta_5 + \left[4 f_5 \frac{1}{\tau_{r3}} \right] \theta_5^4 - \left[f_4 \frac{1}{\tau_{c4}} \right] \theta_2, \tag{5.15e}$$

$$c_6 \frac{dz_0^{(6)}}{dt} + \left[4 \left(f_6 \frac{1}{\tau_{r5}} + \frac{1}{\tau_{r6}} \right) \theta_6^3 \right] z_0^{(6)} - \left[4 f_6 \frac{1}{\tau_{r5}} \theta_3^3 \right] z_0^{(3)}$$

$$= 4 \left[f_6 \frac{1}{\tau_{r5}} + \frac{1}{\tau_{r6}} \right] \theta_6^4 - 4 \left[f_6 \frac{1}{\tau_{r5}} \right] \theta_3^4, \tag{5.15f}$$

$$c_3 \frac{dz_0^{(7)}}{dt} + \left[\frac{4}{\tau_{r2}}(\theta_3 + \epsilon_{32})^3\right] z_0^{(7)} - \frac{4}{\tau_{r2}}\left[\theta_3^3 - (\theta_3 + \epsilon_{32})^3\right] z_0^{(3)}$$

$$= \left[\frac{4}{\tau_{r2}}\right](\theta_3 + \epsilon_{32})^4 - \left[\frac{4}{\tau_{r2}}\right]\theta_3^4 - \frac{4}{\tau_{r2}}(\theta_0 - 1)\left[\theta_0 + K_0(\theta_0 - 1)\right]^3 K_0,$$

$$t \ \geq \ 0, \tag{5.15g}$$

subject to the initial conditions

$$z_0^{(i)}(0) \ = \ 1, \quad i = 1, 2, \ldots, 7. \tag{5.15h}$$

Likewise, a similar series of equations is generated for each set of sensitivity functions, $\{z_m^{(i)}\}_{m=1}^{11}$ where the initial conditions are given by

$$\left\{z_0^{(i)}\right\}_{m=1}^{11}(0) \ = \ 0, \quad i = 1, 2, \ldots, 7. \tag{5.15i}$$

These equations may be solved by using conventional time-stepping routines or by treating time elliptically and employing a Weighted Residuals Method [113].

5.3.3 Minimization

The final step which must be performed for each iteration is the determination of the sensitivity coefficients, $\{\bar{b}_m\}_{m=1}^{NP}$, which correspond to the unknown system parameters. This calculation is accomplished by means of a discrete least-squares minimization using the measured temperature data sets described in Eq. (5.6a,b). Reconstructing the temperature functions for both the reference and sample plates, residual functions may be written as

$$\bar{R}_1(\bar{\theta}_1(t_i)) = z_0^{(1)}(t_i) + \sum_{m=1}^{NP} \bar{b}_m z_m^{(1)}(t_i) - \theta_{1,i}, \quad i = 0, 1, \ldots, M, \tag{5.16a}$$

$$\bar{R}_2(\bar{\theta}_2(t_i)) = z_0^{(2)}(t_i) + \sum_{m=1}^{NP} \bar{b}_m z_m^{(2)}(t_i) - \theta_{2,i}, \quad i = 0, 1, \ldots, M. \tag{5.16b}$$

Implementation of the discrete least-squares method generates a new system of linear equations for the sensitivity coefficients which become

$$\begin{aligned} &\sum_{i=0}^{M} \sum_{m=1}^{NP} \bar{b}_m \Big(z_m^{(1)}(t_i) z_k^{(1)}(t_i) + z_m^{(2)}(t_i) z_k^{(2)}(t_i) \Big) \\ &\quad = \sum_{i=0}^{M} \Big[\Big(\theta_{1,i} - z_0^{(1)}(t_i) \Big) z_k^{(1)}(t_i) + \Big(\theta_{2,i} - z_0^{(2)}(t_i) \Big) z_k^{(2)}(t_i) \Big], \\ &\qquad\qquad k = 1, 2, \ldots, NP. \end{aligned} \tag{5.17}$$

Solution of this system yields updated values for the unknown system parameters which are then used to reconstruct updated temperature profiles for all components of the model. The iterative process described in this section is repeated until satisfactory convergence of the parameters is achieved.

5.4 Numerical Results

In order to demonstrate the validity and robust nature of the parameter estimation algorithm, a benchmark problem using defined parameters and based on Eqs. (5.1a–f) and (5.5a) has been formulated to provide computationally generated temperature data for both the reference and sample plates. Both errorless and noisy data are used as input for the algorithm. Given that $T_1(t_i)$ and $T_2(t_i), i = 0, 1, \ldots, M$ represent the exact solution for reference and sample plate temperatures, respectively, both errorless and noisy data can be generated with an exact initial condition, i.e.,

$$T_{1,i} = T_1(t_i) = T_1(0) = T_o, \qquad i = 0, \tag{5.18a}$$

$$T_{2,i} = T_2(t_i) = T_2(0) = T_o, \qquad i = 0, \tag{5.18b}$$

and a data stream in accordance to

$$T_{1,i} = T_1(t_i) + \epsilon\, Rand(i)\, T_1(0), \qquad i = 1, \cdots, M, \tag{5.18c}$$

$$T_{2,i} = T_2(t_i) + \epsilon\, Rand(i)\, T_2(0), \qquad i = 1, \cdots, M, \tag{5.18d}$$

where $t_i = i\Delta t$, with $\Delta t = t_{max}/M$, M is the total number of data points, ϵ is the noise factor chosen from the closed interval [0,1], and $Rand(i)$ represents the i^{th} randomly drawn real number from the closed interval [-1,1] based on a normal distribution. The data streams are normalized with respect to T_o before their application in the algorithm to accommodate the use of dimensionless temperature in the governing system.

A computational algorithm, written in ANSI Standard Fortran, has been developed based on the function decomposition model described above. The basic logic for this algorithm is illustrated by the flowchart in Fig. 5.2. Temperature data for the sample and reference plates are obtained from separate files. Next, it is necessary to develop initial temperature profiles to be used in the quasilinearization process. Because the quasilinearization scheme is based on the Newton-Raphson method, the 'guesses' employed as established values for the first iteration can considerably influence the rate of convergence and, if physically unrealistic, the final result. It is therefore beneficial to begin the process with educated estimates. For the algorithm presented here, initial values for the unknown parameters can be determined based on the physical characteristics of each DSC component as well as empirical observation which provides estimates within the proper order of magnitude. Initial component temperature profiles are then obtained by solving a direct problem using the assumed parameter values. These values are used to begin the iterative resolution process which is considered complete when convergence is satisfied. Convergence criteria are based on comparison of system parameters of successive iterations.

Table 5.1 shows the resolved parameters obtained for errorless input data generated using values of α which correspond to heating rates of 10 K/min, 20 K/min and 30 K/min. In all cases, the method produces results that are accurate to the number of significant digits used in the defined parameters. This excellent parameter recovery and component temperature reconstruction verify the inverse algorithm. It should be noted that the number of iterations needed for convergence is dependent on the quality of the initial guesses for each parameter.

In the practical operation of a DSC, a small amount of error (noise) is expected in the plate thermocouple readings. This level of error does not have a substantial effect on the stability or accuracy of a direct algorithm. However, inverse problems are known to be ill-posed in the sense of Hadamard which means that a small change in the input data can produce a significant change in the output. While parameter estimation problems are generally considered to be only mildly ill-posed, the similarity of the DSC component temperature profiles combined with the number of parameters which must be recovered can induce instability and magnify error in the inverse algorithm. This situation can be illustrated by an intuitive examination of the sensitivity functions.

Figures 5.3 and 5.4 depict the sensitivity functions that are generated for the reference plate (using errorless data) and that are associated with the conductive and radiative parameters, respectively. For stable operation of the FDM technique, these functions must remain linearly independent or else the minimization matrix will tend to become singular. As can be seen in the figures, both sets of sensitivity functions are beginning to show signs of linear dependency in some of the curves. As noise is introduced into the input data, the likelihood of linear dependence increases and thus the stability and accuracy of the inverse routine may begin to fail.

To see the magnitude of this effect, input data with various levels of noise have been used with the empty pan model parameter estimation scheme. The results are presented in Table 5.2, where ϵ has been chosen to produce maximum noise of $\pm$ 0.03 K, $\pm$ 0.06 K, and $\pm$ 0.15 K, respectively. It is readily apparent that as the amount of data noise increases, accuracy and stability begin to degrade. For the case of $\pm$ 0.15 K maximum noise, no convergence is achieved. These issues suggest the introduction of a multistep scheme that resolves two subsets of the parameter list.

The answer to this problem is to construct a two-step calibration sequence which can determine all parameters satisfactorily. The first step involves the resolution of a model where both the reference and sample pans have been removed (no pan model). This model can easily be constructed by returning to Eqs. (5.1a–f) and eliminating Eqs. (5.1d,e) as well as heat balance terms that are associated with pan temperatures. This new governing system only requires the estimation of eight unknown parameters, five of which (τ_{c1},τ_{c2},τ_{r2},τ_{r5}, and τ_{r6}) can be used as known parameters in the empty pan model. Recovery of the six remaining unknown parameters using the empty pan model comprises the second step. Both steps of the sequence retain sufficient accuracy and stability to provide good results, as illustrated in Tab. 5.3.

An additional demonstration of the effectiveness of the two-step calibration sequence can be found by comparing the reconstructed and exact benchmark temperature profiles. Comparisons for two key DSC components are shown in Figs. 5.5 and 5.6 in the form of percent differences. Even in the presence of relatively significant input error, the reconstructed temperatures agree closely with the exact, especially in the higher temperature regime. Since this is the range where sample phase change is likely to occur, the performance of the calibration sequence is highly encouraging.

Chapter 6

Inverse Heat Transfer Problem - Conduction in a Slab

The use of inverse analysis for both function reconstruction-estimation and thermal design problems represents an important area of study from which numerous practical applications can be derived. For example, investigations of casting processes involving solidification design [102, 155, 156] have derived great benefit from the use of inverse techniques. Other applications of interest include the calculation of process control for heat treatment, the determination of surface heat flux in fire experiments, and the estimation of reentry surface temperatures and heat fluxes for space vehicles. These applications are of diverse complexity, but they all can be classified as inverse heat conduction problems. This chapter details the application of both the Global Time Method (GTM) and Function Decomposition Method (FDM) to a standard one-dimensional inverse heat conduction problem [4].

6.1 Introduction

In general, inverse heat conduction analysis utilizes the measured temperature history at one or more internal locations to estimate unknown boundary conditions, energy generation rates, or, as discussed in the previous chapter, thermophysical properties [7]. Problems can be further classified depending upon the quantity or function to be determined. As with other inverse problems, the main difficulty in developing a suitable solution algorithm evolves from the tendency of the inverse heat conduction problem to be ill-posed in the sense of Hadamard [2]. Previous attempts to overcome the inherent instability have involved the utilization of future information, Tikhonov regularization and Conjugate Gradient techniques [1, 4, 6].

Both the Global Time Method (GTM) and Function Decomposition Method (FDM) are offered to resolve the aforementioned inverse heat conduction problem. Here, a brief overview is helpful. For the case of the GTM, the entire space-time domain is resolved simultaneously with functional reconstruction accomplished by means of a weighted-residuals technique. As with the direct problem presented in Chapter 4, a spectral basis set is chosen to represent both space and time [102]. In this method, the prescribed one-sided boundary conditions retain exactness in the approximate solution series expansion. For the case of the FDM, a functional representation for either the unknown surface temperature or surface heat flux is assumed. The dependent variable is then decomposed into a finite sum of functions defined in terms of a baseline function and a finite set of sensitivity functions. This decomposition results in a series of concurrent, well-posed partial differential equations which can be resolved by a weighted-residuals technique using a spectral basis representation for both space and time. The sensitivity coefficients needed in the reconstruction of the assumed boundary condition and dependent variable can likewise be obtained via a weighted-residuals technique, i.e., an appropriate least-squares method or orthogonal collocation. With the FDM, exactness of the "data" boundary condition used to find the sensitivity coefficients is not retained in the series representation for the temperature. This permits some lack of precision that can be exploited in the actual implementation process. Neither approach requires the specification of a classical regularization parameter but instead provides regularization through the retention of expansion terms. Hence, the problem is stabilized by adding higher frequencies back to the solution.

6.2 Mathematical Formulation

As an illustrative example of both methodologies, the traditional one-dimensional inverse heat conduction problem with over-specified boundary conditions at the back wall is considered. For this well-documented problem [4, 7], shown in Fig. 6.1, a one-dimensional parallel plate of unit dimensionless length is subject to a transient, dimensionless heat flux, $q(t)$, at the front surface, $x = 0$, while the back surface, $x = 1$, is insulated. Using the dimensionless forms of Ozisik [7], and Frankel and Keyhani [157], the governing heat conduction equation is written as

$$\frac{\partial^2 T}{\partial x^2}(x,t) = \frac{\partial T}{\partial t}(x,t), \quad x \in [0,1], \quad t \geq 0, \tag{6.1a}$$

with the imposed boundary conditions

$$-\frac{\partial T}{\partial x}(0,t) = q(t), \tag{6.1b}$$

$$\frac{\partial T}{\partial x}(1,t) = 0, \quad t > 0, \tag{6.1c}$$

and the initial condition

$$T(x,0) = 0, \quad x \in [0,1]. \tag{6.1d}$$

The dimensionless terms can be defined as

$$T = \frac{T^* - T_o}{T_o}, \tag{6.2a}$$

$$x = \frac{x^*}{L}, \tag{6.2b}$$

$$t = \frac{\alpha t^*}{L^2}, \tag{6.2c}$$

where T^*, x^*, and t^* represent dimensional temperature, space and time, respectively. Likewise, α is the material thermal diffusivity and L is the dimensional plate thickness.

An analytic solution for the problem given by Eq. (6.1) may readily be obtained using the finite integral transform method [7]. Using such a technique produces

$$T(x,t) = \sum_{m=0}^{\infty} \frac{\cos(\lambda_m x)}{N_m} \int_0^t q(\tau) e^{-\lambda_m^2 (t-\tau)} d\tau, \quad x \in [0,1], \quad t \geq 0, \tag{6.3}$$

where $\lambda_m = m\pi, \ m = 0, 1, ...,$ represents the discrete spectrum of eigenvalues and $N_0 = 1, N_m = \frac{1}{2}, \ m = 1, 2, ...,$ are the normalization integrals. Evaluating Eq. (6.3) at the insulated boundary yields

$$T(1,t) = \sum_{m=0}^{\infty} \frac{(-1)^m}{N_m} \int_0^t q(\tau) e^{-\lambda_m^2 (t-\tau)} d\tau, \quad t \geq 0. \tag{6.4}$$

The temperature field $T(x,t)$, shown in Eq. (6.3) is defined in terms of the dimensionless heat flux and so is well-posed if $q(t)$ is known. However, for the classical inverse heat conduction problem, $T(1,t)$ is given by either a continuous function (thermal design) or discrete data (diagnostic deduction) and $q(t)$ must be determined. Examination of Eq. (6.4) reveals that it is necessary to resolve a Volterra integral equation of the first kind in order to calculate heat flux. This type of integral equation is known to be ill-posed [41], hence, the inverse heat conduction problem is likewise ill-posed and care must be taken in choosing an accurate but stable prediction technique.

At this point, it is possible to investigate two different types of inverse problem depending upon the nature of the information at the back boundary. The first type of problem is known as the diagnostic deduction problem and is a class of inverse heat conduction problem which utilizes discrete data for one of the boundary conditions to form an over-specified or one-sided boundary statement, thus leading to a Cauchy problem. The data are normally obtained from a thermocouple embedded at (or near) an insulated back surface. The use of multiple embedded probe locations is also possible. The second type of problem is the thermal design problem which requires the determination of one or more boundary conditions based on a prescribed continuous specification. Here, the same one-dimensional inverse heat conduction problem with over-specified boundary conditions is treated, with the exception that the discrete back wall boundary condition is now given as a continuous function.

For the diagnostic deduction problem where discrete temperature data are given at the insulated surface, the over-specified boundary conditions for the governing equation, Eq. (6.1a), become

$$T(1, t_i) \;=\; F_i, \quad i = 1, 2, ..., M, \tag{6.5a}$$

where M represents the number of time sampled temperatures and

$$\frac{\partial T}{\partial x}(1, t) \;=\; 0, \quad t > 0. \tag{6.5b}$$

Here, F_i can be qualitatively given by

$$F_i = F(t_i) + \epsilon_i, \quad i = 1, 2, ..., M, \tag{6.5c}$$

where $F(t_i)$ is the exact temperature and ϵ_i is the measurement noise for each sample time $i = 1, 2, \ldots, M$. For the case of the thermal design problem, the boundary condition in Eq. (6.5a) is replaced by

$$T(1, t) = F(t), \quad t \geq 0. \tag{6.5d}$$

In both cases, the initial condition remains that given by Eq. (6.1d).

Since it is intended to incorporate a weighted-residuals technique with spectral basis functions into the solution methodology, it is convenient to now transform the temporal and spatial coordinates to the Chebyshev domain by the linear mapping functions [157]

$$\eta = 2x - 1, \quad \eta \in [-1, 1], \quad x \in [0, 1], \tag{6.6a}$$

$$\xi = \frac{t}{\lambda} - 1, \quad \xi \in [-1, 1], \quad t \in [0, t_{max}], \tag{6.6b}$$

where $\lambda = \frac{t_{max}}{2}$ and t_{max} represents the maximum dimensionless time of interest for the time evolution of the problem. Following the mathematical formulation of Frankel and Keyhani [157], the nondimensional heat conduction equation in the Chebyshev domain is given by

$$L[\theta(\eta, \xi)] = 0, \quad (\eta, \xi) \in [-1, 1], \tag{6.7a}$$

where the differential operator is defined as

$$L \equiv \frac{\partial^2}{\partial \eta^2} - \frac{1}{4\lambda} \frac{\partial}{\partial \xi}. \tag{6.7b}$$

The over-specified boundary conditions for the diagnostic deduction problem become

$$\theta(1, \xi_i) = f_i, \quad i = 1, 2, ..., M, \tag{6.7c}$$

$$\frac{\partial \theta}{\partial \eta}(1, \xi) = 0, \quad \xi \in [-1, 1], \tag{6.7d}$$

while for the thermal design problem, the boundary condition given by Eq. (6.5d) becomes

$$\theta(1, \xi) = f(\xi), \quad \xi \in [-1, 1]. \tag{6.7e}$$

The corresponding initial condition for both types of problem is

$$\theta(\eta, -1) = 0, \quad \eta \in [-1, 1]. \tag{6.7f}$$

The nondimensionalized temperature is now expressed as $\theta(\eta, \xi) = T(\frac{1+\eta}{2}, \lambda(1 + \xi))$ and the boundary input data is given by $f_i = \theta_i,\ i = 1, 2, ..., M$. By inspection of the mapping functions, Eq. (6.6a) and Eq. (6.6b), it is apparent that the new problem domain is defined over a square space-time region. Finally, the unknown surface heat flux can be calculated from the expression

$$Q(\xi) = -2\frac{\partial \theta}{\partial \eta}(-1, \xi), \quad \xi \in [-1, 1]. \tag{6.7g}$$

Techniques that have been applied to this type of problem in the past include Beck's future information method [4], dynamic programming [40], and regularization methods [1, 10].

6.3 Solution Technique: Global Time Method

6.3.1 Diagnostic Deduction

To begin, the unknown temperature distribution can be represented in terms of the infinite series expansion

$$\theta(\eta, \xi) \;=\; \sum_{m=0}^{\infty} a_m(\xi) T_m(\eta), \quad (\eta, \xi) \in [-1, 1], \tag{6.8}$$

where the spatial basis functions $\{T_m(\eta)\}_{m=0}^{\infty}$ are Chebyshev polynomials of the first kind [106] and the unknown time-varying expansion coefficients are denoted by the infinite set $\{a_m(\xi)\}_{m=0}^{\infty}$. In practice, this infinite series representation must be truncated after a finite number of terms, say $N+1$, and thus Eq. (6.8) must be reformed in the approximate sense as

$$\theta(\eta, \xi) \;\approx\; \theta_N(\eta, \xi) \;=\; \sum_{m=0}^{N} a_m^N(\xi) T_m(\eta), \quad (\eta, \xi) \in [-1, 1], \tag{6.9}$$

where $a_m(\xi) \approx a_m^N(\xi)$, $m = 0, 1, ..., N$ for sufficiently large N. At this point, it is possible to remove a potential source of error from the numerical solution by incorporating the known boundary and initial conditions. From the boundary condition in Eq. (6.7d), it can be written

$$\frac{\partial \theta}{\partial \eta}(1, \xi) \;=\; \frac{\partial \theta_N}{\partial \eta}(1, \xi) \;=\; \sum_{m=0}^{N} a_m^N(\xi) \frac{dT_m}{d\eta}(1) \;=\; 0, \quad \xi \in [-1, 1]. \tag{6.10}$$

Releasing the $m = 0$ (where $\frac{dT_0}{d\eta}(1) = 0$) and $m = 1$ (where $\frac{dT_1}{d\eta}(1) = 1$) terms from the expansion in Eq. (6.10) leads to the relation

$$a_1^N(\xi) \;=\; -\sum_{m=2}^{N} a_m^N(\xi)\frac{dT_m}{d\eta}(1), \quad \xi \in [-1,1], \tag{6.11}$$

which upon substitution into Eq. (6.9) yields

$$\theta_N(\eta,\xi) \;=\; a_0^N(\xi) + \sum_{m=2}^{N} a_m^N(\xi)\left[T_m(\eta) - \eta\frac{dT_m}{d\eta}(1)\right], \quad (\eta,\xi) \in [-1,1]. \tag{6.12}$$

For convenience, the time-varying expansion coefficients and basis functions can be redefined as

$$b_1^N(\xi) \;=\; a_0^N(\xi), \tag{6.13a}$$

$$b_m^N(\xi) \;=\; a_m^N(\xi), \quad m = 2,3,\ldots,N, \tag{6.13b}$$

$$\omega_m(\eta) \;=\; \begin{cases} 1, & \text{if } m = 1; \\ T_m(\eta) - \eta\frac{dT_m}{d\eta}(1) & \text{if } m = 2,3,...,N, \end{cases} \tag{6.13c}$$

therefore $\theta_N(\eta,\xi)$ is now presented in the form

$$\theta_N(\eta,\xi) \;=\; \sum_{m=1}^{N} b_m^N(\xi)\omega_m(\eta), \quad (\eta,\xi) \in [-1,1]. \tag{6.14}$$

Similarly, the initial condition can be incorporated into the approximate expansion. Recalling Eq. (6.7f),

$$\theta(\eta,-1) \;=\; \theta_N(\eta,-1) \;=\; 0 \;=\; \sum_{m=1}^{N} b_m^N(-1)\omega_m(\eta), \quad \eta \in [-1,1], \tag{6.15a}$$

which, due to the linear independence of the spatial trial functions, requires that

$$b_m^N(-1) \;=\; 0, \quad m = 1, 2, \ldots, N. \tag{6.15b}$$

Expressing the time-varying expansion coefficients $\{b_m^N(\xi)\}_{m=1}^N$ as a finite sum of Chebyshev polynomials of the first kind, i.e.,

$$b_m^N(\xi) \;=\; \sum_{n=0}^{P_m} b_n^m T_n(\xi), \quad \xi \in [-1, 1], \tag{6.16a}$$

and using the requirement in Eq. (6.15b), it can be written

$$b_m^N(-1) \;=\; 0 \;=\; \sum_{n=0}^{P_m} b_n^m T_n(-1) \;=\; \sum_{n=0}^{P_m} b_n^m (-1)^n, \quad m = 1, 2, \ldots, N. \tag{6.16b}$$

Releasing the $n = 0$ term and applying this condition to the expansion for the time-varying coefficients gives

$$b_m^N(\xi) \;=\; \sum_{n=1}^{P_m} b_n^m \left[T_n(\xi) + (-1)^{n+1}\right], \quad \xi \in [-1, 1], \quad m = 1, 2, \ldots, N. \tag{6.17}$$

Finally, substitution of Eq. (6.17) into Eq. (6.14) yields

$$\theta_N(\eta, \xi) \;=\; \sum_{m=1}^{N} \sum_{n=1}^{P_m} b_n^m \Omega_{m,n}(\eta, \xi), \quad (\eta, \xi) \in [-1, 1], \tag{6.18a}$$

where

$$\Omega_{m,n}(\eta, \xi) \;=\; \left[T_n(\xi) + (-1)^{n+1}\right] \omega_m(\eta), \quad (\eta, \xi) \in [-1, 1],$$

$$n = 1, 2, \ldots, P_m; \quad m = 1, 2, \ldots, N. \tag{6.18b}$$

Because discrete data are being used at the boundary, the condition in Eq. (6.7c) cannot be incorporated into the expansion but must be included in a later step. It is therefore necessary at this point to determine the unknown expansion coefficients. For this purpose, a Weighted Residuals Method is employed. Substituting the series expansion in Eq. (6.18a) into the heat equation shown in Eq. (6.7a) leads to the residual statement

$$R_N(\theta_N(\eta,\xi)) \;=\; L[\theta_N(\eta,\xi)] \;=\; \sum_{m=1}^{N}\sum_{n=1}^{P_m} b_n^m L[\Omega_{m,n}(\eta,\xi)],$$

$$(\eta,\xi) \in [-1,1], \qquad (6.19)$$

where $R_N(\theta_N(\eta,\xi))$ is the residual function which arises from the approximate nature of the series expansion and the heat equation operator, L is given in Eq. (6.7b). Because discrete data are provided at discrete times, it is proposed that orthogonal collocation be used in space while a discrete least-squares approach be used in time. By necessity, two separate inner product statements must be introduced for probe and nonprobe locations. For the spatial collocation, a closed rule is used [106], namely

$$\eta_j \;=\; \cos\left(\frac{(j-1)\pi}{N-1}\right), \quad j = 1, 2, \ldots, N. \qquad (6.20)$$

By choosing a closed rule, it is ensured that the endpoints are included in the collocation scheme and thus the probe location at the insulated boundary will coincide with a collocation point, i.e., when $j = 1$ or $\eta_1 = 1$. In this instance, the orthogonality statement for the discrete least-squares method yields

$$\left\langle \hat{R}_N^1(\xi), \frac{\partial \hat{R}_N^1}{\partial b_k^1}(\xi) \right\rangle_1 \;=\; 0, \quad j = 1, \qquad (6.21)$$

where the residual function $\hat{R}_N^1(\xi)$ is determined using the known, discrete data stream at the probe location. For all other collocation points, i.e., those that do not correspond to a probe location, the orthogonality statement for collocation and the discrete least-squares method is given by

$$\left\langle R_N^j(\xi), \frac{\partial R_N^j}{\partial b_k^j}(\xi) \right\rangle_1 \;=\; 0, \quad j = 2, 3, \ldots, N, \tag{6.22a}$$

where

$$R_N^j(\xi) \;=\; \langle R_N(\theta_N(\eta, \xi)), \delta(\eta - \eta_j) \rangle_1 \,, \quad j = 1, 2, \ldots, N, \tag{6.22b}$$

and δ represents the Dirac delta function. For the case of Eqs. (6.22a,b), the residual function $R_N^j(\xi)$ is described by Eq. (6.19). Substitution of Eq. (6.19) into Eq. (6.22b) leads to the expression

$$R_N^j(\xi) \;=\; \sum_{m=1}^{N} \sum_{n=1}^{P_m} b_n^m L[\Omega_{m,n}(\eta_j, \xi)], \quad j = 1, 2, \ldots, N, \tag{6.23}$$

where time ξ is still represented as a continuous function at each spatial collocation point η_j. It should be noted that while Eq. (6.23) is valid at the probe location ($j = 1$) it is disregarded here in favor of the known data stream. The case would be similar for any other collocation point corresponding with a probe location should multiple probes be available.

It is next incumbent to apply the discrete least-squares method to the inner product statement for the probe location and nonprobe locations, respectively. For the inner product statement at the probe location, the discrete least-squares method can be utilized in the form

$$S_1\left(\{b_n^m\}\right) \;\triangleq\; S_1 \;=\; \|\hat{R}_N^1\|_2^2 \;=\; \sum_{i=1}^{M} \left(\theta_N(\eta_j, \xi_i) - \theta_i\right)^2 . \tag{6.24}$$

Substituting the expansion for $\theta_N(\eta, \xi)$ as given by Eq. (6.18a) into Eq. (6.24) leads to the expression

$$S_1 \;=\; \sum_{i=1}^{M} \left(\sum_{m=1}^{N} \sum_{n=1}^{P_m} b_n^m \Omega_{m,n}(\eta_1, \xi_i) - \theta_i \right)^2 . \tag{6.25}$$

Minimizing Eq. (6.25) with respect to the expansion coefficients $b_k^1, k = 1, 2, \ldots, P_1$ yields

$$\frac{\partial S_1}{\partial b_k^1} \;=\; 2 \sum_{i=1}^{M} \left(\sum_{m=1}^{N} \sum_{n=1}^{P_m} b_n^m \Omega_{m,n}(\eta_1, \xi_i) - \theta_i \right) \Omega_{1,k}(\eta_1, \xi_i) \;=\; 0,$$

$$k = 1, 2, \ldots, P_1, \tag{6.26a}$$

or

$$\sum_{m=1}^{N} \sum_{n=1}^{P_m} b_n^m \left(\sum_{i=1}^{M} \Omega_{m,n}(\eta_1, \xi_i) \Omega_{1,k}(\eta_1, \xi_i) \right)$$

$$= \sum_{i=1}^{M} \theta_i \Omega_{1,k}(\eta_1, \xi_i), \quad k = 1, 2, \ldots, P_1. \tag{6.26b}$$

For the inner product expression at nonprobe locations, it can be written

$$S_j \left(\{ b_n^m \} \right) \;\triangleq\; S_j \;=\; \| R_N^j \|_2^2 \;=\; \sum_{i=1}^{M} \left(\sum_{m=1}^{N} \sum_{n=1}^{P_m} b_n^m L \left[\Omega_{m,n}(\eta_j, \xi_i) \right] \right)^2 ,$$

$$j = 2, 3, \ldots, N. \tag{6.27}$$

Minimizing Eq. (6.27) with respect to $b_k^j (k = 1, 2, \ldots, P_j)$ gives [158]

$$\frac{\partial S_j}{\partial b_k^j} \; = \; 2 \sum_{i=1}^{M} \left(\sum_{m=1}^{N} \sum_{n=1}^{P_m} b_n^m L\left[\Omega_{m,n}(\eta_j, \xi_i)\right] \right) L\left[\Omega_{j,k}(\eta_j, \xi_i)\right] \; = \; 0,$$

$$k = 1, 2, \ldots, P_j; \quad j = 2, 3, \ldots, N, \tag{6.28a}$$

or

$$\sum_{m=1}^{N} \sum_{n=1}^{P_m} b_n^m \left(\sum_{i=1}^{M} L\left[\Omega_{m,n}(\eta_j, \xi_i)\right] L\left[\Omega_{j,k}(\eta_j, \xi_i)\right] \right) \; = \; 0,$$

$$k = 1, 2, \ldots, P_j; \quad j = 2, 3, \ldots, N. \tag{6.28b}$$

Equations (6.26b) and (6.28b) form a linear system of equations which can be solved for the set of expansion coefficients b_m^n. Recovery of these coefficients allows for the reconstruction of the approximate solution $\theta_N(\eta, \xi)$ using Eq. (6.18a).

6.3.2 Thermal Design

Application of the Global Time Method to the thermal design problem begins with the same series expansion representation for $\theta(\eta, \xi)$ found in Eq. (6.8), i.e.,

$$\theta(\eta, \xi) \; = \; \sum_{m=0}^{\infty} a_m(\xi) T_m(\eta), \quad (\eta, \xi) \in [-1, 1], \tag{6.29}$$

where again the spatial basis functions $\{T_m(\eta)\}_{m=0}^{\infty}$ are chosen as Chebyshev polynomials of the first kind [106] and the unknown time-varying expansion coefficients are denoted by the infinite set $\{a_m(\xi)\}_{m=0}^{\infty}$. Truncation of the infinite series after a finite number of terms, say $N+2$, the approximate solution can be written in the form

$$\theta(\eta,\xi) \approx \Theta_{N+1}(\eta,\xi) \;=\; \sum_{m=0}^{N+1} a_m^{N+1}(\xi) T_m(\eta), \quad (\eta,\xi) \in [-1,1], \tag{6.30}$$

where $a_m(\xi) \approx a_m^{N+1}(\xi)$, $m = 0, 1, \ldots, N, N+1$ for sufficiently large N. As with the diagnostic deduction problem, the auxiliary conditions given by Eqs. (6.7d,f) can be incorporated into the approximate series expansion to retain exactness at the boundary. Additionally, the condition given by Eq. (6.7e) can be included since the temperature at the insulated wall is defined by a function as opposed to a discrete data stream. Hence, from Eq. (6.7e) it is known

$$\Theta(1,\xi) \;=\; \Theta_{N+1}(1,\xi) \;=\; f(\xi) \;=\; \sum_{m=0}^{N+1} a_m^{N+1}(\xi) T_m(1), \quad \xi \in [-1,1], \tag{6.31}$$

and since $T_m(1) = 1$ for $m = 0, 1, \ldots, \infty$, Eq. (6.31) becomes

$$\sum_{m=0}^{N+1} a_m^{N+1}(\xi) \;=\; f(\xi), \quad \xi \in [-1,1]. \tag{6.32}$$

Releasing the $m = 0$ term leads to the expression

$$a_0^{N+1}(\xi) \;=\; f(\xi) - \sum_{m=1}^{N+1} a_m^{N+1}(\xi), \quad \xi \in [-1,1]. \tag{6.33}$$

Likewise, from the boundary condition in Eq. (6.7d), it can be determined

$$\frac{\partial\Theta}{\partial\eta}(1,\xi) \;=\; \frac{\partial\Theta_{N+1}}{\partial\eta}(1,\xi) \;=\; 0 \;=\; \sum_{m=0}^{N+1} a_m^{N+1}(\xi) \frac{dT_m}{d\eta}(1), \quad \xi \in [-1,1], \tag{6.34a}$$

and noting that

$$\frac{dT_0}{d\eta}(1) \;=\; 0, \quad \text{and} \quad \frac{dT_1}{d\eta}(1) \;=\; 1, \tag{6.34b}$$

releasing the $m = 0$ and $m = 1$ terms leads to the expression

$$a_1^{N+1}(\xi) \;=\; -\sum_{m=2}^{N+1} a_m^{N+1}(\xi)\frac{dT_m}{d\eta}(1), \quad \xi \in [-1, 1]. \tag{6.34c}$$

Introducing the relations in Eqs. (6.33) and (6.34c) into the approximate series expansion described in Eq. (6.30) yields

$$\begin{aligned}\Theta_{N+1}(\eta, \xi) \;=\; & f(\xi) + \left[\sum_{m=2}^{N+1} a_m^{N+1}(\xi)\frac{T_m}{d\eta}(1)\right](1-\eta) \\ & + \sum_{m=2}^{N+1} a_m^{N+1}(\xi)T_m(1) - \sum_{m=2}^{N+1} a_m^{N+1}, \quad (\eta, \xi) \in [-1, 1],\end{aligned} \tag{6.35}$$

or in the more compact form

$$\theta_N(\eta, \xi) \;=\; f(\xi) + \sum_{m=1}^{N} c_m^N(\xi)\Psi_m(\eta), \quad (\eta, \xi) \in [-1, 1], \tag{6.36a}$$

where $\theta_N(\eta, \xi) = \Theta_{N+1}(\eta, \xi)$, and $c_m^N(\xi) = a_{m+1}^{N+1}(\xi)$, with

$$\Psi_m(\eta) \;=\; T_{m+1}(\eta) + (1-\eta)\frac{dT_{m+1}}{d\eta}(1) - 1, \quad m = 1, 2, \ldots, N. \tag{6.36b}$$

As with the spatial approximation, it is possible to express the time-varying expansion coefficients in terms of a finite series such that

$$c_m^N(\xi) \;=\; \sum_{n=0}^{P_m} b_n^m T_n(\xi), \quad m = 1, 2, \ldots, N, \tag{6.37}$$

where Chebyshev polynomials of the first kind are chosen for the basis set. Substitution of Eq. (6.37) into Eq. (6.36a) produces

$$\theta(\eta,\xi) \;\approx\; \theta_N(\eta,\xi) \;=\; f(\xi) + \sum_{m=1}^{N}\sum_{n=0}^{P_N} b_n^m T_n(\xi)\Psi_m(\eta), \quad (\eta,\xi) \in [-1,1]. \tag{6.38}$$

At this point, the initial condition found in Eq. (6.7f) is incorporated into the approximate expansion for $\theta_N(\eta,\xi)$. Following the form of previous analytical manipulations, this incorporation provides

$$\theta(\eta,\xi) \;\approx\; \theta_N(\eta,\xi) \;=\; f(\xi) + \sum_{m=1}^{N}\sum_{n=1}^{P_N} b_n^m \left(T_n(\xi) + (-1)^{n+1}\right)\Psi_m(\eta),$$

$$(\eta,\xi) \in [-1,1]. \tag{6.39}$$

With this expansion, all known auxiliary conditions are exactly satisfied when continuity is maintained.

The set of unknown expansion coefficients b_n^m, $n = 1, 2, ..., P_N$; $m = 1, 2, ..., N$, is now determined via the Weighted Residuals Method of orthogonal collocation. Substitution of the approximation $\theta_N(\eta,\xi)$ into the governing equation found in Eq. (6.7a) produces the residual function $R_N(\theta_N(\eta,\xi))$ given by

$$R_N(\theta_N(\eta,\xi)) \;=\; L[\theta_N(\eta,\xi)], \quad (\eta,\xi) \in [-1,1], \tag{6.40}$$

where the heat equation operator is given in Eq. (6.7b). The collocation method is defined through the orthogonality statement

$$\langle R_N\left(\theta_N(\eta,\xi)\right), \delta(\eta-\eta_j,\xi-\xi_k)\rangle_1 \;=\; 0,$$

$$k=1,2,...,P_N; \quad j=1,2,...,N, \tag{6.41a}$$

where ξ_k, $k=1,2,...,P_N$ and η_j, $j=1,2,...,N$ are prescribed temporal and spatial collocation points, respectively and δ represents the Dirac delta function. The collocation points are explicitely stated by the open rules [106]

$$\eta_j \;=\; \cos\left(\frac{(2j-1)\pi}{2N}\right), \quad j=1,2,...,N, \tag{6.41b}$$

$$\xi_k \;=\; \cos\left(\frac{(2k-1)\pi}{2P_N}\right), \quad k=1,2,...,P_N. \tag{6.41c}$$

Substitution of Eq. (6.40) into Eq. (6.41a) where Eq. (6.39) is explicitly used in place of $\theta_N(\eta,\xi)$ yields

$$\sum_{m=1}^{N}\sum_{n=1}^{P_N} b_n^m L\left[\left(T_n(\xi_k)+(-1)^{n+1}\right)\Psi_m(\eta_j)\right] \;=\; -\,L\left[f(\xi_k)\right],$$

$$k=1,2,...,P_N; \quad j=1,2,...,N. \tag{6.42}$$

Equation (6.42) describes a system of linear algebraic equations for the unknown expansion coefficients $\{b_n^m\}$, $n=1,2,...,P_N$; $m=1,2,...,N$. Calculation of these coefficients allows the reconstruction of the approximate solution $\theta_N(\eta,\xi)$ through Eq. (6.39).

6.4 Solution Technique: Function Decomposition Method

6.4.1 Diagnostic Deduction

When resolving the described inverse heat conduction problem, it is generally desired to know both the temperature, $\theta(-1,\xi)$, and heat flux, $-2\frac{\partial\theta}{\partial\eta}(-1,\xi) = Q(\xi)$, at the control surface. The Function Decomposition Method accomplishes this task by recasting the original mathematical formulation into a series of direct problems. For the purpose of this methodology, it is necessary to formulate an expansion for the unknown boundary condition at the front wall ($\eta = -1$) which is constructed from a basis set having unknown expansion coefficients $\{a_j\}_{j=0}^{P}$. The form chosen for the front wall condition is termed the boundary variant, and there are a number of possible choices which hold physical meaning. The two boundary variants, γ which are discussed in the present context can be written in general terms as

$$B_\gamma[\theta(-1,\xi)] \;=\; a + \sum_{j=0}^{P} a_j \Phi_j(\xi), \quad \gamma = I, II, \quad \xi \in [-1,1], \tag{6.43a}$$

where $B_\gamma, \gamma = I, II$ is introduced as the boundary operator

$$B_I \;=\; 1, \quad B_{II} \;=\; \frac{\partial}{\partial\eta}, \tag{6.43b}$$

and "a" is an additional unknown constant. It can readily be seen from Eq. (6.43b) that the first kind boundary variant, B_I, specifies temperature at the front wall while the second kind, B_{II}, specifies the temperature gradient proportional to heat flux. The type of boundary variant chosen can be an important factor in the quality of problem resolution, especially in the presence of noisy data.

As with the boundary variants, several possible basis functions can be used in the expansion for the unknown boundary condition. This investigation utilizes a set of radially symmetric basis functions, that is, the Hardy multiquadric basis [105, 159, 160], which can be given by the expression

$$\Phi_j(\xi) \; = \; \sqrt{\beta_j + (\xi - \hat{\xi}_j)^2}, \quad j = 0, 1, ..., P. \tag{6.44a}$$

The points $\{\hat{\xi}_j\}_{j=0}^{P}$ in Eq. (6.44a) are called centers while the points $\{\beta_j\}_{j=0}^{P}$ are their corresponding shape parameters. In general, the centers may be located in many different patterns, however, good results are obtained from equidistant positioning so this study adopts the definition $\hat{\xi}_j = -1 + 2j/P$, $j = 0, 1, ..., P$. Likewise, for simplification, the shape parameters are assumed to be a constant for all centers, i.e., $\beta_j = \beta$, for $j = 0, 1, ..., P$. In order to assure uniform boundedness on the function expansion [160], it is necessary to impose the constraint

$$\sum_{j=0}^{P} a_j \; = \; 0. \tag{6.44b}$$

Using this additional constraint and requiring continuity to exist between the initial condition and the boundary at $\xi = -1$, the unknown boundary expansion becomes

$$B_\gamma[\theta(-1, \xi)] \; = \; \sum_{j=0}^{P} a_j \phi_j(\xi), \quad \gamma = I, II, \quad \xi \in [-1, 1], \tag{6.44c}$$

where

$$\begin{aligned} \phi_j(\xi) \; = & \sqrt{\beta + (\xi - \hat{\xi}_j)^2} - \sqrt{\beta + (-1 - \hat{\xi}_j)^2} + \sqrt{\beta} \\ & - \sqrt{\beta + (1 + \xi)^2}, \quad \xi \in [-1, 1], \quad j = 1, 2, ..., P. \end{aligned} \tag{6.44d}$$

The decomposition process is initiated by approximating the unknown temperature field, $\theta(\eta, \xi)$, as a linear combination of the baseline function, $\hat{z}(\eta, \xi)$, and the sensitivity functions, $z_n(\eta, \xi)$, that is,

$$\theta(\eta, \xi) \;\approx\; \theta^P(\eta, \xi) \;=\; \hat{z}(\eta, \xi) \;+\; \sum_{n=1}^{P} a_n z_n(\eta, \xi), \quad (\eta, \xi) \in [-1, 1]. \tag{6.45}$$

Equation (6.45) is valid regardless of the boundary variant used. Nevertheless, it should be noted that each boundary variant produces different baseline and sensitivity functions; therefore, the approximate solution will depend on the choice of γ.

The definition for $\theta^P(\eta, \xi)$ is now substituted into the heat equation described by Eq. (6.7a) as well as the boundary and initial conditions shown in Eqs. (6.7c), (6.7d), and (6.7f). Collecting terms containing common coefficients from the set $\{1, a_1, a_2, ..., a_P\}$ produces a system of uncoupled partial differential equations governing the baseline and sensitivity functions. Performing this procedure leads to the baseline system

$$\frac{\partial^2 \hat{z}}{\partial \eta^2}(\eta, \xi) \;=\; \frac{1}{4\lambda}\frac{\partial \hat{z}}{\partial \xi}(\eta, \xi), \quad (\eta, \xi) \in [-1, 1], \tag{6.46a}$$

subject to the boundary conditions

$$B_\gamma[\hat{z}(-1, \xi)] \;=\; 0, \quad \gamma = I, II, \tag{6.46b}$$

$$\frac{\partial \hat{z}}{\partial \eta}(1, \xi) \;=\; 0, \qquad \xi \in [-1, 1], \tag{6.46c}$$

and the initial condition

$$\hat{z}(\eta, -1) \;=\; 0, \quad \eta \in [-1, 1]. \tag{6.46d}$$

It can easily be seen that the system described in Eq. (6.46) results in the trivial solution $\hat{z}(\eta, \xi) = 0,\ (\eta, \xi) \in [-1, 1],\ \gamma = I, II$; thus, the baseline function need not be considered for this example.

In a similar fashion, the sensitivity system is

$$\frac{\partial^2 z_n}{\partial \eta^2}(\eta, \xi) \;=\; \frac{1}{4\lambda}\frac{\partial z_n}{\partial \xi}(\eta, \xi), \quad (\eta, \xi) \in [-1, 1], \quad n = 1, 2, ..., P, \tag{6.47a}$$

subject to the boundary conditions

$$B_\gamma[z_n(-1, \xi)] \;=\; \phi_n(\xi), \quad \gamma = I, II, \tag{6.47b}$$

$$\frac{\partial z_n}{\partial \eta}(1, \xi) = 0, \qquad \xi \in [-1, 1], \tag{6.47c}$$

and the initial condition

$$z_n(\eta, -1) \;=\; 0, \quad \eta \in [-1, 1], \quad n = 1, 2, ..., P. \tag{6.47d}$$

Equation (6.47) produces a series of direct, well-posed problems and so represents an improvement over the ill-posed governing statement defined in Eq. (6.7).

There are a number of exact and approximate techniques that can be used to solve the sensitivity system described in Eq. (6.47). In this case, the Weighted Residuals Method is employed to determine the approximate solutions for $\{z_n(\eta, \xi)\}_{n=1}^{P}$. The linear system of parabolic, partial differential equations is resolved by orthogonal collocation in both space and time. Initially, each sensitivity function is characterized as the infinite series expansion

$$z_n(\eta,\xi) \;=\; \sum_{m=0}^{\infty} a_{m,n}(\xi)T_m(\eta), \quad (\eta,\xi)\in[-1,1], \quad n=1,2,...,P, \tag{6.48}$$

where the general form of Eq. (6.48) is independent of the chosen boundary variant. The global spatial basis functions, $\{T_m(\eta)\}_{m=0}^{\infty}$, are defined as Chebyshev polynomials of the first kind [110]. As previously mentioned, this particular basis set possesses several advantageous computational attributes and has been used with considerable success to solve problems in the disciplines of fluid mechanics [137], solid mechanics [138], and radiative heat transfer [118, 161]. The infinite sets $\{a_{m,n}(\xi)\}$ in Eq. (6.48) denote the unknown time-varying expansion coefficients. For matters of practicality, it is necessary to truncate the infinite series expansion to a finite number of terms, say $N+2$, which produces the approximate representation

$$z_n(\eta,\xi) \;\approx\; Z_n^{N+1}(\eta,\xi) \;=\; \sum_{m=0}^{N+1} a_{m,n}^{N+1}(\xi)T_m(\eta), \quad (\eta,\xi)\in[-1,1], \quad n=1,2,...,P. \tag{6.49}$$

where $a_{m,n} \;\approx\; a_{m,n}^{N+1},\; m=0,1,...,N+1,\; n=1,2,...,P$, for sufficiently large N. At this point, a potential source of error in the numerical solution can be eliminated by incorporating the known boundary conditions given by Eqs. (6.47b) and (6.47c) into the expansion. By performing this procedure and letting $k=m-1$, Eq. (6.49) becomes

$$z_n(\eta,\xi) \;\approx\; z_n^N(\eta,\xi) \;=\; F_n^{\gamma}(\eta,\xi) \;+\; \sum_{k=1}^{N} b_{k,n}^N(\xi)\omega_k^{\gamma}(\eta),$$
$$(\eta,\xi)\in[-1,1], \quad n=1,2,...,P, \quad \gamma=I,II, \tag{6.50}$$

with $z_n^N(\eta,\xi) = Z_n^{N+1}(\eta,\xi)$ and $b_{k,n}^N(\xi) = a_{m,n}^{N+1}(\xi)$, $k = 1,2,...,N$, and where the spatial trial function $\omega_k^\gamma(\eta)$ and the function $F_n^\gamma(\eta,\xi)$ both depend on the chosen boundary variant γ. It can be shown that for the first kind boundary variant ($\gamma = I$), these functions are given by

$$\omega_k^I(\eta) \ = \ T_{k+1}(\eta) \ + \ (-1)^k \ - \ (\eta+1)T'_{k+1}(1), \quad k = 1,2,...,N, \tag{6.51a}$$

and

$$F_n^I(\eta,\xi) \ = \ \phi_n(\xi), \quad n = 1,2,...,P, \tag{6.51b}$$

where $\phi_n(\xi)$ is given in (6.44d). Likewise, the second kind boundary variant ($\gamma = II$) yields the functional relations

$$\omega_k^{II}(\eta) \ = \ \begin{cases} 1, & \text{if } k = 1; \\ \varpi_k(\eta) & \text{if } k = 2,3,...,N, \end{cases} \tag{6.52a}$$

where

$$\begin{aligned} \varpi_k(\eta) \ &= \ T_{k+1}(\eta) \ - \ \eta T'_{k+1}(1) \\ &\quad - \ \frac{T_2(\eta) \ - \ \eta T'_2(1)}{T'_2(-1) \ - \ T'_2(1)} \left(T'_{k+1}(-1) \ - \ T'_{k+1}(1)\right); \end{aligned} \tag{6.52b}$$

and

$$F_n^{II}(\eta,\xi) \ = \ \frac{T_2(\eta) \ - \ \eta T'_2(1)}{T'_2(-1) \ - \ T'_2(1)} \ \phi_n(\xi), \quad n = 1,2,...,P. \tag{6.52c}$$

Following the development of the spatial approximation, the time-varying coefficients $b_{k,n}^N(\xi)$ can be expanded in the form

$$b_{k,n}^N(\xi) \ = \ \sum_{j=0}^{P_N} b_{j,n}^k T_j(\xi), \quad \xi \in (-1,1), \tag{6.53}$$

where Chebyshev polynomials of the first kind have again been used as the basis set for the expansion. Substitution of Eq. (6.53) into Eq. (6.50) and incorporation of the known initial condition as given by Eq. (6.47d) leads to the expression

$$z_n(\eta,\xi) \;\approx\; z_n^N(\eta,\xi) \;=\; F_n^\gamma(\eta,\xi) \;+\; \sum_{k=1}^{N}\sum_{j=1}^{P_N} b_{j,n}^k \Omega_{j,k}^\gamma(\eta,\xi),$$

$$(\eta,\xi) \in [-1,1], \quad n = 1,2,...,P. \tag{6.54a}$$

The new space-time trial function $\Omega_{j,k}^\gamma(\eta,\xi)$ in Eq. (6.54a) is defined as

$$\Omega_{j,k}^\gamma(\eta,\xi) \;=\; \omega_k^\gamma(\eta)\left(T_j(\xi) \;+\; (-1)^{j+1}\right),$$

$$j = 1,2,...,P_N; \quad k = 1,2,...,N, \quad \gamma = I, II, \tag{6.54b}$$

and remains common to each sensitivity function $z_n^N(\eta,\xi)$. This attribute of the sensitivity functions is quite convenient, as will be seen shortly. The expansion coefficients $\{b_{j,n}^k\}$ can be accurately determined by application of the orthogonal collocation method.

The first step in the collocation method is the formation of the residual functions $R_N^n(z_n^N(\eta,\xi)),\ n = 1,2,...P$. These residuals are obtained by substituting the expansion for the sensitivity functions as given by Eq. (6.54a) into the governing partial differential equation given in Eq. (6.47a). Hence, the residual functions are specified by the relationship

$$R_N^n(z_n^N(\eta,\xi)) \;=\; L[z_n^N(\eta,\xi)], \quad n = 1,2,...,P, \quad \gamma = I, II, \tag{6.55}$$

where the differential operator L is defined by Eq. (6.7b). As a consequence of the approximate nature of the truncated series expansion, it is unlikely that the residual function $R_N^n(z_n^N(\eta,\xi))$ would vanish completely within the problem domain. However, suitable expansion coefficients can be obtained which minimize the residual function in some sense. The collocation method determines the expansion coefficients required for each sensitivity function by imposing the orthogonality condition

$$\begin{aligned} \left\langle R_N^n(z_n^N(\eta,\xi)), \delta(\xi-\xi_l, \eta-\eta_m)\right\rangle_1 &= 0, \\ l=1,2,...,P_N; \quad m=1,2,...,N, \quad n=1,2,...,P, \end{aligned} \tag{6.56a}$$

where the spatial and temporal collocation points are chosen according to the open rules [106]

$$\xi_l = \cos\left(\frac{(2l-1)\pi}{2P_N}\right), \quad l=1,2,...,P_N, \tag{6.56b}$$

$$\eta_m = \cos\left(\frac{(2m-1)\pi}{2N}\right), \quad m=1,2,...,N. \tag{6.56c}$$

Evaluation of the inner product in Eq. (6.56a) yields a system of linear equations for each set of expansion coefficients ($n=1,2,...,P$)

$$\begin{aligned} \sum_{k=1}^{N}\sum_{j=1}^{P_N} b_{j,n}^k L[\Omega_{j,k}^{\gamma}(\eta_m,\xi_l)] &= -L[F_n^{\gamma}(\eta_m,\xi_l)], \\ \gamma = I, II, \quad l=1,2,...,P_N; \quad m=1,2,...,N, &\quad n=1,2,...,P. \end{aligned} \tag{6.57}$$

Equation (6.57) produces a $N\times P_N$ linear system of equations for each n-set of expansion coefficients. The advantage of a common space-time trial function is now evident, since only one matrix inversion is required to resolve all n sets of expansion coefficients. As normally assumed, the sensitivity functions $\{z_n(\eta,\xi)\}_{n=1}^{P}$ are recovered in the limit; namely,

$$z_n(\eta,\xi) = \lim_{N\to\infty}\lim_{P_N\to\infty} z_n^N(\eta,\xi), \quad n = 1, 2, ..., P, \quad \gamma = I, II, \tag{6.58a}$$

where the approximate temperature is

$$\theta_N^P(\eta,\xi) = \sum_{n=1}^{P} a_{n,N} z_n^N(\eta,\xi), \quad \gamma = I, II, \tag{6.58b}$$

since $\hat{z}(\eta,\xi) = 0$. Similarly, the theoretically exact temperature is recovered in the limit through

$$\begin{aligned}\theta^P(\eta,\xi) &= \lim_{N\to\infty}\lim_{P_N\to\infty} \theta_N^P(\eta,\xi) \\ &= \lim_{N\to\infty}\lim_{P_N\to\infty} \sum_{n=1}^{P} a_{n,N} z_n^N(\eta,\xi), \quad \gamma = I, II.\end{aligned} \tag{6.58c}$$

Up to this point in the formulation, the measured data described by the boundary condition in Eq. (6.7c) has not been used. Hence, it can be observed that while the development of the sensitivity functions is dependent upon the chosen boundary variant and basis set, it is independent of the input data. This characteristic gives the FDM flexibility to handle multiple sets or types of data with only a minimal amount of additional computational effort.

Having obtained the n-set expansion coefficients, the only remaining task is the approximation of the sensitivity coefficients $\{a_n\}_{n=1}^P$ or, more precisely $\{a_{n,N}\}_{n=1}^P$ where $a_{n,N} \approx a_n$ for sufficiently large P_N, N. The input data provided in Eq. (6.7c) is now employed by equating it with the evaluation of $\theta_N^P(\eta,\xi)$ at $\eta = 1$ as described in Eq. (6.58c)

$$\theta(1,\xi_i) \;=\; f_i \;\approx\; \theta_N^P(1,\xi_i) \;=\; \sum_{n=1}^{P} a_{n,N} z_n^N(1,\xi_i),$$

$$\xi \in [-1,1], \quad i = 1,2,...,M, \tag{6.59a}$$

or

$$R_N^B(\theta_N^P(1,\xi_i)) \;=\; \theta_N^P(1,\xi_i) \;-\; f_i \;=\; \sum_{n=1}^{P} a_{n,N} z_n^N(1,\xi_i) \;-\; f_i,$$

$$\xi \in [-1,1], \quad i = 1,2,...,M, \tag{6.59b}$$

where $R_N^B(\theta_N^P(1,\xi_i))$ is representative of a boundary residual function. As such, Eq. (6.59b) is suggestive of a boundary residual statement that appears in the Weighted Residuals Method, and so should be minimized by some manner. Because the input data are discrete, the FDM requires the implementation of the discrete least-squares method for determining the sensitivity coefficients. The total least-squares error for Eq. (6.59b) is given by

$$\begin{aligned} S_1\left(\{a_{n,N}\}_{n=1}^{P}\right) \;&=\; \sum_{i=1}^{M} \left(\theta(1,\xi_i) \;-\; f_i\right)^2 \\ &=\; \sum_{i=1}^{M} \left(\sum_{n=1}^{P} a_n^N z_n^N(1,\xi_i) \;-\; f_i\right)^2 . \end{aligned} \tag{6.60}$$

In accordance with the discrete least-squares method, the error $S_1\left(\{a_{n,N}\}_{n=1}^{P}\right)$ in Eq. (6.60) is minimized with respect to each unknown sensitivity coefficient through the relation

$$\frac{\partial S_1\left(\{a_{n,N}\}_{n=1}^{P}\right)}{\partial a_{k,N}} \;=\; 0, \quad k = 1, 2, ..., P. \tag{6.61}$$

Applying Eq. (6.61) to the expression given in Eq. (6.60) generates a new system of linear equations for the sensitivity coefficients, which can be written as

$$\sum_{n=1}^{P} a_n^N \left(\sum_{i=1}^{M} z_n^N(1, \xi_i) z_k^N(1, \xi_i) \right) \;=\; \sum_{i=1}^{M} f_i z_k^N(1, \xi_i), \qquad k = 1, 2, ..., P. \tag{6.62}$$

Solving this system leads to an approximation for the sensitivity coefficients $\{a_n^N\}_{n=1}^{P}$ for fixed P_N, N. The sensitivity coefficients can then be used to reconstruct the temperature function $\theta_N^P(\eta, \xi)$.

6.4.2 Thermal Design

The development of the FDM for the thermal design problem is the same as that for the diagnostic deduction problem with the exception that the prescribed back boundary temperature function given by Eq. (6.7e) is incorporated into the approximation instead of discrete data. Thus, evaluating $\theta_N^P(\eta, \xi)$ at $\eta = 1$ as described in Eq. (6.58b) and equating this to the data provided in Eq. (6.7e) yields

$$\theta(1, \xi) \;=\; f(\xi) \;\approx\; \theta_N^P(1, \xi) \;=\; \sum_{n=1}^{P} a_{n,N} z_n^N(1, \xi), \quad \xi \in [-1, 1], \tag{6.63a}$$

or

$$R_N^B(\theta_N^P(1, \xi)) \;=\; \theta_N^P(1, \xi) - f(\xi) \;=\; \sum_{n=1}^{P} a_{n,N} z_n^N(1, \xi) - f(\xi), \quad \xi \in [-1, 1], \tag{6.63b}$$

where $R_N^B(\theta_N^P(1,\xi))$ is representative of a boundary residual function. Equation (6.63b) is reminiscent of a boundary residual statement that appears in the Weighted Residuals Method. Again, the objective involves minimizing the boundary residual by some manner. As such, the methods of collocation, Galerkin, and continuous least-squares come to mind to accomplish this task. In the diagnostic deduction problem where discrete data are offered at this juncture, the FDM would require using the discrete least-squares method for determining the sensitivity coefficients. Following an analogous argument, the availability of continuous data suggests implementing a continuous least-squares approach for determining the sensitivity coefficients. This method is costly from the CPU point of view. Alternatively, it can be observed that the GTM only requires the use of collocation. Thus, it appears warranted to demonstrate that the collocation method can also be used to find $\{a_{n,N}\}_{n=1}^{P}$ where the set of centers $\{\hat{\xi}_n\}_{n=1}^{N}$ is used to define the collocation points.

Option A: Continuous Least-Squares

In a general weighted-residuals framework, the continuous least-squares for a provided boundary variant γ is expressible as

$$\left\langle \frac{\partial R_N^B(\theta_N^P(1,\xi))}{\partial a_{k,N}}, R_N^B(\theta_N^P(1,\xi)) \right\rangle_1 \;=\; 0, \quad k=1,2,...,P, \quad \gamma = I, II, \qquad (6.64\text{a})$$

where $R_N^B(\theta_N^P(1,\xi))$ is given in Eq. (6.63b). Substituting Eq. (6.63b) into Eq. (6.64a) and performing the indicated differentiation yields

$$\sum_{n=1}^{P} a_{n,N} \int_{\xi=-1}^{1} z_n^N(1,\xi) z_k^N(1,\xi) d\xi \;=\; \int_{\xi=-1}^{1} f(\xi) z_k^N(1,\xi) d\xi,$$

$$k=1,2,...,P, \quad \gamma = I, II. \quad (6.64\text{b})$$

Solving this system leads to the sensitivity coefficients $\{a_{n,N}\}_{n=1}^{P}$ for fixed P_N, N, γ as needed in reconstructing the temperature function $\theta_N^P(\eta, \xi)$.

Option B: Collocation

The collocation method can be defined in terms of a general weighted-residuals framework as

$$\left\langle R_N^B(\theta_N^P(1,\xi)), \delta(\xi - \hat{\xi}_l) \right\rangle_1 \;=\; 0, \quad l = 1, 2, ..., P, \tag{6.65a}$$

where $R_N^B(\theta_N^P(1,\xi))$ is given in Eq. (6.63b). Upon explicitly introducing the proper components into Eq. (6.65a), it is possible to obtain

$$\sum_{n=1}^{P} a_{n,N} z_n^N(1, \hat{\xi}_l) \;=\; f(\hat{\xi}_l), \quad l = 1, 2, ..., P, \tag{6.65b}$$

which upon solving determines the sensitivity coefficients $\{a_{n,N}\}_{n=1}^{P}$.

After determining the sensitivity coefficients $\{a_{n,N}\}_{n=1}^{P}$, reconstruction of the resolved solution $\theta_N^P(\eta, \xi)$ is available from Eq. (6.58c) for fixed P.

6.5 Numerical Results

In order to illustrate the numerical application of both the GTM and FDM to typical problems of diagnostic deduction and thermal design, the benchmark test case proposed by Beck *et al.* [4] is investigated. In this scenario, a flat plate is subjected to a triangular heat flux at its front surface $(x = 0, \eta = -1)$ and is insulated at the back wall $(x = 1, \eta = 1)$. Solved as a direct problem, the known flux history, $q(t)$, is substituted into Eq. (6.3) to obtain an analytic solution for temperature at both the front and back surfaces. When recast as an inverse problem, the temperature solution for the back wall can be used to generate "input data" for the diagnostic deduction problem or a prescribed condition for the thermal design problem, while the known flux history and analytic front surface temperature provide an exact solution for comparative purposes.

Utilizing the aforementioned procedure, input data sets corresponding to three exemplary test cases have been produced for the diagnostic deduction problem. The data for case (i) are generated without the addition of potential input noise and are considered errorless. This data set is shown in Fig. 6.2. The data generated for case (ii) contain moderate noise and that for case (iii) contain severe noise. These discrete data sets are shown in Figs. 6.3 and 6.4, respectively. All data are given in the mapped coordinate system, i.e., $\theta(1, \xi_i) = \theta_i$, and are composed of $M = 201$ equidistant samples in the domain $\xi \in [-1, 1]$. The random noise is introduced into each set through the relation

$$\theta_i \;=\; \theta_{exact}(1, \xi_i) \;+\; \sigma R(i) \max_{\xi \in [-1,1]} \mid \theta_{exact}(1, \xi) \mid, \tag{6.66}$$

where σ is a noise amplification parameter and $R(i)$ is a random number between [-1,1] as determined by a random number generator with a normal distribution. It can be seen from Eq. (6.66) that the errorless data represented in Fig. 6.2 can be acquired when $\sigma = 0$. In like fashion, the data with moderate noise in Fig. 6.3 and severe noise in Fig. 6.4 have been computed using $\sigma = 0.015$ and $\sigma = 0.025$, respectively.

Similarly, the prescribed temperature boundary condition, $f(\xi)$ at $\eta = -1$, for the thermal design problem is given by the continuous function shown in Fig. 6.5.

Employing the data corresponding to the three test cases, surface temperature and heat flux predictions were calculated using the GTM. These results are displayed in Figs. 6.6–6.11 and have been generated using an optimized algorithm written in ANSI

Standard Fortran. A Lahey Fortran95 Linux Pro compiler (version 6.2) was used to produce the binary code which has been executed on a Dell Inspiron 9100 laptop computer with an Intel 865PE chipset and 1024 MB of system memory. Because of its conceptual simplicity, the computational cost is low with each simulation requiring less than one second to complete.

Case (i) GTM predictions for surface temperature and heat flux are shown in Figs. 6.6 and 6.7, respectively. With exception of the end effect in the neighborhood of $\xi = 1$ ($t = t_{max}$), the GTM produces excellent results which closely match the exact solution when no data noise is present. Convergence has been accomplished with an eye toward minimizing the end effect; however, this effect is generally irrelevant from a physical standpoint since the choice of $t = t_{max}$ can be arbitrarily made. For example, experimental data can be collected beyond the time frame of interest such that any end effect would occur outside the range of the desired solution. Likewise, if the process being investigated is known to reach a steady-state condition, it is possible to impose the added constraint

$$\frac{\partial T}{\partial t}(x, t_{max}) \;=\; 0, \quad x \in [0, 1], \tag{6.67a}$$

or in the mapped coordinate formulation

$$\frac{\partial \theta}{\partial \xi}(\eta, 1) \;=\; 0, \quad \eta \in [-1, 1]. \tag{6.67b}$$

This additional constraint can be incorporated into the series expansion to promote stability and 'tie down' the solution at the endpoint.

Figures 6.8 and 6.9 illustrate converged GTM predictions of surface temperature and heat flux for case (ii) where the input data contains moderate noise. While the GTM is still able to match the exact solution with general success, the influence of noisy input data is evident, particularly at the endpoints. This influence is even more pronounced for case (iii) as illustrated in Figs. 6.10 and 6.11. In this case, the severe noise in the input data begins to dominate the solution and makes convergence difficult but not impossible to achieve. One noteworthy observation is that as data noise level increases, the number of temporal collocation points, P_m required for a converged result decreases. This trend makes sense when one considers that the number of expansion terms in the GTM approximation correspond to the frequency content retained in the predicted solution. Because diffusion is by nature a low frequency phenomenon, high frequency noise that appears in the data will tend to promote instability. Thus there will be a point when the addition of higher frequencies becomes counterproductive.

The predicted solutions generated by utilizing the FDM for the three test cases are presented in Figs. 6.12–6.23. In all cases, first and second kind boundary variants have been employed in the decomposition process. The results have been generated using an optimized algorithm written in ANSI Standard Fortran. As before, a Lahey Fortran95 Linux Pro compiler (version 6.2) was used to produce the binary code which has been executed on a Dell Inspiron 9100 laptop computer with an Intel 865PE chipset and 1024 MB of system memory. Each related numerical experiment was completed in less than one second. Like the GTM, the impressive speed demonstrated by the FDM provides a tangible display of its computational advantages.

Figures 6.12 and 6.13 show the predicted surface temperature at $\eta = -1$ based on use of the first kind and second kind boundary variants, respectively, for case (i). Both types of boundary variant yield exceptional results for discrete errorless input. In fact, the endpoint anomaly (near t_{max}) which commonly occurs in most techniques has been substantially reduced and, in the case of the second kind boundary variant, virtually eliminated. This accuracy is echoed in the estimation of surface heat flux depicted in

Figs. 6.14 and 6.15. It is clear that the chosen orthogonal polynomial basis sets are able to recover the triangular flux solution, even in the presence of three discontinuous derivatives. The endpoint anomaly for the first kind boundary variant (Fig. 6.14) has been slightly amplified by differentiation of the expansion but is still undetectable in the second kind boundary variant solution (Fig. 6.15). Other than the endpoint effect, there is very little difference between solutions based on the two choices of boundary variant. It should be noted, however, that the higher boundary variant has been found to produce faster convergence in more complex, real problems. The boundary variant also affects the quality of the function estimations when noise is introduced into the input data, as will be seen presently. The results in Figs. 6.12–6.15 agree favorably with those obtained using more complicated regularization techniques [4].

Figures 6.16–6.19 illustrate the predicted surface temperature and heat flux, respectively, for case (ii) where a moderate amount of noise in the input data has been introduced. The effect of boundary variant choice, while not overwhelmingly obvious, is nevertheless present. Its manifestation is mainly in the necessity for the first kind boundary variant to utilize additional spatial collocation points to achieve similar output as that obtained from the second kind boundary variant. A comparison with the results for case (i) shows that, as expected, the scattering of data has a nominal impact on the function approximation. For the noise levels displayed in Fig. 6.3, this impact is felt mostly along the flat regions of the solution which is accentuated by a more prominent endpoint anomaly. In the region of interest, however, the quality of the temperature and heat flux estimations has remained high. This excellent level of accuracy is an indication of the ability of the FDM to stabilize an inherently ill-posed problem. Again, the solutions represented in Figs. 6.16–6.19 coincide robustly with analogous numerical experiments using other methodologies.

Finally, the predicted surface temperature and heat flux for case (iii) are presented in Figs. 6.20, 6.21 and 6.22, 6.23, respectively. Even though the input data are quite scattered (Fig. 6.4), the FDM is able to achieve an accurate resolution for both temperature and heat flux with only a moderate amount of fluctuation around the endpoints. The estimated functions produced using the second kind boundary variant (Figs. 6.21 and 6.23) are particularly impressive. These results also demonstrate a more substantial difference in solution quality with regards to the choice of boundary variant. In particular, a closer investigation of the predicted surface heat flux shows that the first kind boundary variant prediction is having difficulty maintaining the triangular form while that of the second kind boundary variant remains consistent. These observations underscore the importance and utility of the capability of the FDM to tailor a boundary trial function to conform with physical expectations.

With respect to the thermal design problem, representative results for the predicted surface temperature and heat flux at $\eta = -1$ as obtained using the Global Time and Function Decomposition Methods are illustrated in Figs. 6.24–6.29. Based on superior results for the second kind boundary variant, as seen above, FDM solutions are presented with this form only. It can be seen that both methods perform exceptionally well for the benchmark problem. The GTM is conceptually simpler than the FDM and can be applied to complex problems. Additionally, by exactly matching the "data" at $\eta = 1$, the GTM is capable of nearly replicating the projected values at $\eta = -1$ for the surface temperature and heat flux. Exceptions occur in the neighborhood of the temporal endpoint and locations where discontinuous derivatives exist. The FDM solutions indicate that good projections can also be accomplished by not exactly matching the "data" at $\eta = 1$ for $\xi \in [-1, 1]$ but rather by minimizing the boundary residual function displayed in Eq. (6.63b) in some sense. This concept is important in the actual implementation process. It should also be noted that the minimization processes used for this example (continuous least squares and orthogonal collocation) produced equally good results. As with the diagnostic deduction problem, the FDM permits the user to cast the boundary trial functions based on the particular nature of the physical problem.

Chapter 7

Conclusions and Recommendations

7.1 Summary

Two innovative and robust numerical approaches, the Global Time Method (GTM) and the Function Decomposition Method (FDM), have been developed and demonstrated for the resolution of direct and inverse problems of radiative and conductive heat transfer. These techniques are capable of rendering time and space in a global fashion thus resolving the temporal and spatial domains simultaneously. This process effectively treats time elliptically or as a fourth spatial dimension. A Weighted Residuals Method (WRM) is utilized in the mathematical formulation wherein the unknown function is approximated in terms of a finite series expansion. Regularization of the solution is achieved by retention of expansion terms as opposed to smoothing in the classical Tikhonov sense.

In order to demonstrate the merit and flexibility of these approaches, they have been applied to representative problems of direct and inverse heat transfer. First, the GTM has been applied to the case of transient, one-dimensional cooling in an absorbing medium bounded by black surfaces. The method is able to prove its effectiveness in handling the type of partial integro-differential equations found in radiative transport problems, even under conditions of stiffness. Second, the FDM was employed to resolve a complex parameter estimation problem found in Differential Scanning Calorimetry (DSC). In this case, the calculation of seven unknown variables and the resolution of eleven unknown parameters were required. The FDM was able to accomplish this task in the presence of noisy data with the adaptation of a two-part calibration scheme. Lastly, the GTM and FDM were both employed to resolve a one-dimensional inverse heat conduction problem (IHCP). Two cases were considered. The first was a diagnostic deduction problem for which discrete data are known at the over-specified boundary. The second was a thermal design problem for which a prescribed function was given as a condition at the over-specified boundary. Both methods provided good results with the FDM performing particularly well in the presence of noisy data. In all instances, the proposed techniques were computationally efficient.

7.2 Future Work

While the GTM and FDM have proven to be powerful methods for the resolution of direct and inverse problems alike, recent developments indicate avenues of advancement upon which future work should be based. One area which merits further study is the correction and/or filtering of input data, particularly as it relates to the heating rate dT/dt. The use of a classical least-squares framework to perform an *a posteriori* analysis of data streams to approximate local measurement errors and predict uncertainty is detailed by Frankel *et al.* [162]. These error estimates can be used to correct the data (in some sense) and produce accurate solutions both in the primitive function and its derivative. They can also be utilized to determine a stopping criterion with respect to the number of temporal expansion terms retained in the functional approximation as illustrated in [162, 163].

A great deal of promise can also be found in filtering the data stream employing a Discrete Fourier Transform (DFT) mechanism to determine an appropriate cut-off frequency and eliminate some noise from the data, as outlined by Frankel [164]. Removal of higher-frequency noise is accomplished via a low-pass, Gaussian digital filter based on the previously established cut-off frequency. This process not only produces better functional resolution but also usable time derivative information. These aforementioned data correction algorithms can be used within the context of the GTM and FDM to improve solution stability and accuracy or incorporated into other methods such as Analytic Continuation (i.e., Taylor series) [163, 164].

The potential for the application of additional constraints on the problem has already been mentioned in Chapter 6 but bears repeating. For instance, many experiments and practical thermal processes involve the transition from one steady-state condition to another. Examples include the experimental determination of properties like thermal diffusivity and quenching in which a heated material is plunged into a cooling bath until its temperature reaches ambient conditions. The second instance of steady state, i.e., $\partial T/\partial t = 0$ at t_{max} can readily be absorbed into the approximate series expansion representation utilized by global time techniques. The exploitation of this added constraint can help to stabilize the solution at the endpoint, particularly when there is excessive noise present in the data, by providing exactness at t_{max}. One can presume that when combined with the data filtering/correction algorithms described above, the added level of exactness will produce exceptional results.

Along with additional constraints, the adaptation of the proposed methodologies to include data streams from multiple probe locations is an extension which could be quite beneficial. In this case, the challenge is not the mere inclusion of more probe locations into the solution schemes but instead the development of a means of analysis to determine the best and most economical probe placement. Such an analysis in itself would be an inverse problem. Again, the aforementioned data filtering/correction algorithms could play an important role.

Another research topic of great interest is the utilization of flux and rate based data streams. The employment of both temperature and heat flux data as well as their rate based quantities is inherent to the concept of Analytic Continuation [163,164] as applied to the inverse heat conduction problem. However, these quantities, especially the instantaneous heating/cooling rate $\partial T/\partial t$, can also provide a stabilizing influence as input data for other methods of resolving thermal inverse problems. Frankel and Keyhani [165] present one of the first published accounts of this observation. It has been noted in Chapter 1 that the time-order of the differential equation gives valuable insight into the best form for data collection. At this point, a brief example involving an inverse heat conduction problem in the half-space will help to demonstrate that changing the data space can have a profound effect on the ill-posed nature of the problem.

Consider the example found in [163] which describes a linear, constant property heat equation problem developed in the half space. The governing equation can be given by

$$\frac{1}{\alpha}\frac{\partial T}{\partial t}(x,t) \;=\; \frac{\partial^2 T}{\partial x^2}(x,t), \quad x \geq 0, \quad t \geq 0, \tag{7.1a}$$

where $T(x,t)$ is the temperature profile, x is the spatial coordinate, t is the temporal coordinate, and $\alpha = k/(\rho C)$ is the thermal diffusivity. Here, k is the thermal conductivity, ρ is the density and C is the heat capacity. Equation (7.1a) is subject to the initial condition

$$T(x,0) \;=\; T_o, \quad x \geq 0. \tag{7.1b}$$

It can be assumed without loss of generality that $T_o = 0$. Also, no explicit boundary condition at $x = 0$ is currently specified. Furthermore, the conventional relationship between temperature and heat flux can be given by Fourier's law

$$q''(x,t) \;=\; -\,k\frac{\partial T}{\partial x}(x,t), \tag{7.1c}$$

which follows classical assumptions regarding parabolic heat conduction [7]. An equivalent integral equation for this system can be constructed based on a boundary element approach [166]. Development of this form (see [163] for more detail) and evaluation of the resulting integral equation at $x = 0$ yields

$$T(0,t) \;=\; \lambda \int_{t_0=0}^{t} \frac{q''(0,t_0)}{\sqrt{t-t_0}}\,dt_0, \quad t \geq 0, \tag{7.2}$$

where it is known from Eq. (7.1c) that $q''(0,t) = -k(\partial T/\partial x)(0,t)$. Furthermore, the parameter λ is defined as $\lambda = 1/\sqrt{k\rho C\pi}$.

Equation (7.2) represents an Abel integral equation [167, 168] for $q''(0,t)$. It can be readily inverted by a conventional approach (see [167] for details) provided some knowledge of $T(0,t)$. Inversion produces

$$q''(0,t) \;=\; \frac{1}{\lambda\pi} \int_{t_0=0}^{t} \frac{\partial T}{\partial t_0}(0,t_0)\frac{dt_0}{\sqrt{t-t_0}}, \quad t \geq 0. \tag{7.3}$$

It is evident from Eq. (7.3) that if temperature data $T(0,t)$ are collected, it will be necessary to differentiate them with respect to time in some fashion. If these data are discrete and noisy, numerical differentiation can prove to be problematic. It should be noted that integration by parts of Eq. (7.3) neither removes nor deters the true nature of the problem [163].

Contemplation of this issue leads to the conclusion that a change in the data space could improve solution stability. In other words, if one could measure $\partial T/\partial t(0, t)$ with reasonable accuracy either actively or passively, the difficulties associated with differentiating discrete and noisy data would disappear and solution stability would be considerably improved. Frankel and his colleagues [163, 165, 169–172] have advanced this line of thinking. Recently, Frankel *et al.* [172] proposed a novel approach for a sensor that indirectly measures dT/dt by relating voltage rate to heating rate. The potential also exists for the design of sensors utilizing materials which are sensitive to heating rates and subsequently possess a property with a known dependency. For example, pyroelectric materials respond to small changes in temperature [173] and could be adapted for use in heating rate sensors. Under any circumstance, both the GTM and FDM can easily be modified to exploit alternative types of input data.

Finally, adaptation of the proposed global methods to real-time or near real-time analysis is a subject which should be considered. Issues such as health management in hostile thermal environments require indepth sensors which must be able to provide timely feedback and control. A computationally efficient technique like the GTM can provide an excellent platform for resolving inverse problems of this type, particularly when combined with near real-time data filtering algorithms.

7.3 Conclusions

As more applications evolve that require operation in high temperature, high heat flux, or otherwise harsh thermal environments, the need for accurate and reliable thermal inverse analytical techniques will continue to grow. The methods proposed in this dissertation show great promise in meeting these challenges. Moreover, adaptation of the suggested future work can help to create even more powerful solution techniques.

Bibliography

Bibliography

[1] O. M. Alifanov, *Inverse Heat Transfer Problems.* New York: Springer-Verlag, 1994.

[2] J. Hadamard, *Lectures on Cauchy's Problem in Linear Differential Equations.* New Haven, CT: Yale University Press, 1923.

[3] A. N. Tikhonov and V. Y. Arsenin, *Solutions of Ill-Posed Problems.* Washington, DC: Winston and Sons, 1977.

[4] J. V. Beck, B. Blackwell, and C. R. St. Clair, Jr., *Inverse Heat Conduction.* New York: John Wiley and Sons Inc., 1985.

[5] J. V. Beck and A. K. J., *Parameter Estimation in Engineering and Science.* New York: John Wiley and Sons Inc., 1977.

[6] M. N. Ozisik and H. R. B. Orlande, *Inverse Heat Transfer: Fundamentals and Applications.* New York: Taylor and Francis, 2000.

[7] M. N. Ozisik, *Heat Conduction.* New York: John Wiley and Sons Inc., 1993.

[8] J. I. Frankel, "Course notes for Engineering Science 681: Advanced Topics in Engineering Mechanics," Fall 1997.

[9] J. Baumeister, *Stable Solution of Inverse Problems.* Germany: Friedr. Vieweg and Sons, 1987.

[10] K. Kurpisz and A. J. Nowak, *Inverse Thermal Problems.* Southampton, UK: Computational Mechanics Publications, 1995.

[11] H. W. Engl, M. Hanke, and A. Neubauer, *Regularization of Inverse Problems.* Dordrecht: Kluwer Academic Publishers, 2000.

[12] A. N. Tikhonov, "Solution of incorrectly formulated problems and the regularization method," *Soviet Math. Dokl.*, vol. 4, no. 4, pp. 1035–1038, 1963.

[13] A. N. Tikhonov, "Regularization of incorrectly posed problems," *Soviet Math. Dokl.*, vol. 4, no. 6, pp. 1624–1627, 1963.

[14] A. N. Tikhonov, "On the regularization of ill-posed problems," *Lectures of Academy of Sciences USSR*, vol. 153, pp. 49–52, 1963. in Russian.

[15] A. N. Tikhonov, "On stability of inverse problems," *Lectures of Academy of Sciences USSR*, vol. 39, pp. 195–198, 1943. in Russian.

[16] V. A. Morozov, *Methods for Solving Incorrectly Posed Problems.* New York: Springer, 1984.

[17] P. C. Hansen and P. O'Leary, "The use of the L-curve in the regularization of discrete ill-posed problems," tech. rep., Danish Computing Center for Research and Education, Technical University of Denmark, DK-2800 Lyngby, Denmark, 1991. Technical Report UNI*C, UMIACS-TR-91-142.

[18] P. C. Hansen, "Analysis of discrete ill-posed problems by means of the L-curve," *SIAM Review*, vol. 34, no. 4, pp. 561–580, 1992.

[19] K. Levenberg, "A method for the solution of certain non-linear problems in least squares," *Quarterly of Applied Mathematics*, vol. 2, pp. 164–168, 1944.

[20] D. W. Marquardt, "An algorithm for least squares estimation of nonlinear parameters," *SIAM Journal on Applied Mathematics*, vol. 11, pp. 431–441, 1963.

[21] Y. B. Bard, *Nonlinear Parameter Estimation*. New York: Academic Press, 1974.

[22] W. H. Press, B. P. Flannery, S. A. Teukolsky, and W. T. Vetterling, *Numerical Recipes*. Cambridge University Press, 1987.

[23] J. W. Daniel, *The Approximate Minimization of Functionals*. Englewood Cliffs: Prentice Hall, 1971.

[24] O. M. Alifanov, "Determination of heat loads from a solution of the nonlinear inverse problem," *High Temperature*, vol. 15, pp. 498–504, 1977.

[25] C. W. Groetsch, *Inverse Problems in the Mathematical Sciences*. Braunschweig: Vieweg, 1993.

[26] Plato, *The Republic*. London: Penguin, 2003. Translated with an introduction by Desmond Lee.

[27] W. H. Giedt, "The determination of transient temperatures and heat transfer in a gas-metal interface applied to a 40-mm gun barrel," *Jet Propulsion*, vol. 25, pp. 158–162, 1955.

[28] N. V. Shumakov, "A method for the experimental study of the process of heating a solid body," *Soviet Physics – Technical Physics*, vol. 2, p. 771, 1957. Translated by the American Institute of Physics.

[29] G. Stolz, "Numerical solutions to an inverse problem of heat conduction for simple shapes," *Journal of Heat Transfer*, vol. 82, no. 1, pp. 20–26, 1960.

[30] J. V. Beck, "Surface heat flux determination using an integral method," *Nuclear Engineering and Design*, vol. 7, pp. 170–178, 1968.

[31] J. V. Beck, "Calculation of a surface heat flux from an internal temperature history." ASME Paper, 62-HT-46, 1970.

[32] J. V. Beck and H. Wolf, "The nonlinear inverse heat conduction problem." ASME Paper, 65-HT-40, 1970.

[33] J. V. Beck, "Nonlinear estimation applied to the nonlinear heat conduction problem," *International Journal of Heat and Mass Transfer*, vol. 13, pp. 703–716, 1970.

[34] A. N. Tikhonov, "Inverse problems in heat conduction," *Journal of Engineering Physics*, vol. 29, no. 1, pp. 816–820, 1975.

[35] J. V. Beck, "Criteria for comparison of methods of solution of the inverse heat conduction problem," *Nuclear Engineering and Design*, vol. 53, pp. 11–22, 1979.

[36] L. Elden, "Numerical solution of the sideways heat equation," in *Inverse Problems in Diffusion Processes: Proceedings of the GAMM-SIAM Symposium*, (Lake St. Wolfgang in the Austrian Alps), June 27–July 1 1994.

[37] P. K. Lamm, "A survey of regularization methods for first-kind Volterra equations," in *Surveys on Solution Methods for Inverse Problems* (D. Colton, ed.), pp. 53–82, Vienna: Springer, 2000.

[38] N. S. Mera, L. Elliott, D. B. Ingham, and D. Lesnic, "A comparison of different regularization methods for a Cauchy problem in anisotropic heat conduction,"

International Journal of Numerical Methods for Heat and Fluid Flow, vol. 13, no. 5, pp. 528–546, 2003.

[39] D. Murio, *The Mollification Method and the Numerical Solution of Ill-Posed Problems*. New York: John Wiley and Sons Inc., 1993.

[40] D. M. Trujillo and H. R. Busby, *Practical Inverse Analysis in Engineering*. New York: CRC Press, 1997.

[41] G. M. Wing, *A Primer on Integral Equations of the First Kind*. Philadelphia, PA: SIAM, 1991.

[42] A. M. Osman and J. V. Beck, "Nonlinear inverse problem for the estimation of time-and-space dependent heat transfer coefficients," *Journal of Thermophysics and Heat Transfer*, vol. 3, no. 2, pp. 146–152, 1989.

[43] A. M. Osman and J. V. Beck, "Investigation of transient heat transfer coefficients in quenching experiments," *Journal of Heat Transfer*, vol. 112, pp. 843–848, 1990.

[44] J. V. Beck, B. Blackwell, and A. Haji-Sheikh, "Comparison of some inverse heat conduction methods using experimental data," *International Journal of Heat and Mass Transfer*, vol. 39, pp. 3649–3657, 1996.

[45] A. M. Osman, K. J. Dowding, and J. V. Beck, "Numerical solution of the general two-dimensional inverse heat conduction problem," *Journal of Heat Transfer*, vol. 119, pp. 38–45, 1997.

[46] G. Blanc, J. V. Beck, and M. Raynaud, "Solution of the inverse heat conduction problem with a time-variable number of future temperatures," *Numerical Heat Transfer, Part B*, vol. 32, pp. 437–451, 1997.

[47] S. M. Lin, C. K. Chen, and Y. T. Yang, "A modified sequential approach for solving inverse heat conduction problems," *International Journal of Heat and Mass Transfer*, vol. 47, pp. 2669–2680, 2004.

[48] A. Behbahani-nia and F. Kowsary, "A dual reciprocity BE-based sequential function specification solution method for inverse heat conduction problems," *International Journal of Heat and Mass Transfer*, vol. 47, pp. 1247–1255, 2004.

[49] X. Ling, H. P. Cherukuri, and M. F. Horstemeyer, "A hybrid regularization method for inverse heat conduction problems," *International Journal for Numerical Methods in Engineering*, vol. 65, pp. 2246–2264, 2006.

[50] M. T. Nair, "On Morozov's method for Tikhonov regularization as an optimal yielding algorithm," *Journal for Analysis and its Applications*, vol. 18, no. 1, pp. 37–46, 1999.

[51] W. B. Muniz, F. M. Ramos, and H. F. de Campos Velho, "Entropy- and Tikhonov-based regularization techniques applied to the backwards heat equation," *Computers and Mathematics with Applications*, vol. 40, no. 8, pp. 1071–1084, 2000.

[52] O. Scherzer, H. W. Engl, and K. Kunisch, "Optimal a posteriori parameter choice for Tikhonov regularization for solving nonlinear ill-posed problems," *SIAM Journal on Numerical Analysis*, vol. 30, no. 6, pp. 1796–1838, 1993.

[53] O. Scherzer, "The use of Morozov's discrepancy principle for Tikhonov regularization for solving nonlinear ill-posed problems," *Computing*, vol. 51, no. 1, pp. 45–60, 1993.

[54] J. Qi-nian, "Applications of the modified discrepancy principle to Tikhonov regularization of nonlinear ill-posed problems," *SIAM Journal on Numerical Analysis*, vol. 36, no. 2, pp. 475–490, 1999.

[55] S. Lu, S. V. Pereverzev, and R. Ramlan, "An analysis of Tikhonov regularization for nonlinear ill-posed problems under a general smoothness assumption," *Inverse Problems*, vol. 23, pp. 217–230, 2007.

[56] T. Reginska, "A regularization parameter in discrete ill-posed problems," *SIAM Journal on Scientific Computing*, vol. 17, no. 3, pp. 223–228, 1996.

[57] D. Lesnic, L. Elliott, D. B. Ingham, and A. Zeb, "The boundary element method for solving an inverse problem associated to the biharmonic equation," in *Third International Conference on Dynamic System Identification and Inverse Problems*, (Moscow, Russia), May 30 – June 5 1998.

[58] N. S. Mera, "The method of fundamental solutions for the backward heat conduction problem," *Inverse Problems in Science and Engineering*, vol. 13, no. 1, pp. 65–78, 2005.

[59] G. Rodriguez and D. Theis, "An algorithm for estimating the optimal regularization parameter by the L-curve," *Rendiconti di Matematica, Serie VII*, vol. 25, pp. 69–84, 2005.

[60] M. Belge, M. E. Kilmer, and E. L. Miller, "Efficient determination of multiple regularization parameters in a generalized L-curve framework," *Inverse Problems*, vol. 18, pp. 1161–1183, 2002.

[61] C. R. Vogel, "Non-convergence of the L-curve regularization parameter selection method," *Inverse Problems*, vol. 12, pp. 535–547, 1996.

[62] M. Hansen, "Limitations of the L-curve method in ill-posed problems," *BIT Numerical Mathematics*, vol. 36, no. 2, pp. 287–301, 1996.

[63] G. Wahba, "A survey of some smoothing problems and the method of general cross-validation for solving them," in *Applications of Statistics* (P. R. Krishnaiah, ed.), pp. 507 – 524, Amsterdam, The Netherlands: North-Holland, 1977.

[64] Y. Jarny, M. N. Ozisik, and J. P. Bardon, "A general optimization method using adjoint equation for solving multidimensional inverse heat conduction," *International Journal of Heat and Mass Transfer*, vol. 34, pp. 2911–2919, 1991.

[65] H. J. Reinhardt and J. Frohne, "On multidimensional inverse heat conduction problems," in *International Conference on Inverse and Ill-Posed Problems of Mathematical Physics*, (Novosibirsk, Russia), August 20–25 2007.

[66] Y. K. Hong and S. W. Baek, "Inverse analysis for estimating the unsteady inlet temperature distribution for two-phase laminar flow in a channel," *International Journal of Heat and Mass Transfer*, vol. 49, pp. 1137–1147, 2006.

[67] D. N. Hao, "A noncharacteristic Cauchy problem for linear parabolic equations II: a variational method," *Numerical Functional Analysis and Optimization*, vol. 13, pp. 541–564, 1992.

[68] C. H. Huang, M. N. Ozisik, and B. Sawaf, "Conjugate gradient method for determining unknown contact conductance during metal casting," *International Journal of Heat and Mass Transfer*, vol. 35, no. 7, pp. 1779–1786, 1992.

[69] M. Prud'homme and T. H. Nguyen, "Fourier analysis of conjugate gradient method applied to inverse heat conduction problems," *International Journal of Heat and Mass Transfer*, vol. 42, pp. 4447–4460, 1999.

[70] V. A. B. Narayanan and N. Zabaras, "Stochastic inverse heat conduction using a spectral approach," *International Journal for Numerical Methods in Engineering*, vol. 60, no. 9, pp. 1569–1593, 2004.

[71] A. S. Carasso, "Determining surface temperatures from interior observations," *SIAM Journal on Applied Mathematics*, vol. 42, no. 3, pp. 558–574, 1982.

[72] A. S. Carasso, "Space marching difference schemes in the nonlinear inverse heat conduction problem," *Inverse Problems*, vol. 8, pp. 25–43, 1992.

[73] A. S. Carasso, "Slowly divergent space marching schemes in the inverse heat conduction problem," *Numerical Heat Transfer, Part B*, vol. 23, pp. 111–126, 1993.

[74] D. A. Murio, "The mollification method and the numerical solution of the inverse heat conduction problem by finite differences," *Computers and Mathematics with Applications*, vol. 17, no. 10, pp. 1385–1396, 1989.

[75] D. A. Murio and L. Guo, "Discrete stability analysis of the mollification method for numerical differentiation," *Computers and Mathematics with Applications*, vol. 19, no. 6, pp. 15–26, 1990.

[76] D. A. Murio and L. Guo, "A stable space marching finite differences algorithm for the inverse heat conduction problem with no initial filtering procedure," *Computers and Mathematics with Applications*, vol. 19, no. 10, pp. 35–50, 1990.

[77] D. A. Murio, Y. Liu, and H. Zheng, "Numerical experiments in multidimensional IHCP on bounded domains," in *Inverse Problems in Diffusion Processes: Proceedings of the GAMM-SIAM Symposium*, (Lake St. Wolfgang in the Austrian Alps), June 27–July 1 1994.

[78] D. A. Murio, “The mollification method and the numerical solution of an inverse heat conduction problem,” *SIAM Journal on Scientific and Statistical Computing*, vol. 2, pp. 17–34, 1981.

[79] D. A. Murio, “Parameter selection by discrete mollification and the numerical solution of the inverse heat conduction problems,” *Journal of Computational and Applied Mathematics*, vol. 22, no. 1, pp. 25–34, 1988.

[80] B. Sawaf, M. N. Ozisik, and Y. Jarny, “An inverse analysis to estimate linearly temperature dependent thermal conductivity components and heat capacity of an orthotropic medium,” *International Journal of Heat and Mass Transfer*, vol. 38, pp. 3005–3010, 1995.

[81] L. Vozar and T. Sramkova, “Two data reduction methods for evaluation of thermal diffusivity from step-heating measurements,” *International Journal of Heat and Mass Transfer*, vol. 40, pp. 1647–1655, 1997.

[82] L. B. Dantas, H. R. B. Orlande, and R. M. Cotta, “An inverse problem of parameter estimation for heat and mass transfer in capillary porous media,” *International Journal of Heat and Mass Transfer*, vol. 46, pp. 1587–1598, 2003.

[83] N. R. Ou and C. Y. Wu, “Simultaneous estimation of extinction coefficient distribution, scattering albedo and phase function of a two-dimensional medium,” *International Journal of Heat and Mass Transfer*, vol. 45, pp. 4663–4674, 2002.

[84] F. Murphy, T. Kehoe, M. Pietralla, R. Winfield, and L. Floyd, “Development of an algorithm to extract thermal diffusivity for the radial converging wave technique,” *International Journal of Heat and Mass Transfer*, vol. 48, pp. 1395–1402, 2005.

[85] T. Feng, P. Edstrom, and M. Gulliksson, "Levenberg-Marquardt methods for parameter estimation problems in the radiative transfer equation," *Inverse Problems*, vol. 23, pp. 879–891, 2007.

[86] C. E. Siewert, "A new approach to the inverse problem," *Journal of Mathematical Physics*, vol. 19, no. 12, pp. 2619–2621, 1978.

[87] C. E. Siewert, "An inverse source problem in radiative transfer," *Journal of Quantitative Spectroscopy and Radiative Transfer*, vol. 50, no. 6, pp. 603–609, 1993.

[88] C. E. Siewert, "A radiative-transfer inverse-source problem for a sphere," *Journal of Quantitative Spectroscopy and Radiative Transfer*, vol. 52, no. 2, pp. 157–160, 1994.

[89] H. Y. Li and M. N. Ozisik, "Estimation of the radiation source term with a conjugate-gradient method of inverse analysis," *Journal of Quantitative Spectroscopy and Radiative Transfer*, vol. 48, no. 3, pp. 237–244, 1992.

[90] S. Subramaniam and M. P. Menguc, "Solution of the inverse radiation problem for inhomogeneous and anisotropically scattering media using a Monte Carlo technique," *International Journal of Heat and Mass Transfer*, vol. 34, pp. 253–266, 1991.

[91] H. M. Park and W. J. Lee, "An inverse radiation problem of simultaneous estimation of heat transfer coefficient and absorption coefficient in participating media," *International Journal for Numerical Methods in Engineering*, vol. 56, pp. 787–807, 2003.

[92] K. W. Kim and S. W. Baek, "Inverse radiation-conduction design problem in a participating concentric cylindrical medium," *International Journal of Heat and Mass Transfer*, vol. 50, pp. 2828–2837, 2007.

[93] W. Kurz and D. J. Fisher, *Fundamentals of Solidification.* Switzerland: Trans. Tech. Publication, 1984.

[94] N. Zabaras, S. Mukherjee, and O. Richmond, "An analysis of inverse heat transfer problems with phase changes using an integral method," *Journal of Heat Transfer*, vol. 110, no. 3, pp. 554–561, 1988.

[95] N. Zabaras and Y. Ruan, "A deforming finite element method analysis of inverse stefan problems," *International Journal for Numerical Methods in Engineering*, vol. 28, pp. 295–313, 1989.

[96] N. Zabaras, "Inverse finite element techniques for the analysis of solidification processes," *International Journal for Numerical Methods in Engineering*, vol. 29, pp. 1569–1587, 1990.

[97] N. Zabaras, Y. Ruan, and O. Richmond, "Design of two-dimensional Stefan processes with desired freezing front motions," *Numerical Heat Transfer, Part B*, vol. 21, pp. 307–325, 1992.

[98] N. Zabaras and S. Kang, "On the solution of an ill–posed design solidification problem using minimization techniques in finite– and infinite–dimensional function spaces," *International Journal for Numerical Methods in Engineering*, vol. 36, pp. 3973–3990, 1993.

[99] N. Zabaras and T. H. Nguyen, "Control of the freezing interface morphology in solidification process in the presence of natural convection," *International Journal for Numerical Methods in Engineering*, vol. 38, pp. 1555–1578, 1995.

[100] G. Z. Yang and N. Zabaras, “An adjoint method for the inverse design of solidification processes with natural convection,” *International Journal for Numerical Methods in Engineering*, vol. 42, pp. 1121–1144, 1998.

[101] S. W. Hale, M. Keyhani, and J. I. Frankel, “Design and control of interfacial temperature gradients in solidification,” *International Journal of Heat and Mass Transfer*, vol. 43, pp. 3795–3810, 2000.

[102] J. I. Frankel and M. Keyhani, “A new approach for solving inverse solidification design problems,” *Numerical Heat Transfer, Part B*, vol. 30, no. 2, pp. 161–177, 1996.

[103] B. A. Finlayson, *The Method of Weighted Residuals and Variational Principles*. New York: Academic Press, 1972.

[104] M. D. Greenberg, *Foundations of Applied Mathematics*. New Jersey: Prentice Hall, 1978.

[105] M. A. Golberg and C. S. Chen, *Discrete Projection Methods for Integral Equations*. Southampton, UK: Computational Mechanics Publications, 1997.

[106] L. M. Delves and J. L. Mohammad, *Computational Methods for Integral Equations*. Cambridge, UK: Cambridge University Press, 1988.

[107] J. P. Boyd, *Chebyshev and Fourier Spectral Methods*. Dover Publications, Inc., 2nd ed., 1999.

[108] F. W. Byron, Jr. and R. W. Fuller, *Mathematics of Classical and Quantum Physics*. Dover Publications, Inc., 1st ed., 1992.

[109] T. J. Rivlin, *The Chebyshev Polynomials*. New York: John Wiley and Sons Inc., 2nd ed., 1974.

[110] D. Gottlieb and S. A. Orszag, *Numerical Analysis of Spectral Methods*. Philadelphia, PA: SIAM, 1977.

[111] L. C. Andrews, *Special Functions for Engineers and Applied Mathematicians*. New York: Macmillan Publishing Company, 1985.

[112] L. Fox and I. B. Parker, *Chebyshev Polynomials in Numerical Analysis*. Oxford, UK: Oxford University Press, 1968.

[113] G. E. Osborne, J. I. Frankel, and M. Keyhani, "The Function Decomposition Method and its application in thermal inverse analysis," in *International Mechanical Engineering Congress and Exhibition*, (Anaheim, California), November 15–20 1998.

[114] G. Dahlquist, A. Bjorck, and N. Anderson, *Numerical Methods*. Prentice Hall, 1st ed., 1974.

[115] K. K. Prasad and R. G. Hering, "Numerical integration of a nonlinear, singular integro–partial differential equation," *Journal of Computational Physics*, vol. 6, pp. 406–416, 1970.

[116] K. K. Prasad and R. G. Hering, "Transient radiative heat transfer in a plane layer," *International Journal of Heat and Mass Transfer*, vol. 12, pp. 1331–1337, 1969.

[117] J. I. Frankel, "A new orthogonal collocation integral formulation to transient radiative transport," in *Boundary Element Technology IX*, (Southampton: Computational Mechanics Publications), 1994.

[118] J. I. Frankel, "Cumulative variable formulation for transient conductive and radiative transport in participating media," *Journal of Thermophysics and Heat Transfer*, vol. 9, no. 2, pp. 210–218, 1995.

[119] J. I. Frankel, "Implicit solution method for a cumulative variable formulation to radiative/conductive transport," *Journal of Thermophysics and Heat Transfer*, vol. 9, no. 3, pp. 558–560, 1995.

[120] S. N. Tiwari, D. J. Singh, and A. Kumar, "Transient energy transfer by conduction and radiation in nongray gases," *Journal of Thermophysics and Heat Transfer*, vol. 3, no. 2, pp. 167–174, 1989.

[121] R. Siegel and J. R. Howell, *Thermal Radiation Heat Transfer*. Hemisphere Publishing Corporation, 3rd ed., 1992.

[122] R. Siegel, "Some aspects of transient cooling of a radiating rectangular medium," *International Journal of Heat and Mass Transfer*, vol. 32, no. 10, pp. 1955–1966, 1989.

[123] R. Siegel, "Transient cooling in a square region of radiating medium," *Journal of Thermophysics and Heat Transfer*, vol. 5, no. 4, pp. 495–501, 1991.

[124] R. Siegel and F. B. Molls, "Finite difference solution for transient radiative cooling of a conducting semitransparent square region," *International Journal of Heat and Mass Transfer*, vol. 35, no. 10, pp. 2579–2592, 1992.

[125] T. Saitoh, K. Yamazaki, and R. Viskanta, "Effect of thermal radiation on transient combustion of a fuel droplet," *Journal of Thermophysics and Heat Transfer*, vol. 7, no. 1, pp. 94–110, 1993.

[126] A. L. Crosbie and M. Pattabongse, "Transient conductive and radiative transfer in a planar layer with Arrhenius heat generation," *Journal of Quantitative Spectroscopy and Radiative Transfer*, vol. 37, no. 4, pp. 319–329, 1987.

[127] H. C. Kao, "An optically thin radiating gas jet," *ZAMP*, vol. 23, pp. 632–644, 1972.

[128] J. R. Thomas, "Coupled radiation/conduction heat transfer in ceramic liners for diesel engines," *Numerical Heat Transfer*, vol. 21, pp. 109–120, 1992.

[129] T. Tong, D. L. McElroy, and D. W. Yarbrough, "Transient conduction and radiation in porous thermal insulations," *Journal of Thermal Insulation*, vol. 9, pp. 13–19, 1985.

[130] S. Kumar and I. H. Sloan, "A new collocation–type method for Hammerstein integral equations," *Mathematics of Computation*, vol. 48, no. 178, pp. 585–593, 1987.

[131] H. Brunner, "On implicitly linear and iterated collocation methods for Hammerstein integral equations," *J. Integral Equations Applic.*, vol. 3, no. 4, pp. 475–488, 1991.

[132] H. Kaneko and Y. Xu, "Degenerate kernel method for Hammerstein equations," *Math. Comput.*, vol. 56, pp. 141–148, 1991.

[133] K. Atkinson and J. Flores, "The discrete collocation method for nonlinear integral equations," *IMA J. Numer. Anal.*, vol. 13, pp. 195–213, 1993.

[134] J. I. Frankel and S. R. Choudhury, "Some new observations on the classical logistic equation with heredity," *Applied Mathematics and Computation*, vol. 58, pp. 275–308, 1993.

[135] M. Abramowitz and I. A. Stegun, *Handbook of Mathematical Functions.* New York: Dover, 1972.

[136] J. I. Frankel, "A new integral formulation to thermal ignition in radiatively participating media," in *Boundary Element Technology XI*, (Hawaii), 1996.

[137] S. A. Orszag, "Accurate solution of the Orr-Sommerfeld stability equation," *Journal of Fluid Mechanics*, vol. 50, no. 4, pp. 689–703, 1971.

[138] A. C. Kaya and F. Erdogen, "On the solution of integral equations with strongly singular kernels," *Quarterly of Applied Mathematics*, vol. 45, no. 1, pp. 105–122, 1987.

[139] J. I. Frankel, "A Galerkin solution to a regularized Cauchy singular integro-differential equation," *Quarterly of Applied Mathematics*, vol. 53, no. 2, pp. 245–258, 1995.

[140] J. I. Frankel, "Residual-minimization least-squares method for inverse heat conduction," *Computers and Mathematics with Applications*, vol. 32, no. 4, pp. 117–130, 1996.

[141] M. A. Heaslet and R. F. Warming, "Radiative transport and wall temperature slip in an absorbing planar medium," *International Journal of Heat and Mass Transfer*, vol. 8, pp. 979–994, 1965.

[142] G. Hohne, W. Hemminger, and H.-J. Flammershein, *Differential Scanning Calorimetry.* Berlin: Springer, 1996.

[143] M. J. Richardson, "Application of differential scanning calorimetry to the measurement of specific heat," in *Compendium of Thermophysical Property Measurement Methods, Vol. I* (K. D. Maglic, A. Cezairliyan, and V. E. Peletsky, eds.), pp. 669 – 685, New York: Plenum Press, 1984.

[144] I. Moon, R. Androsch, and B. Wunderlich, "A calibration of the various heat-conduction paths for a heat-flux-type temperature-modulated DSC," *Thermochimica Acta*, vol. 357–358, pp. 285–291, 2000.

[145] S.-C. Jeng and S.-W. Chen, "The solidification characteristics of 6061 and A356 aluminum alloys and their ceramic particle-reinforced composites," *Acta Materialia*, vol. 45, no. 12, pp. 4887–4899, 1997.

[146] S.-W. Chen, C.-C. Huang, and J.-C. Lin, "The relationship between the peak shape of a DTA curve and the shape of a phase diagram," *Chemical Engineering Science*, vol. 50, no. 3, pp. 417–431, 1995.

[147] C.-C. Huang and Y.-P. Chen, "Measurements and model prediction of the solid-liquid equilibria of organic binary mixtures," *Chemical Engineering Science*, vol. 55, pp. 3175–3185, 2000.

[148] K. Ishikiriyama, A. Boller, and B. Wunderlich, "Melting of indium by temperature-modulated differential scanning calorimetry," *Journal of Thermal Analysis and Calorimetry*, vol. 50, pp. 553–10000, 1997.

[149] H. B. Dong and J. D. Hunt, "A numerical model of a two-pan heat flux DSC," *Journal of Thermal Analysis and Calorimetry*, vol. 64, pp. 167–176, 2001.

[150] R. Ciach, W. Kapturkiewicz, W. Wolczynski, and A. M. Zahra, "Computer simulation of thermal analysis in heat-flux DSC applied to metal solidification," *Journal of Thermal Analysis*, vol. 38, pp. 1949–1957, 1992.

[151] G. E. Osborne, J. I. Frankel, A. S. Sabau, and W. D. Porter, "Characterization of thermal lags and resistances in a heat-flux DSC," in *EPD Congress 2004*, (Charlotte, North Carolina), March 15–17 2004.

[152] G. E. Osborne, J. I. Frankel, and A. Sabau, "A new parameter estimation method for DSC thermodynamic property evaluation – Part I: analytic development," in *Twenty-Second IASTED International Conference on Modelling, Identification, and Control*, (Innsbruck, Austria), February 10–13 2003.

[153] G. E. Osborne, J. I. Frankel, and A. Sabau, "A new parameter estimation method for DSC thermodynamic property evaluation – Part II: Runge-Kutta implementation," in *Twenty-Second IASTED International Conference on Modelling, Identification, and Control*, (Innsbruck, Austria), February 10–13 2003.

[154] R. E. Bellman and R. E. Kalaba, *Quasilinearization and Nonlinear Boundary Value Problems*. New York: Elsevier, 1965.

[155] S. W. Hale, M. Keyhani, and J. I. Frankel, "Application of the Function Decomposition Method to the solidification design problem," in *International Mechanical Engineering Congress and Exhibition*, (Anaheim, California), November 15–20 1998.

[156] S. W. Hale, M. Keyhani, and J. I. Frankel, "Thermal design aspects in inverse heat conduction," in *Third International Conference on Dynamic System Identification and Inverse Problems*, (Moscow, Russia), May 30 – June 5 1998.

[157] J. I. Frankel and M. Keyhani, "A global time treatment for inverse heat conduction problems," *Journal of Heat Transfer*, vol. 119, no. 4, pp. 673–683, 1997.

[158] J. I. Frankel, "Direct least-squares solutions to integral equations containing discrete data," *Journal of Thermophysics and Heat Transfer*, vol. 10, pp. 181–186, 1996.

[159] R. L. Hardy, "Theory and applications of the multiquadric-biharmonic method," *Computers and Mathematics with Applications*, vol. 19, no. 8,9, pp. 163–208, 1990.

[160] M. D. Buhmann, "New developments in the theory of radial basis function interpolation," *Multivariate Approximation and Wavelets*, pp. 1–39, 1992.

[161] J. I. Frankel and G. E. Osborne, "A new time treatment for solving partial-integro differential equations of radiative transport," *IMA Journal of Numerical Analysis*, vol. 19, pp. 91–103, 1999.

[162] J. I. Frankel, M. Keyhani, and K. Taira, "In-phase error estimation of experimental data and optimal first derivatives," *AIAA Journal*, vol. 42, pp. 1017–1024, 2004.

[163] J. I. Frankel, G. E. Osborne, and K. Taira, "Stabilization of ill-posed problems through thermal rate sensors," *Journal of Thermophysics and Heat Transfer*, vol. 20, no. 2, pp. 238–246, 2006.

[164] J. I. Frankel, "Regularization of inverse heat conduction by combination of rate sensor analysis and analytic continuation," *Journal of Engineering Mathematics*, vol. 57, pp. 181–198, 2007.

[165] J. I. Frankel and M. Keyhani, "Inverse heat conduction: The need of $\partial t/\partial t$ data for design and diagnostic purposes," in *IASTED International Conference on Modelling, Identification, and Control*, (Innsbruck, Austria), February 1999.

[166] C. A. Brebbia, J. C. F. Telles, and L. C. Wrobel, *Boundary Element Techniques*. Berlin: Springer-Verlag, 1984.

[167] F. G. Tricomi, *Integral Equations*. New York: Dover Publications, Inc., 1985.

[168] P. Linz, *Analytical and Numerical Methods for Volterra Equations*. Philadelphia, PA: SIAM, 1985.

[169] J. I. Frankel and G. E. Osborne, "The development of heating/cooling rate dT/dt and heat flux rate dq″/dt sensors for aerospace applications," in *Propulsion Measurement Sensor Development Workshop, Paper 1.2.4*, (Huntsville, AL), NASA, May 2003.

[170] J. I. Frankel and G. E. Osborne, "The prediction of heating/cooling rates in material science investigations," in *Proceedings of the Fourth Conference on Quenching and the Control of Distortion*, (Beijing, PRC), Chinese Heat Treatment Society, November 2003.

[171] J. I. Frankel and G. E. Osborne, "Motivation for the development of heating/cooling rate dT/dt and heat flux rate dq″/dt sensors for engineering applications," in *42nd AIAA Aerospace Sciences Meeting and Exhibit*, (Reno, NV), January 5–8 2004.

[172] J. I. Frankel, R. V. Arimilli, M. Keyhani, and J. Wu, "Heating rate dT/dt measurements developed from in-situ thermocouples using a voltage-rate interface for advanced thermal diagnostics," in *25th AIAA Aerodynamic Measurement Technology and Ground Testing Conference*, (San Francisco, CA), June 5–9 2006.

[173] S. Bauer and S. B. Lang, "Pyroelectric polymer electrets," *IEEE Transactions on Dielectrics and Electrical Insulation*, vol. 3, no. 5, pp. 647–676, 1996.

Appendices

Appendix I

Figures

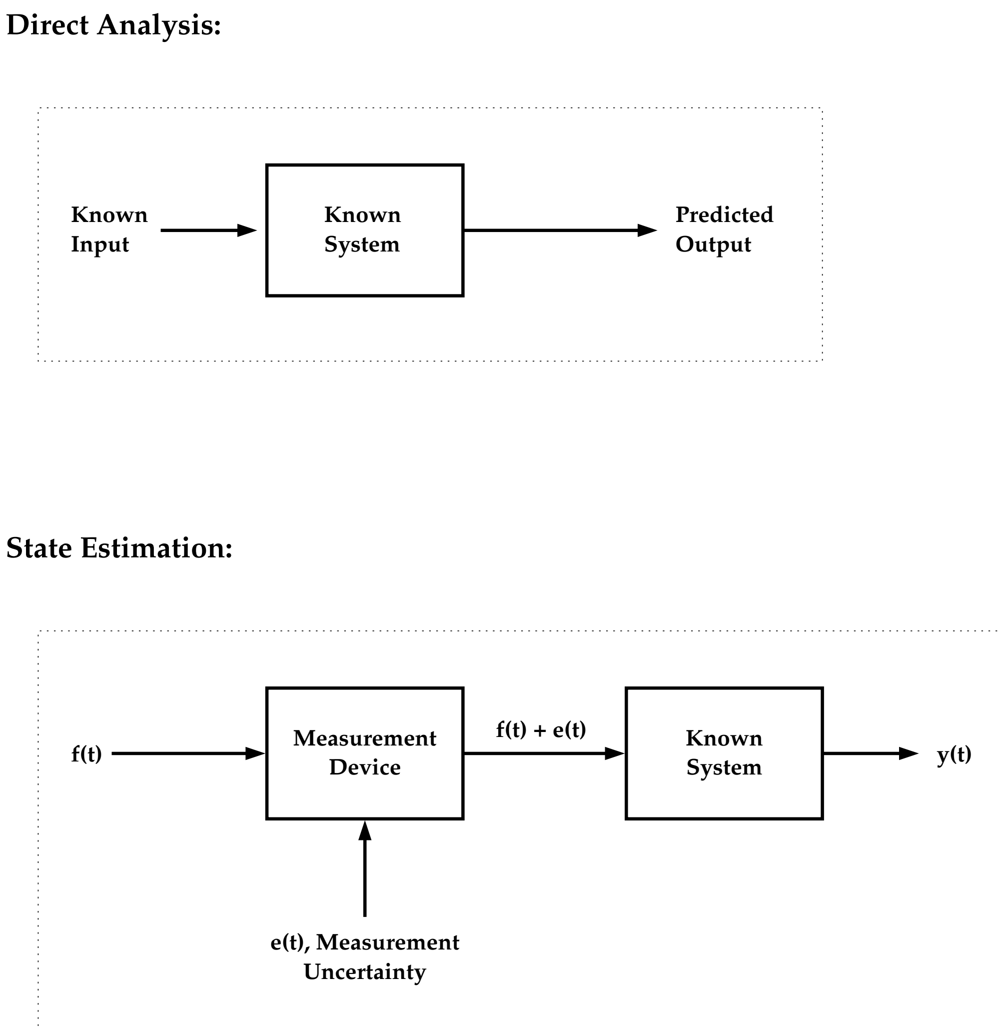

Figure 1.1: Schematic describing (a) direct analysis and (b) state estimation.

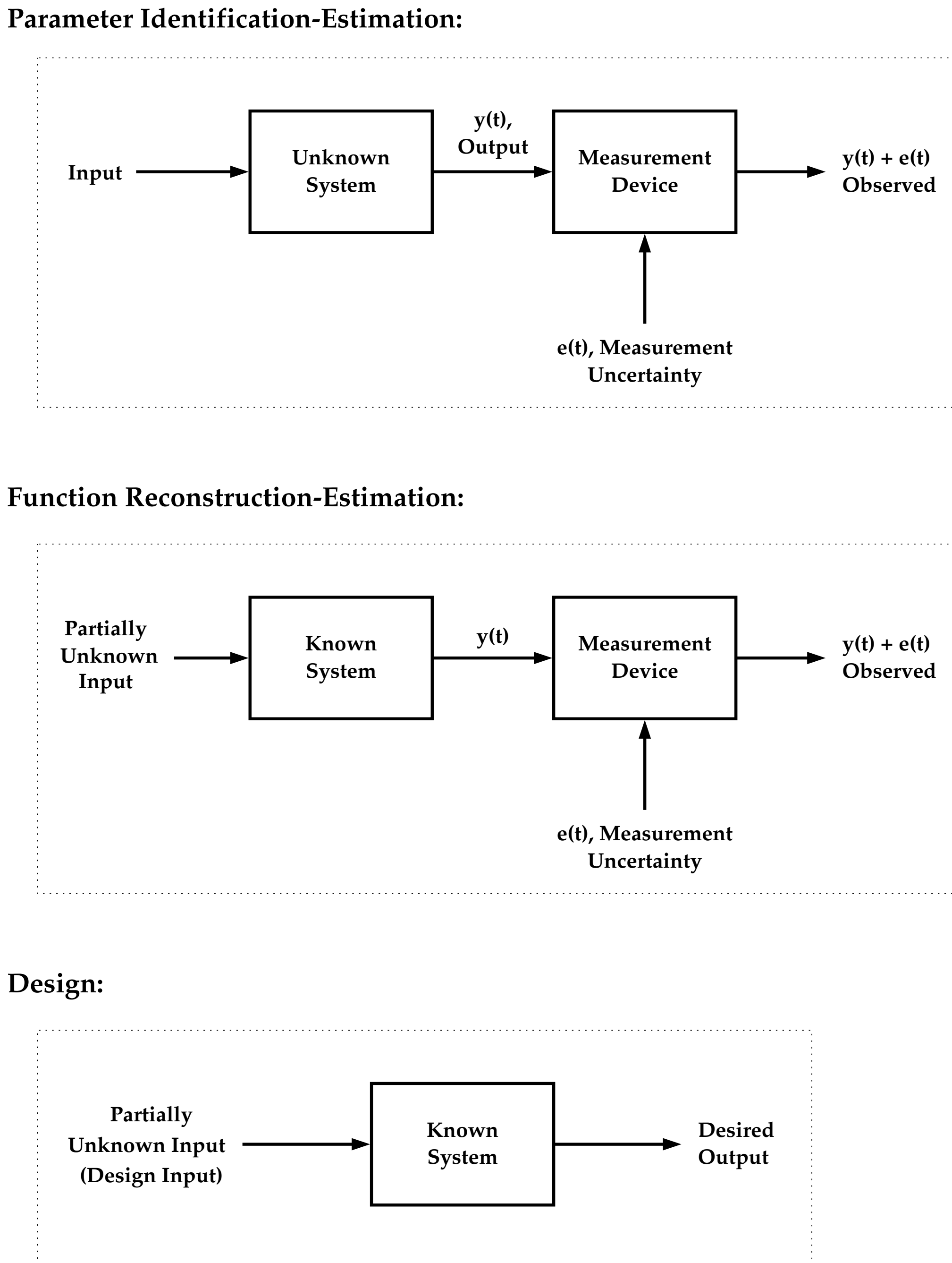

Figure 1.2: Schematic describing (a) parameter identification–estimation, (b) function reconstruction–estimation and (c) thermal design.

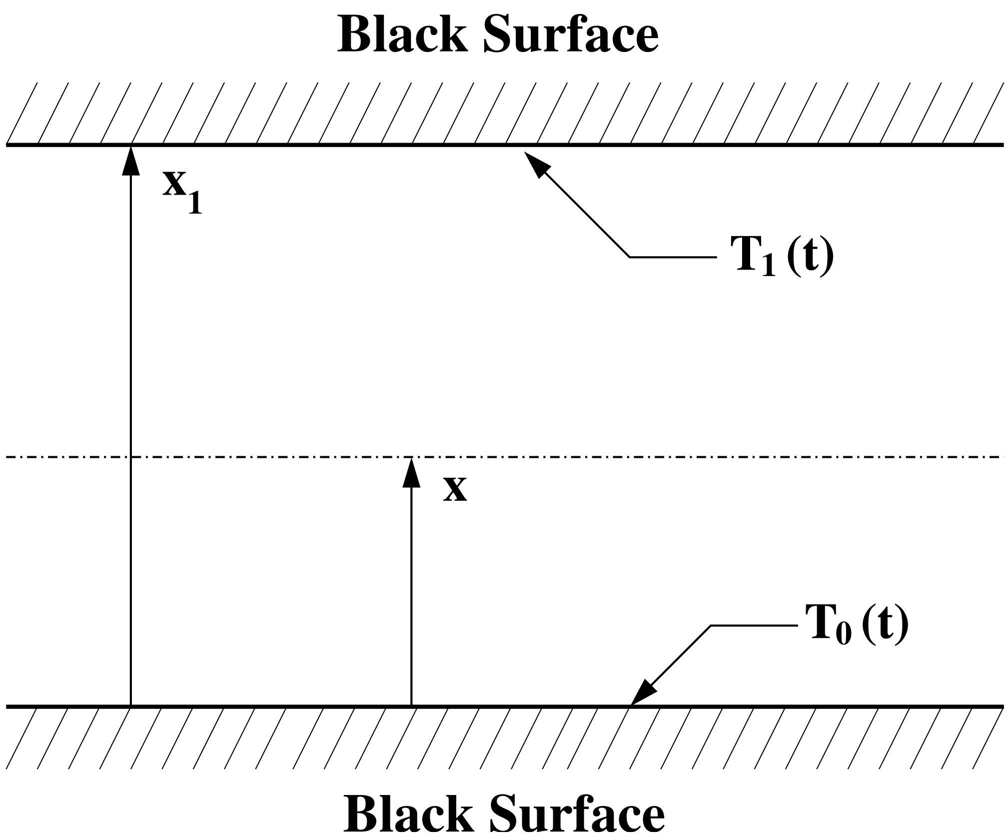

Figure 4.1: Planar absorbing radiating region bounded by black surfaces.

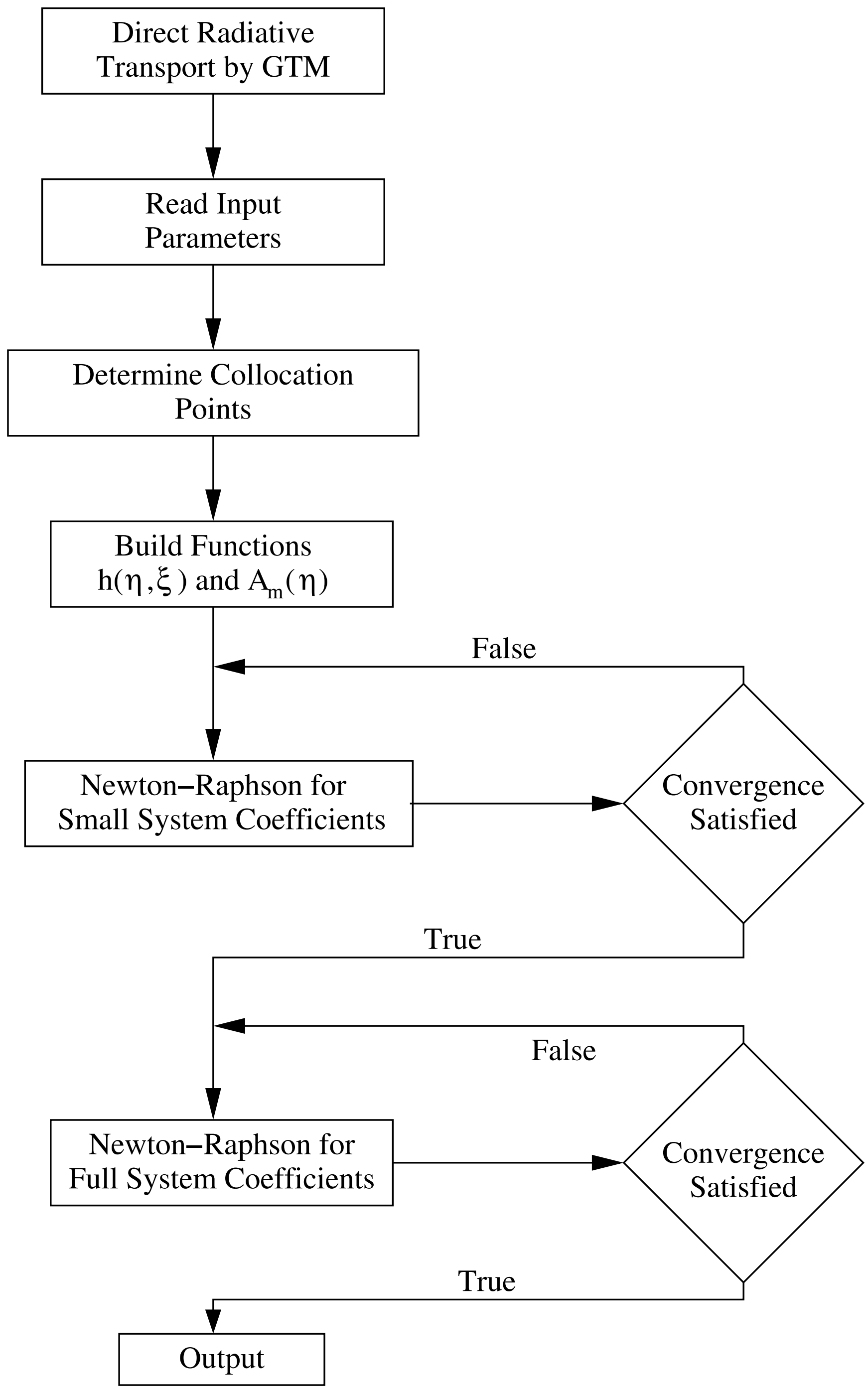

Figure 4.2: Basic flowchart for the GTM direct radiation problem algorithm.

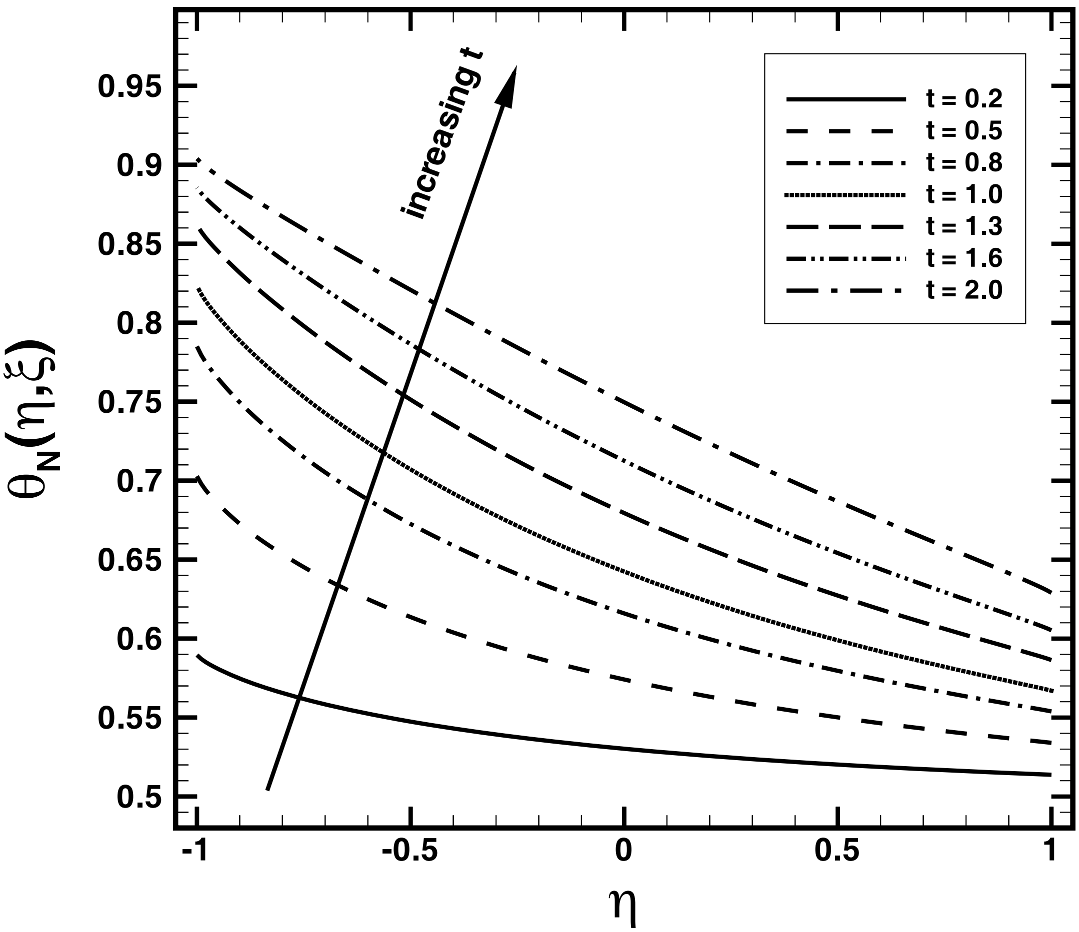

Figure 4.3: Spatial distributions for $\theta_N(\eta, \xi)$ corresponding to various times when $L = 1$, $\theta_1 = 0.5$, and $t_{max} = 2$, and with $N = 20$ and $P = 21$.

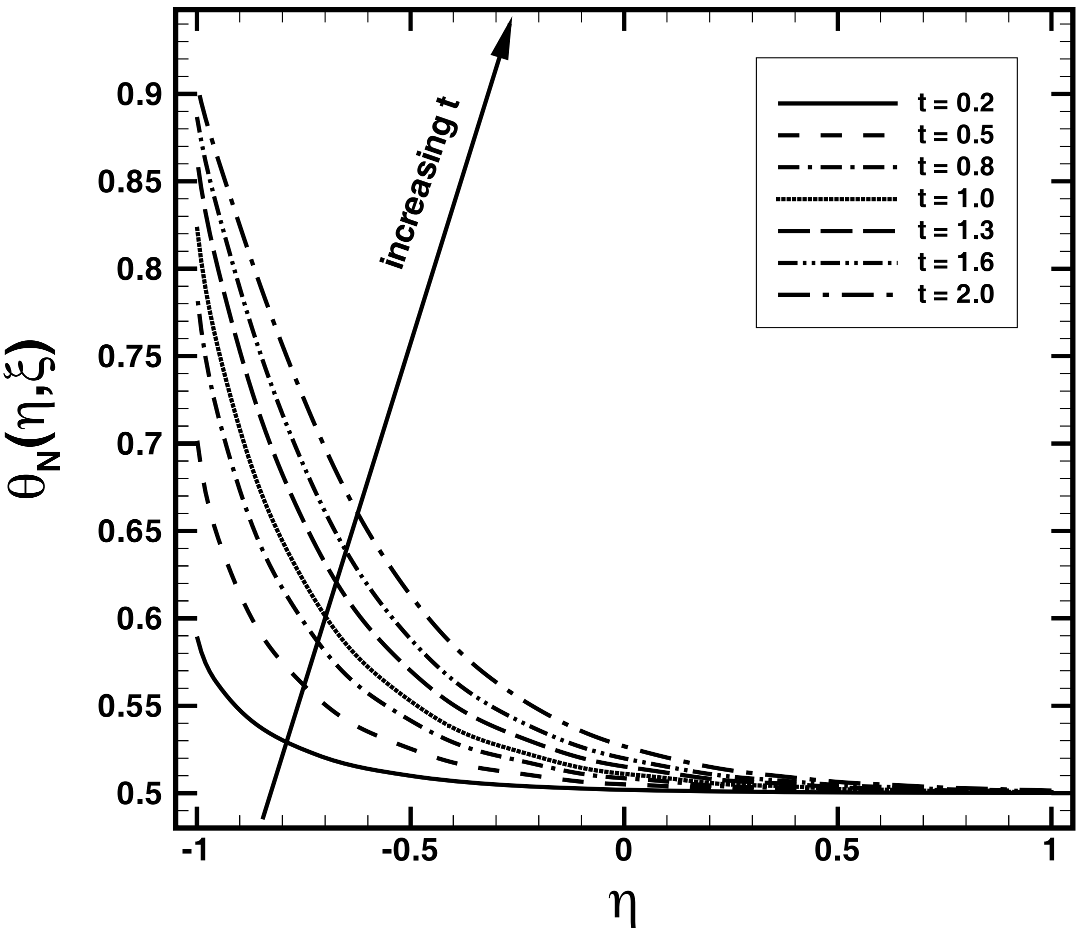

Figure 4.4: Spatial distributions for $\theta_N(\eta, \xi)$ corresponding to various times when $L = 5$, $\theta_1 = 0.5$, and $t_{max} = 2$, and with $N = 20$ and $P = 21$.

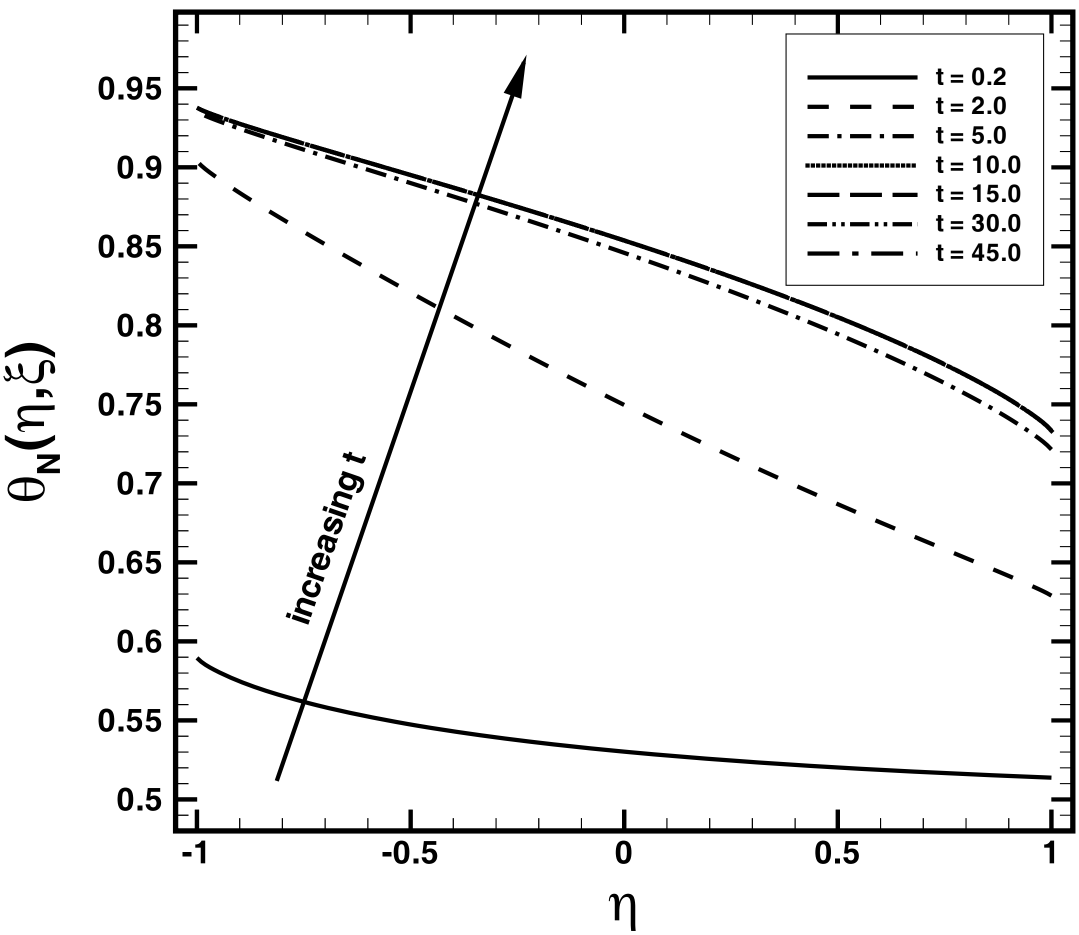

Figure 4.5: Spatial distributions for $\theta_N(\eta, \xi)$ corresponding to various times when $L = 1$, $\theta_1 = 0.5$, and $t_{max} = 45$, and with $N = 20$ and $P = 41$.

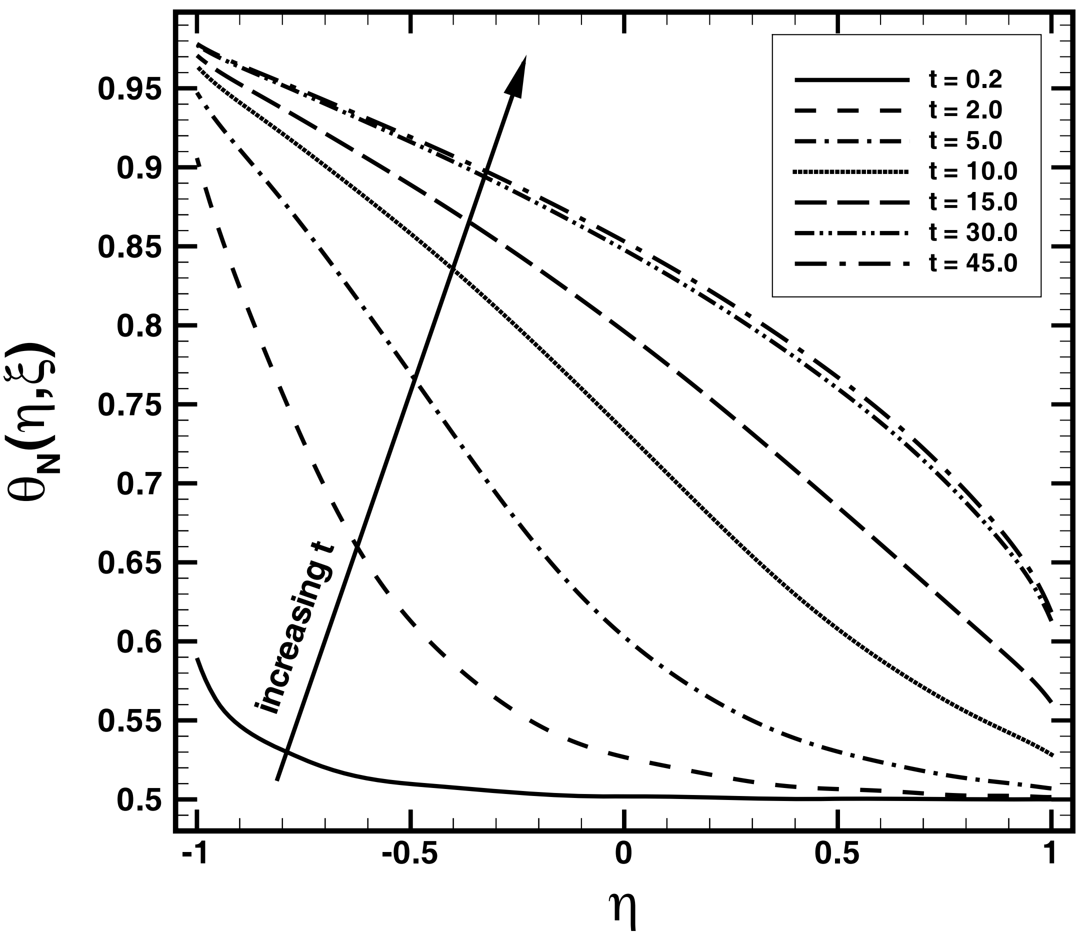

Figure 4.6: Spatial distributions for $\theta_N(\eta, \xi)$ corresponding to various times when $L = 5$, $\theta_1 = 0.5$, and $t_{max} = 45$, and with $N = 20$ and $P = 41$.

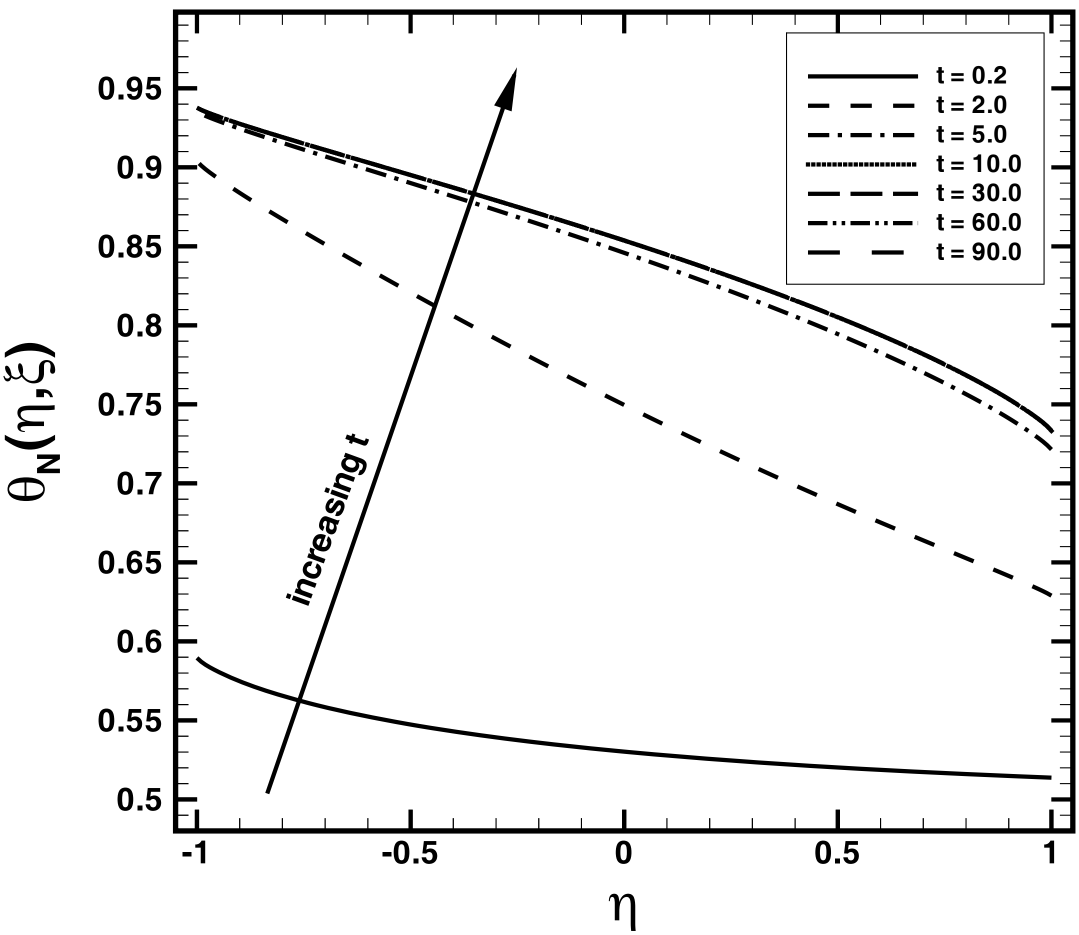

Figure 4.7: Spatial distributions for $\theta_N(\eta, \xi)$ corresponding to various times when $L = 1$, $\theta_1 = 0.5$, and $t_{max} = 90$, and with $N = 20$ and $P = 41$.

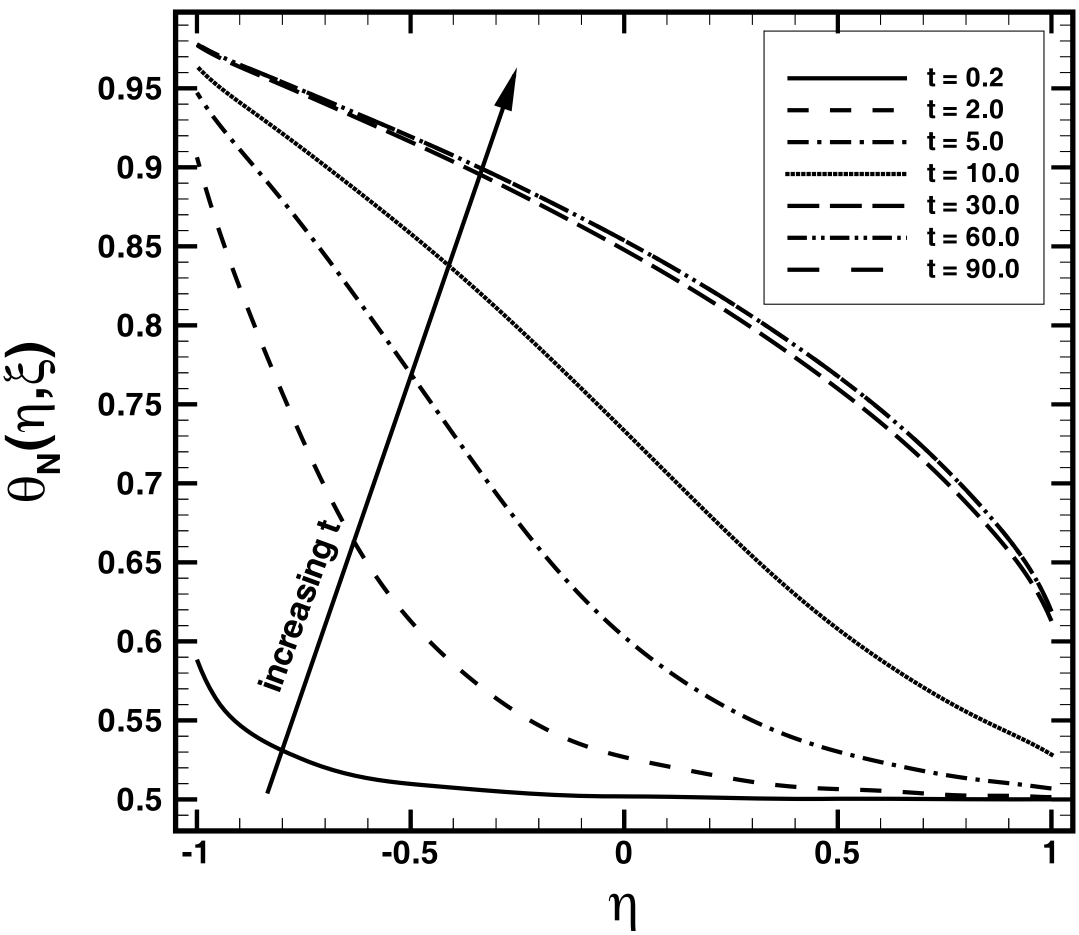

Figure 4.8: Spatial distributions for $\theta_N(\eta, \xi)$ corresponding to various times when $L = 5$, $\theta_1 = 0.5$, and $t_{max} = 90$, and with $N = 20$ and $P = 41$.

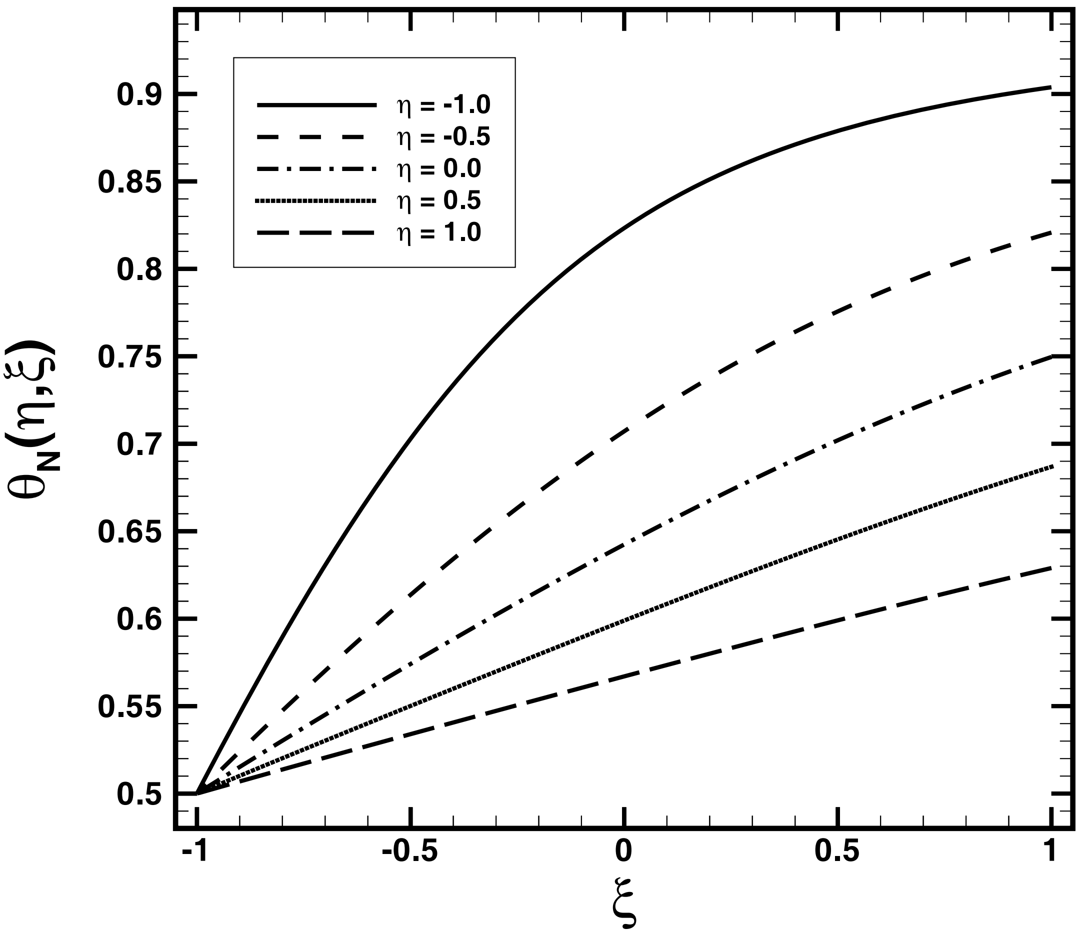

Figure 4.9: Temporal distributions for $\theta_N(\eta, \xi)$ corresponding to various locations when $L = 1$, $\theta_1 = 0.5$, and $t_{max} = 2$, and with $N = 20$ and $P = 21$.

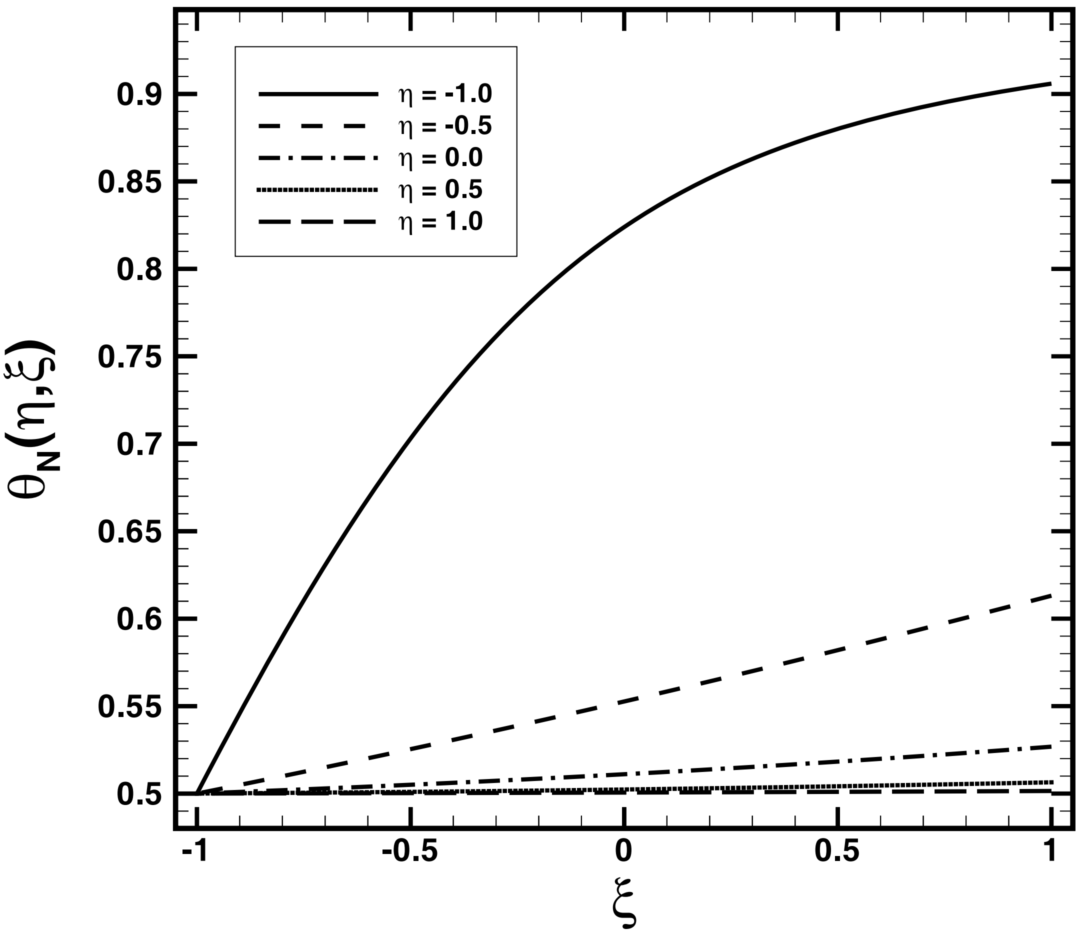

Figure 4.10: Temporal distributions for $\theta_N(\eta, \xi)$ corresponding to various locations when $L = 5$, $\theta_1 = 0.5$, and $t_{max} = 2$, and with $N = 20$ and $P = 21$.

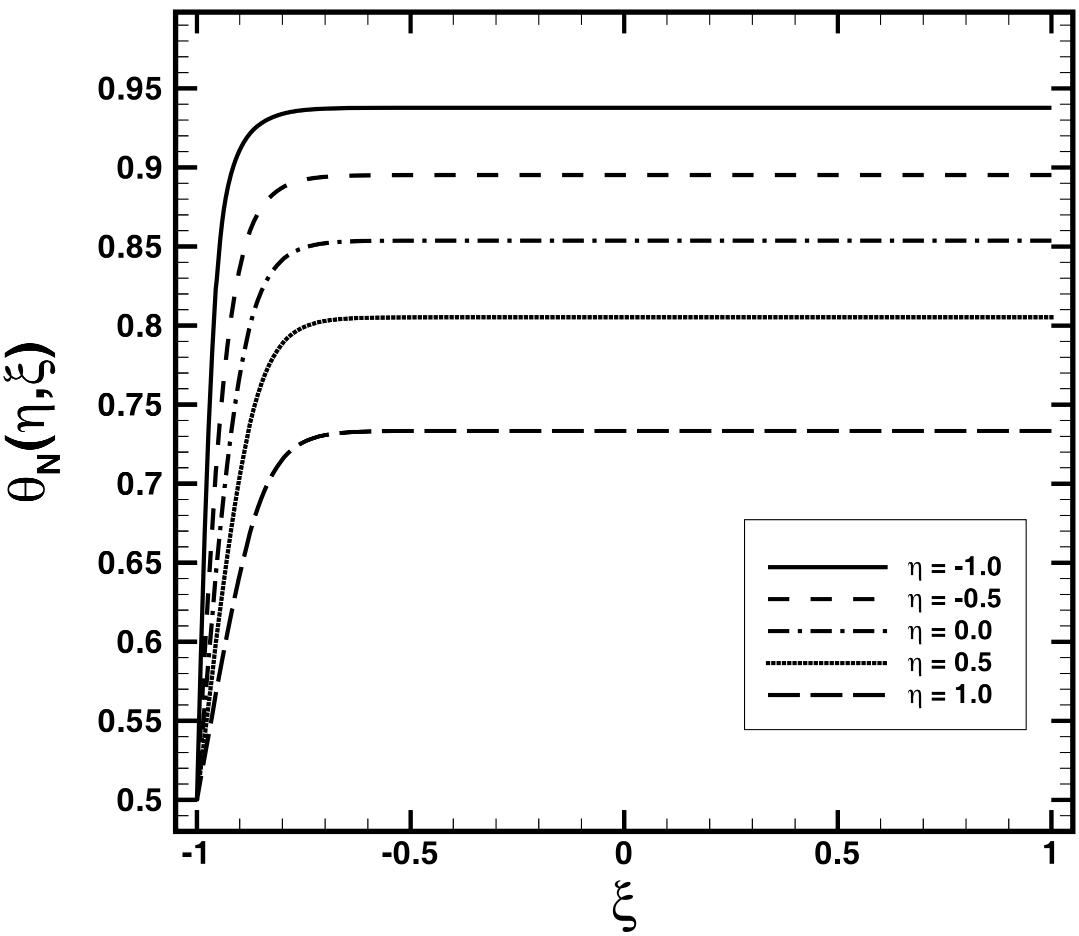

Figure 4.11: Temporal distributions for $\theta_N(\eta, \xi)$ corresponding to various locations when $L = 1$, $\theta_1 = 0.5$, and $t_{max} = 45$, and with $N = 20$ and $P = 41$.

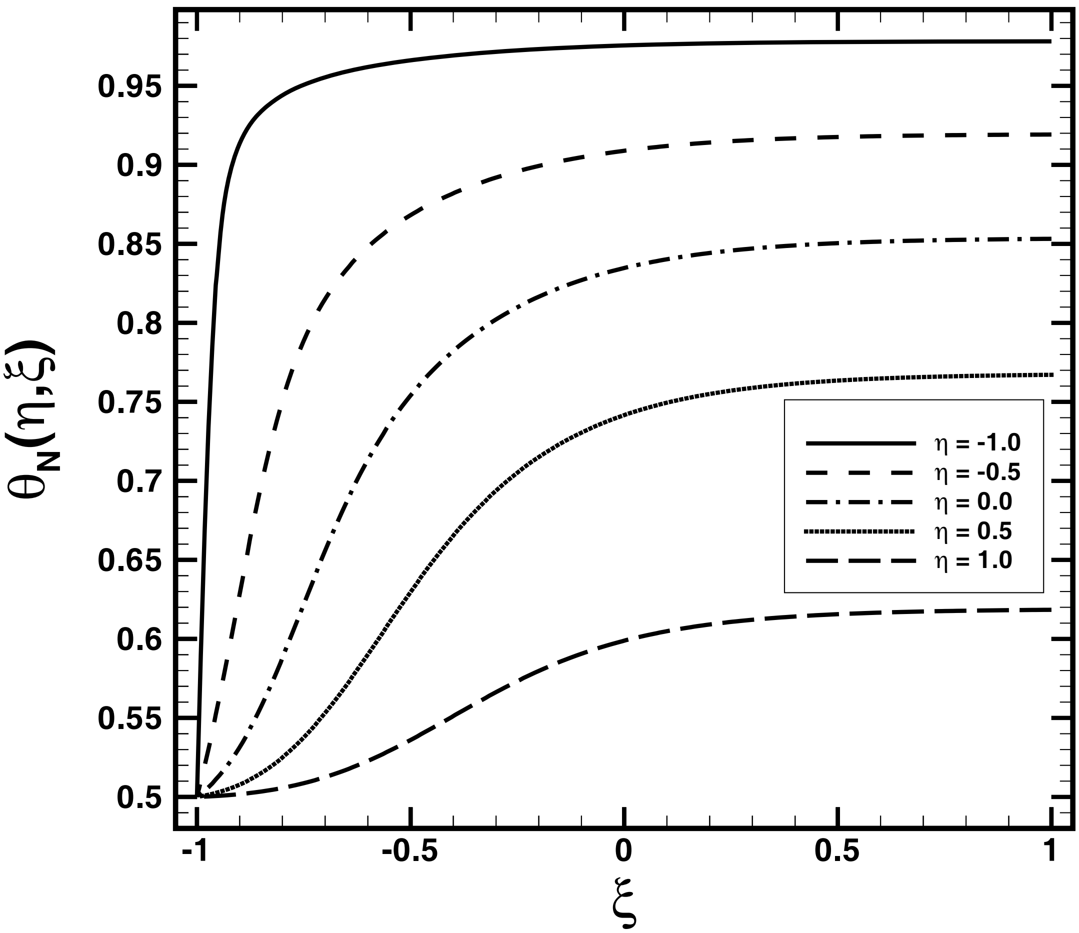

Figure 4.12: Temporal distributions for $\theta_N(\eta, \xi)$ corresponding to various locations when $L = 5$, $\theta_1 = 0.5$, and $t_{max} = 45$, and with $N = 20$ and $P = 41$.

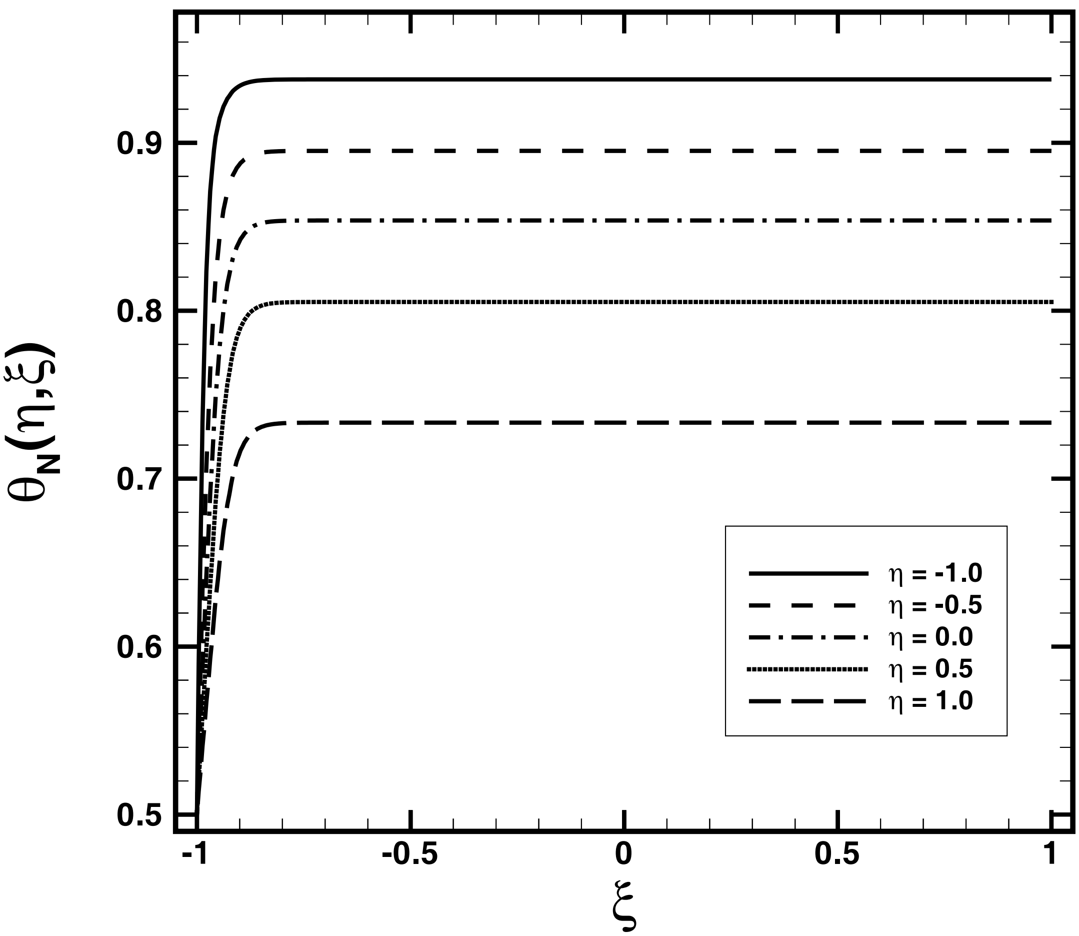

Figure 4.13: Temporal distributions for $\theta_N(\eta, \xi)$ corresponding to various locations when $L = 1$, $\theta_1 = 0.5$, and $t_{max} = 90$, and with $N = 20$ and $P = 41$.

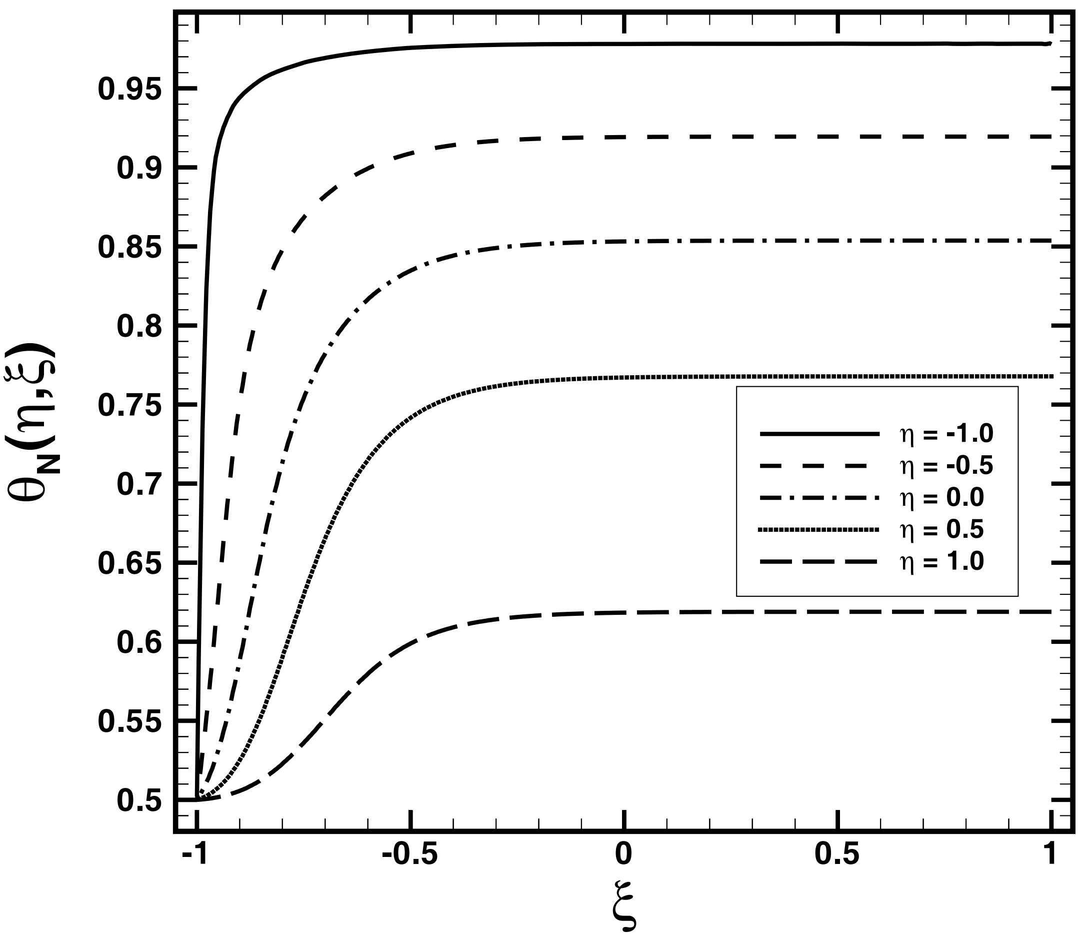

Figure 4.14: Temporal distributions for $\theta_N(\eta, \xi)$ corresponding to various locations when $L = 5$, $\theta_1 = 0.5$, and $t_{max} = 90$, and with $N = 20$ and $P = 41$.

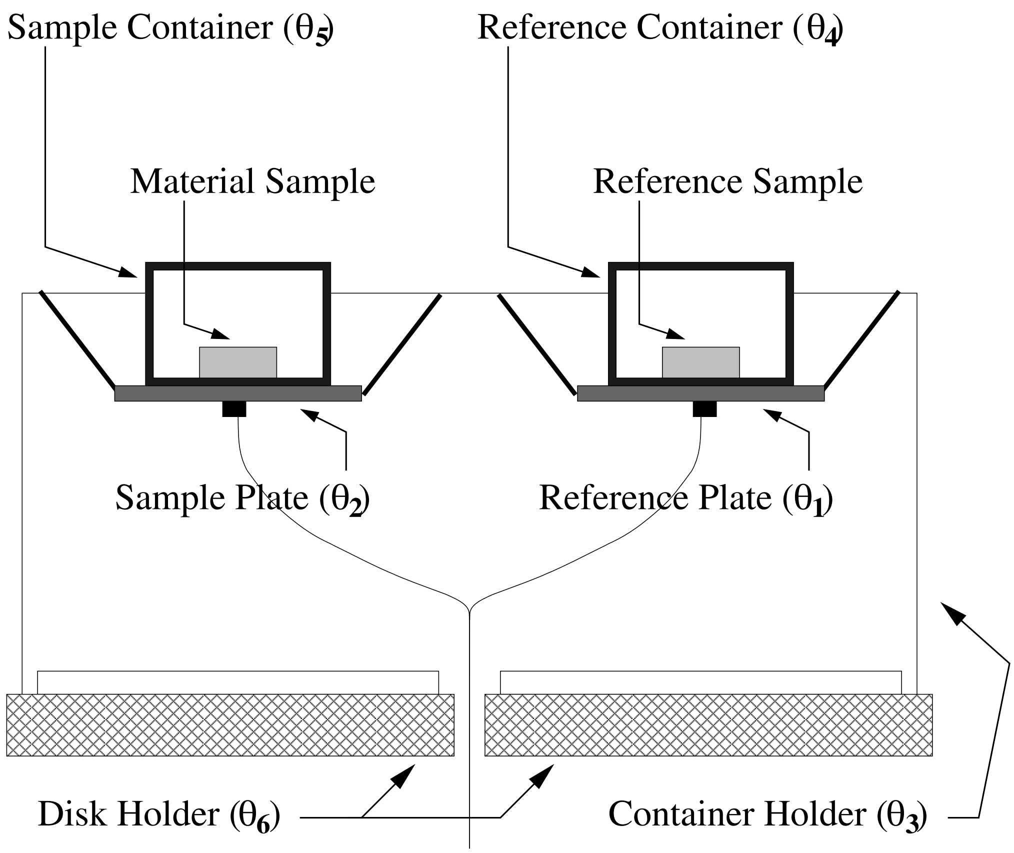

Figure 5.1: Schematic for typical heat flux DSC head system.

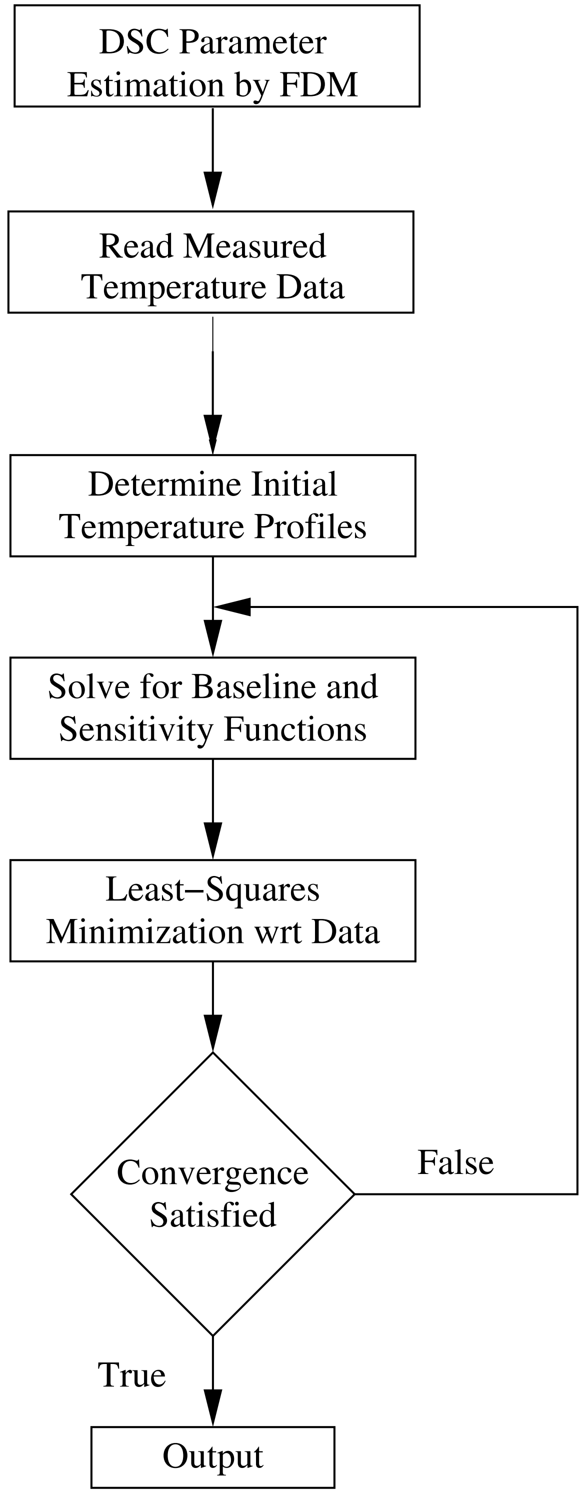

Figure 5.2: Basic flowchart for the DSC parameter estimation algorithm.

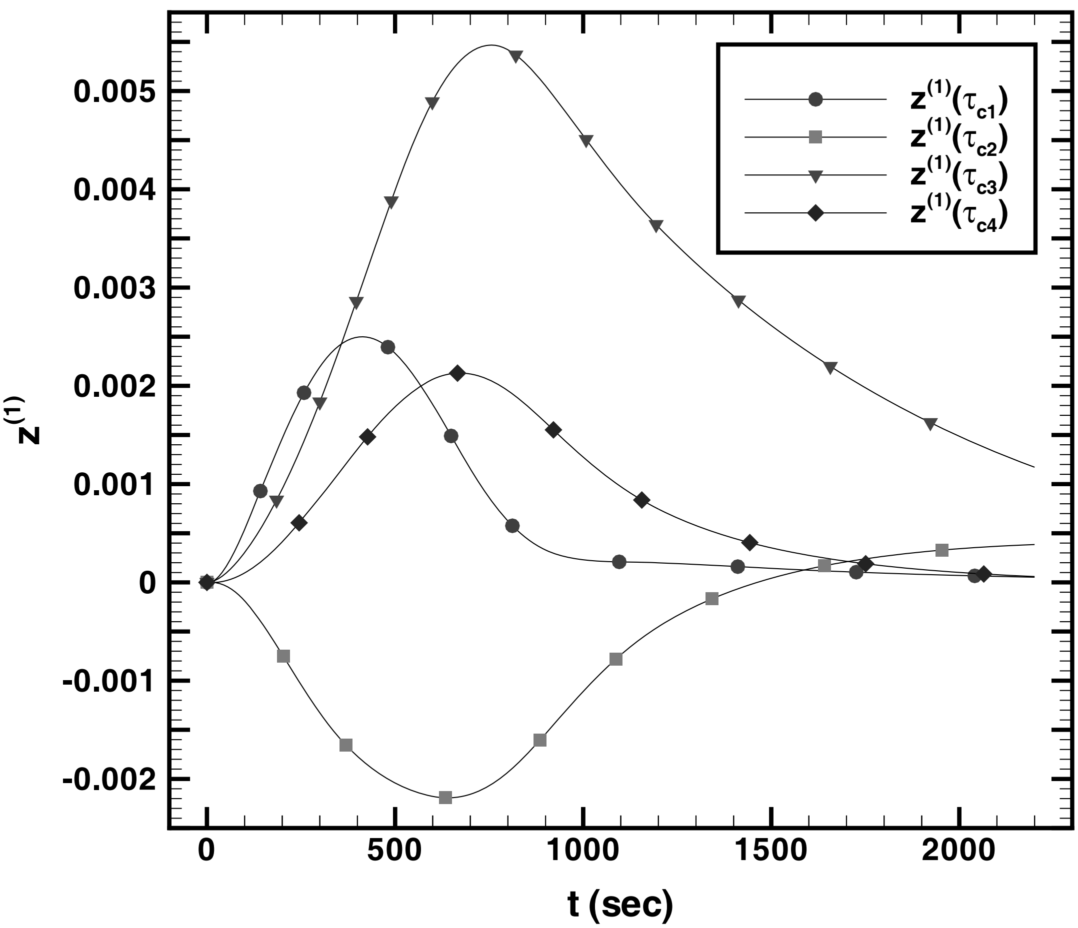

Figure 5.3: Sensitivity functions for reference plate temperature reconstruction that are associated with conductive parameters. There is no error in the input data and α corresponds to a heating rate of 20 K/min.

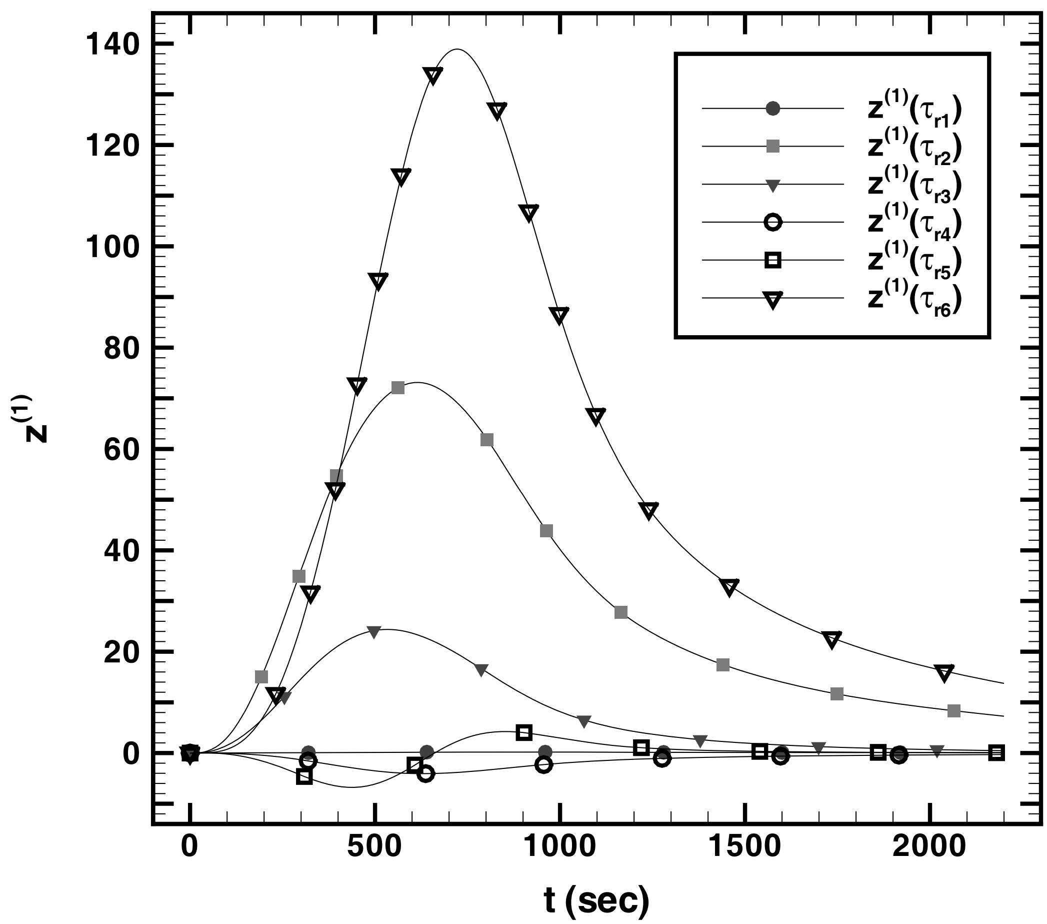

Figure 5.4: Sensitivity functions for reference plate temperature reconstruction that are associated with radiative parameters. There is no error in the input data and α corresponds to a heating rate of 20 K/min.

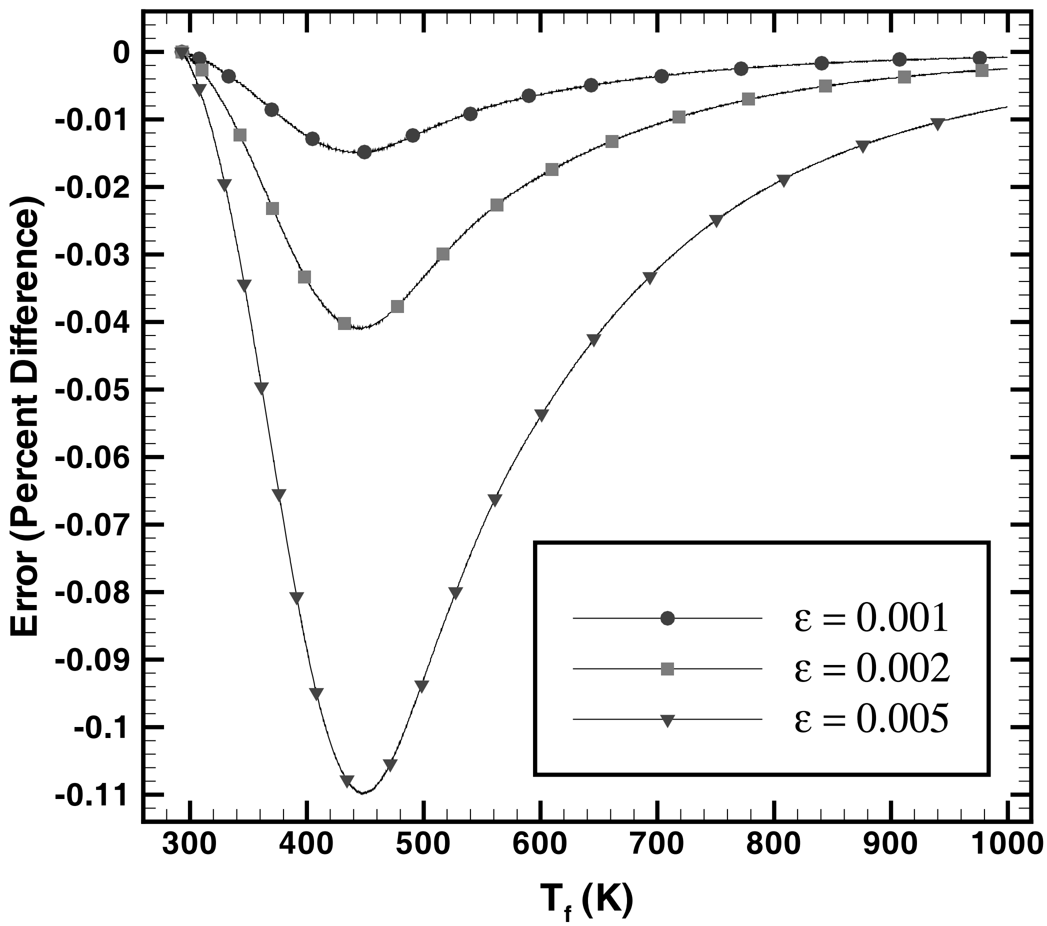

Figure 5.5: Error (% difference) between the reconstructed and exact temperature profiles for the container holder plotted against furnace temperature using input data with increasing levels of noise and α corresponding to a heating rate of 20 K/min.

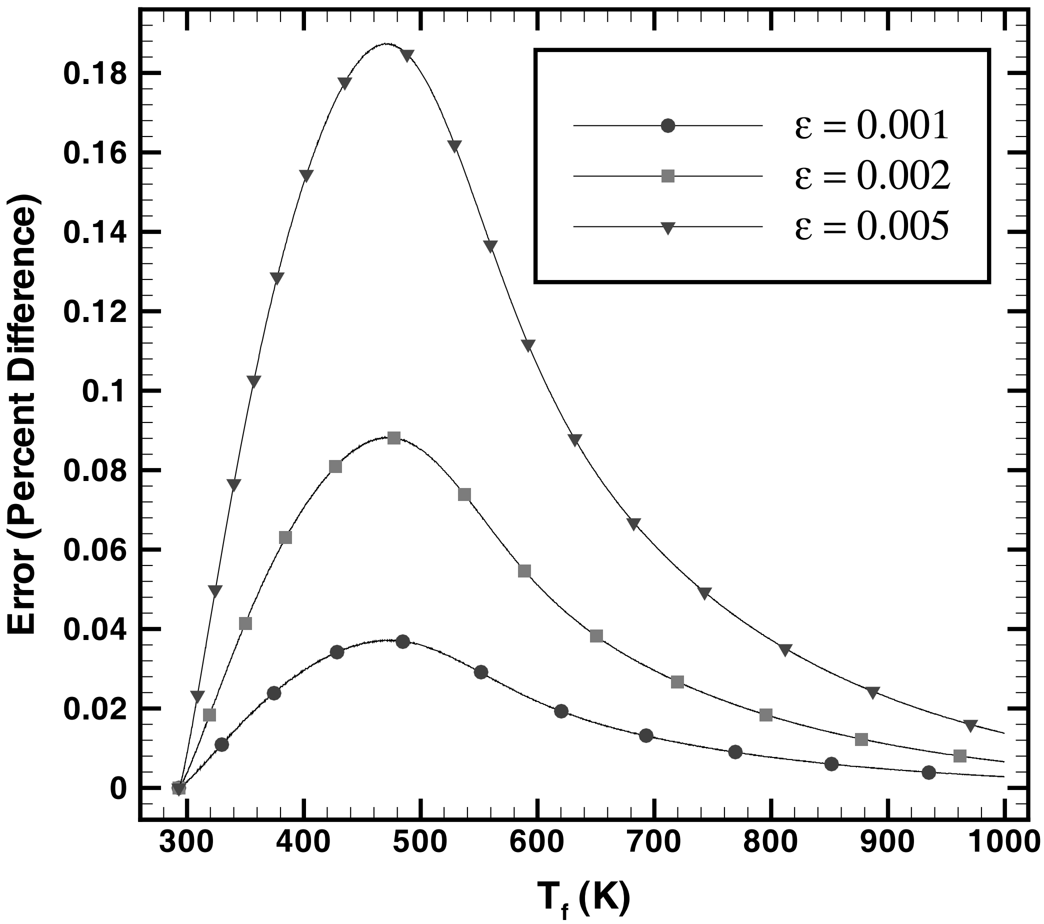

Figure 5.6: Error (% difference) between the reconstructed and exact temperature profiles for the sample pan plotted against furnace temperature using input data with increasing levels of noise and α corresponding to a heating rate of 20 K/min.

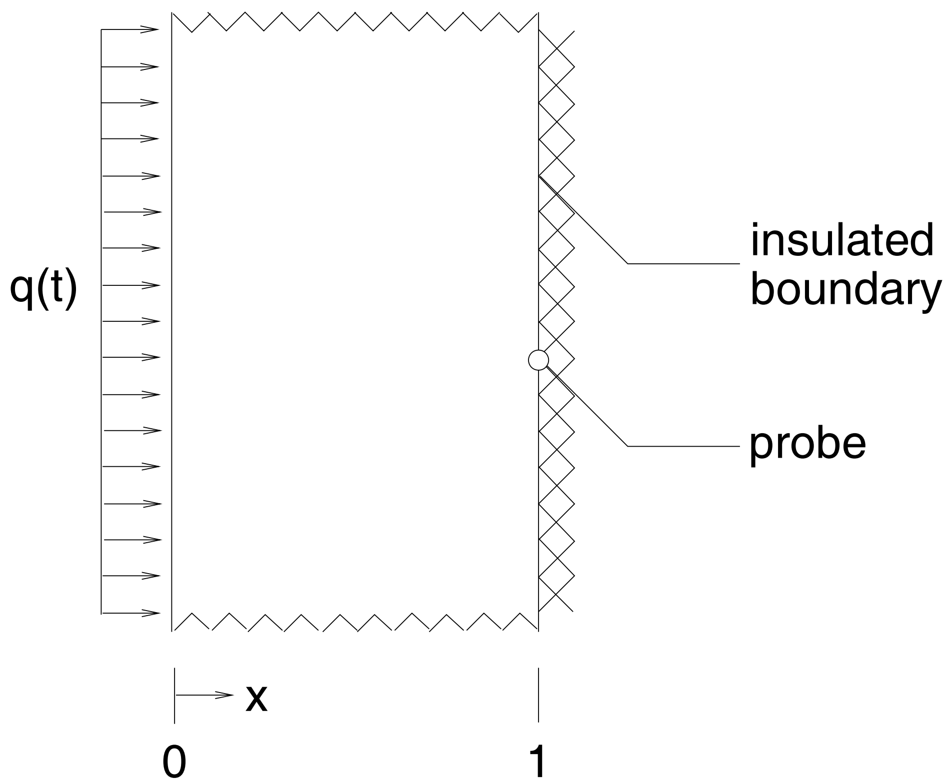

Figure 6.1: Diagram of the one-dimensional inverse heat conduction problem.

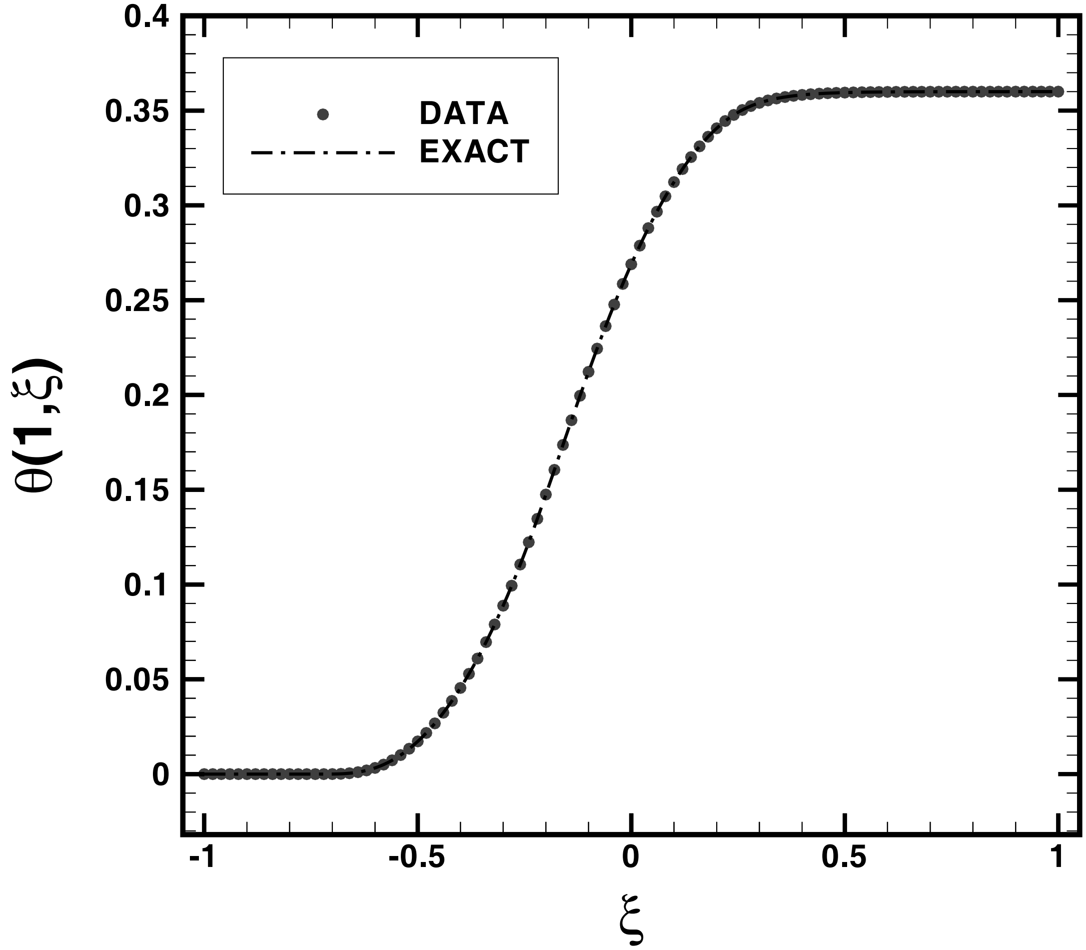

Figure 6.2: Imposed over-specified surface temperature θ_i at $\eta = 1$; discrete errorless data.

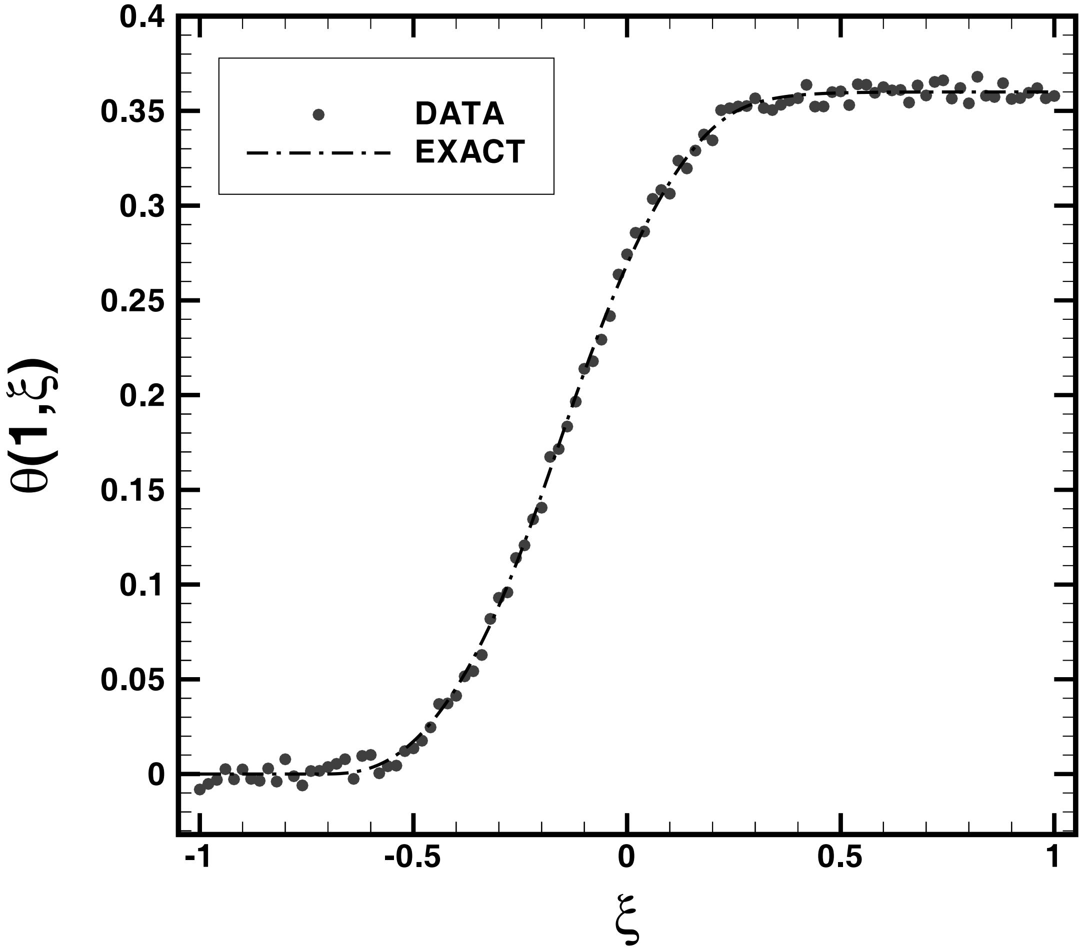

Figure 6.3: Imposed over-specified surface temperature θ_i at $\eta = 1$; discrete noisy data ($\sigma = 0.015$).

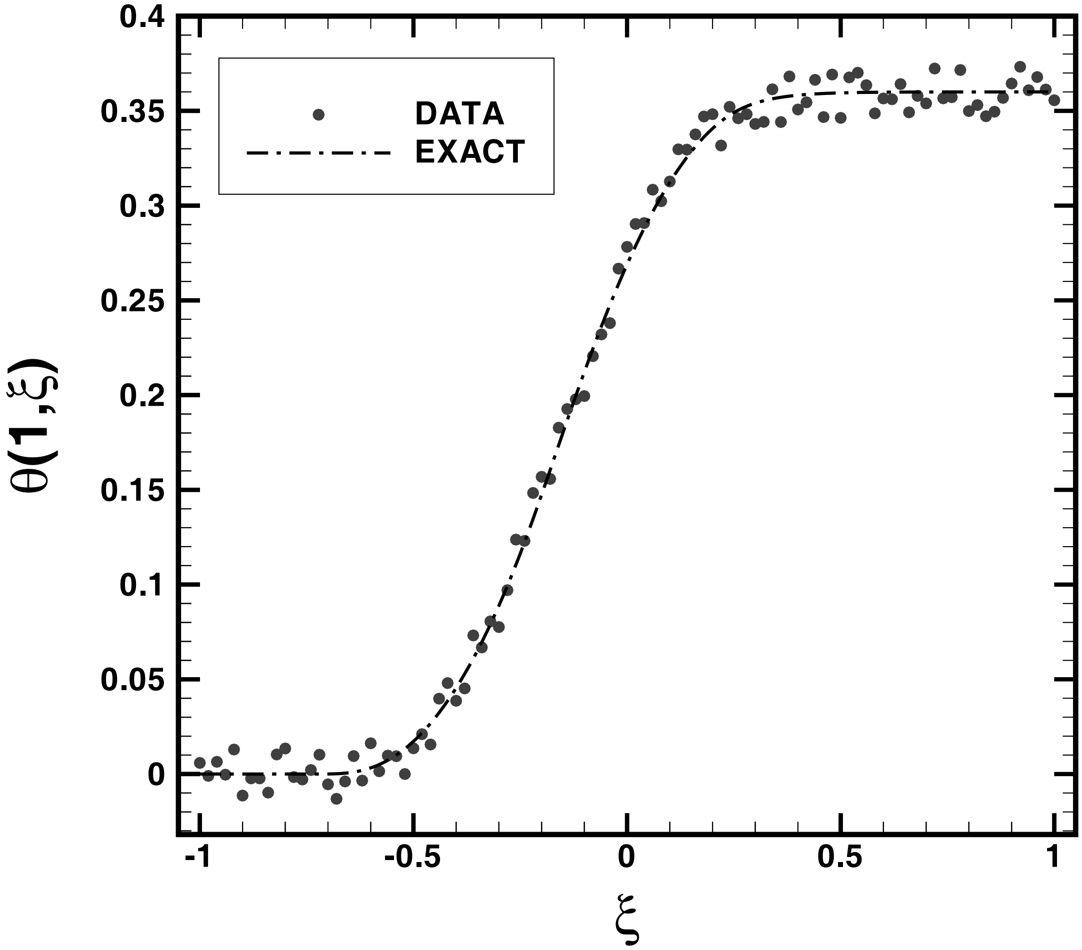

Figure 6.4: Imposed over-specified surface temperature θ_i at $\eta = 1$; discrete noisy data ($\sigma = 0.025$).

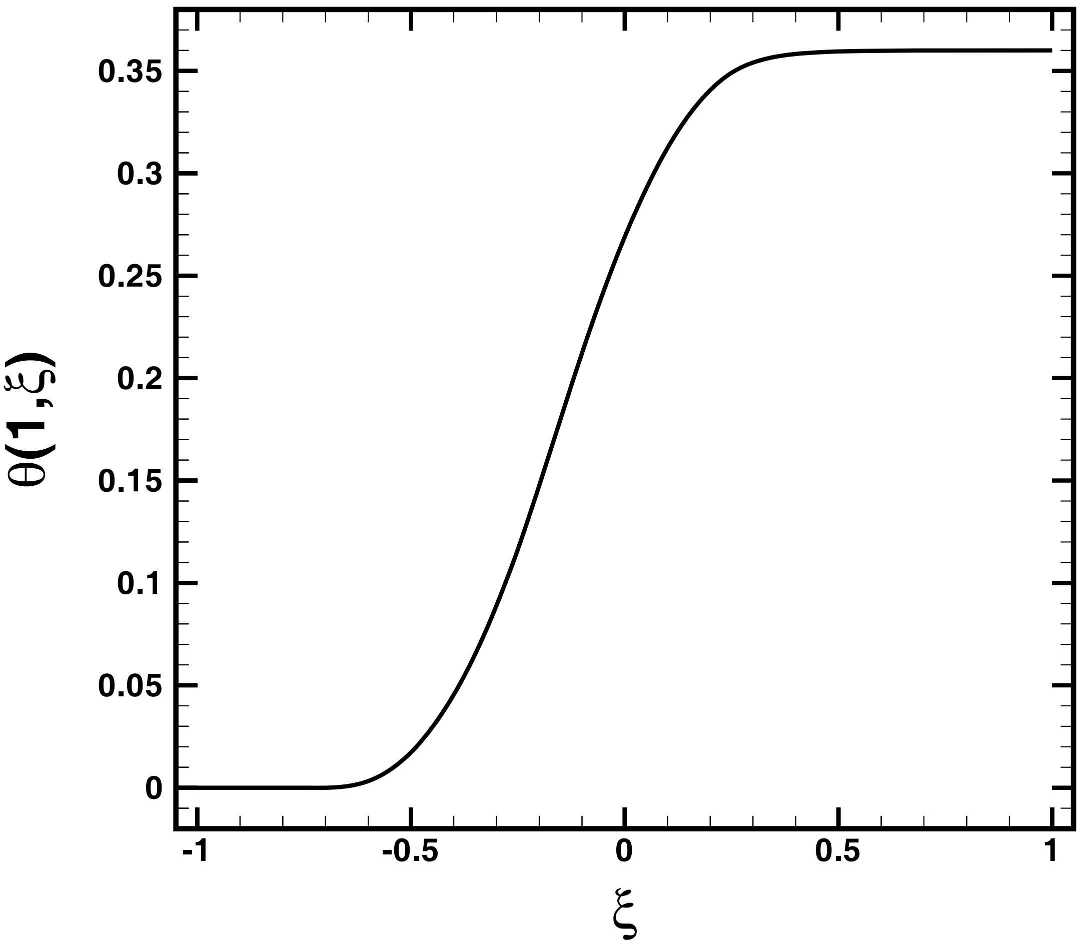

Figure 6.5: Imposed surface temperature $\theta(-1, \xi) = f(\xi)$, $\xi \in [-1, 1], \lambda = 1.25$ for the thermal design problem.

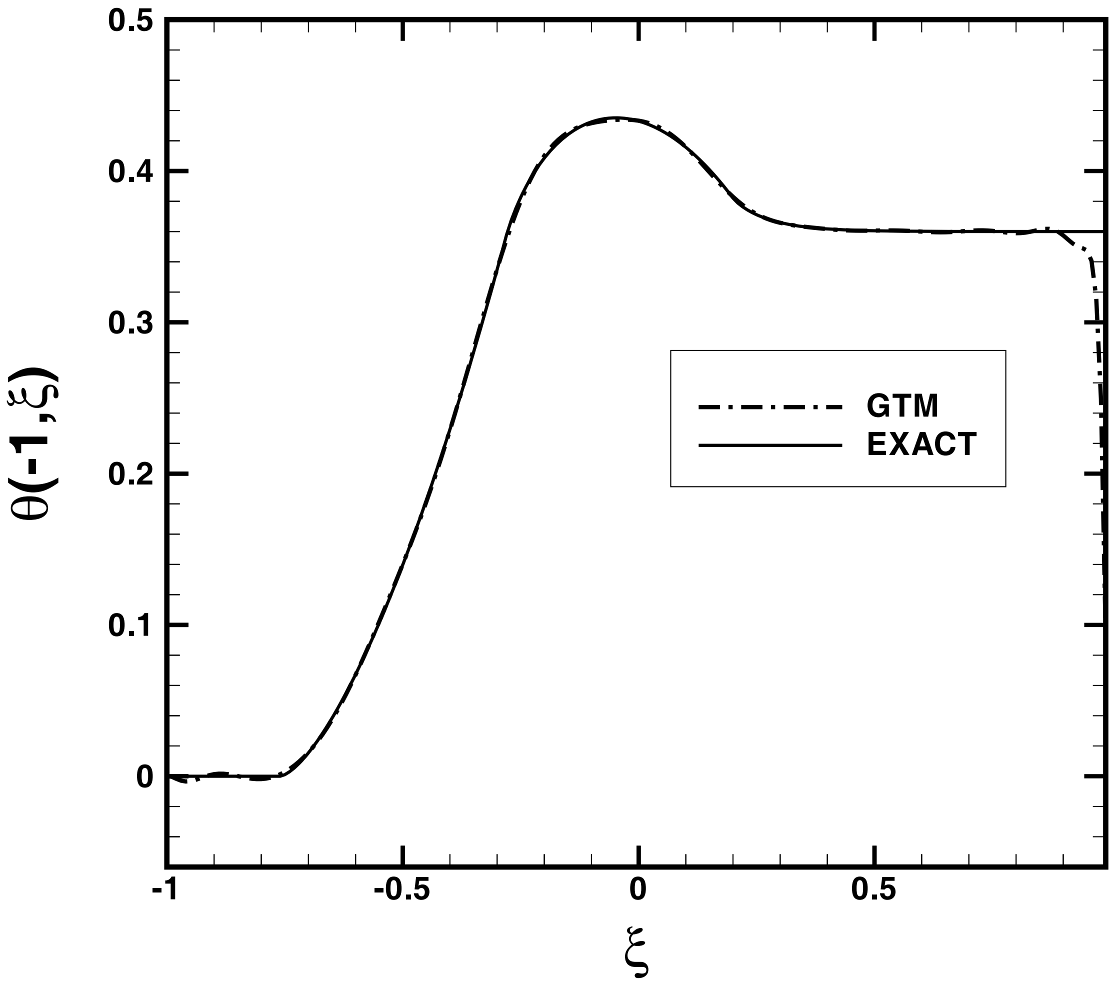

Figure 6.6: Predicted surface temperature at $\eta = -1$ using GTM with errorless data, $N = 8$, $P_m = 24$ and $\lambda = 1.25$.

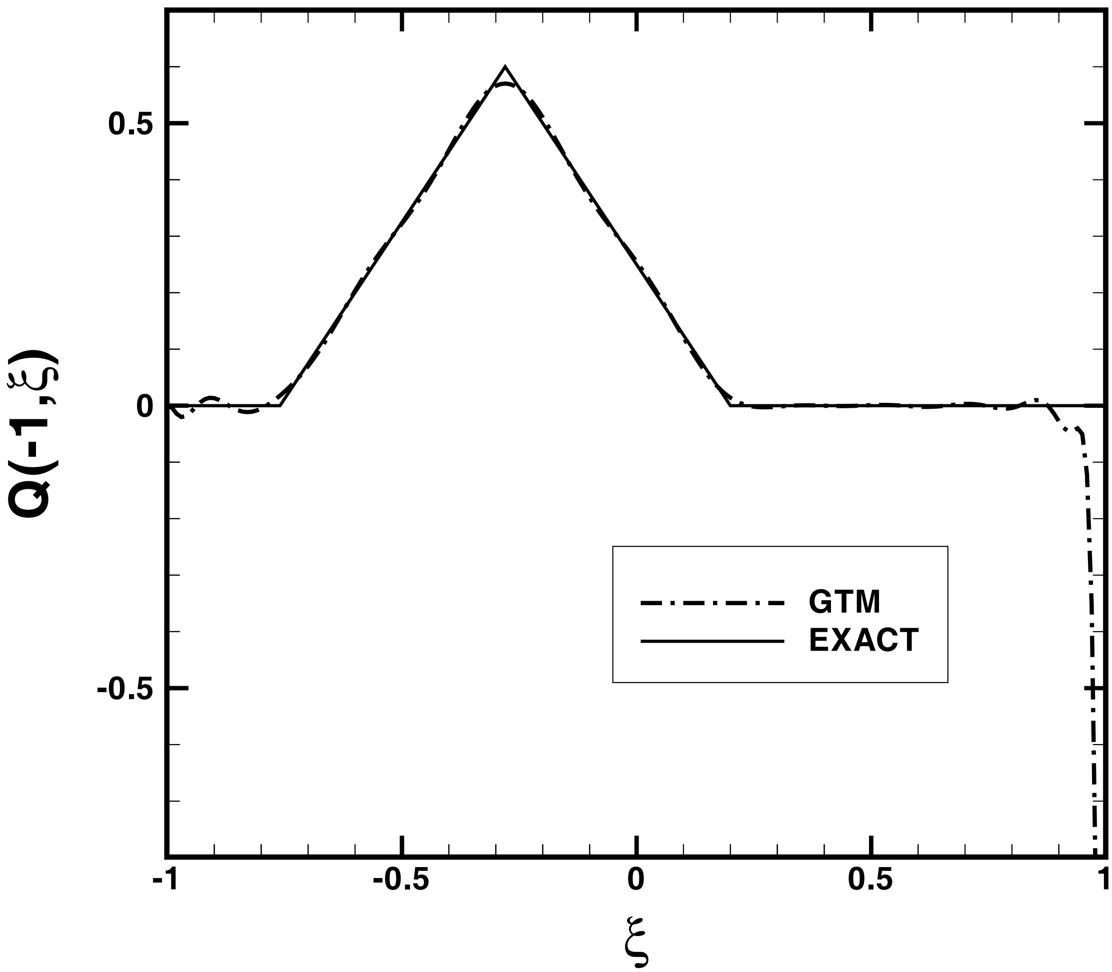

Figure 6.7: Predicted surface heat flux at $\eta = -1$ using GTM with errorless data, $N = 8$, $P_m = 24$ and $\lambda = 1.25$.

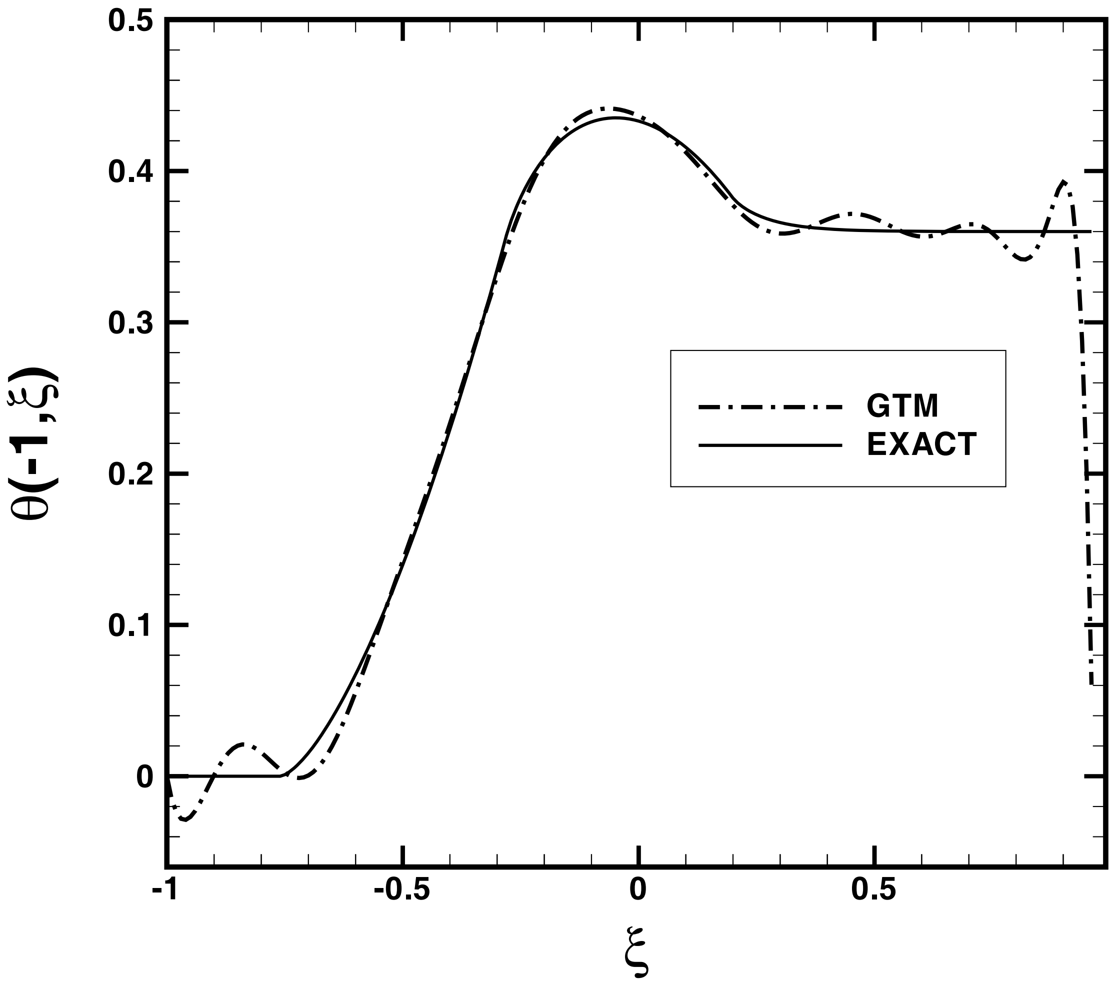

Figure 6.8: Predicted surface temperature at $\eta = -1$ using GTM with moderate noise in the input data, $N = 10$, $P_m = 18$ and $\lambda = 1.25$.

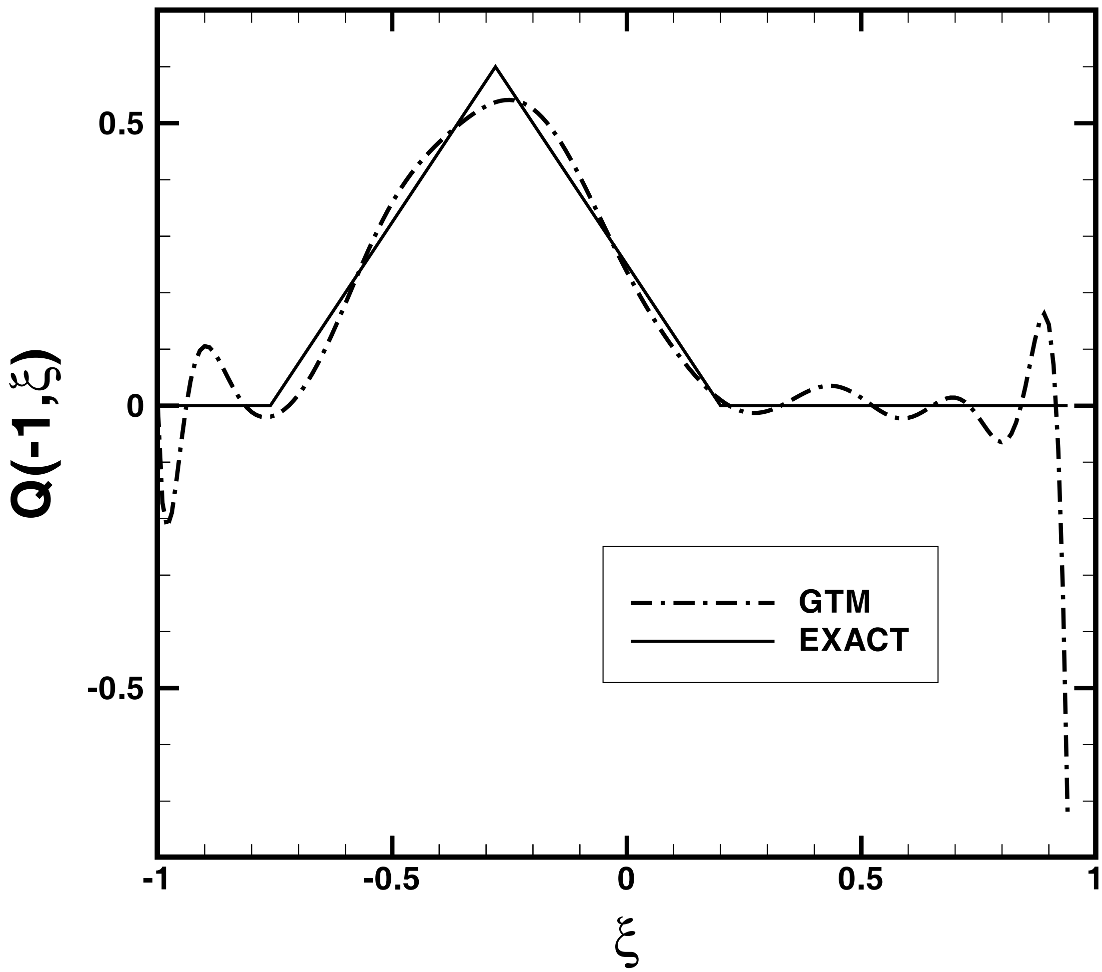

Figure 6.9: Predicted surface heat flux at $\eta = -1$ using GTM with moderate noise in the input data, $N = 10$, $P_m = 18$ and $\lambda = 1.25$.

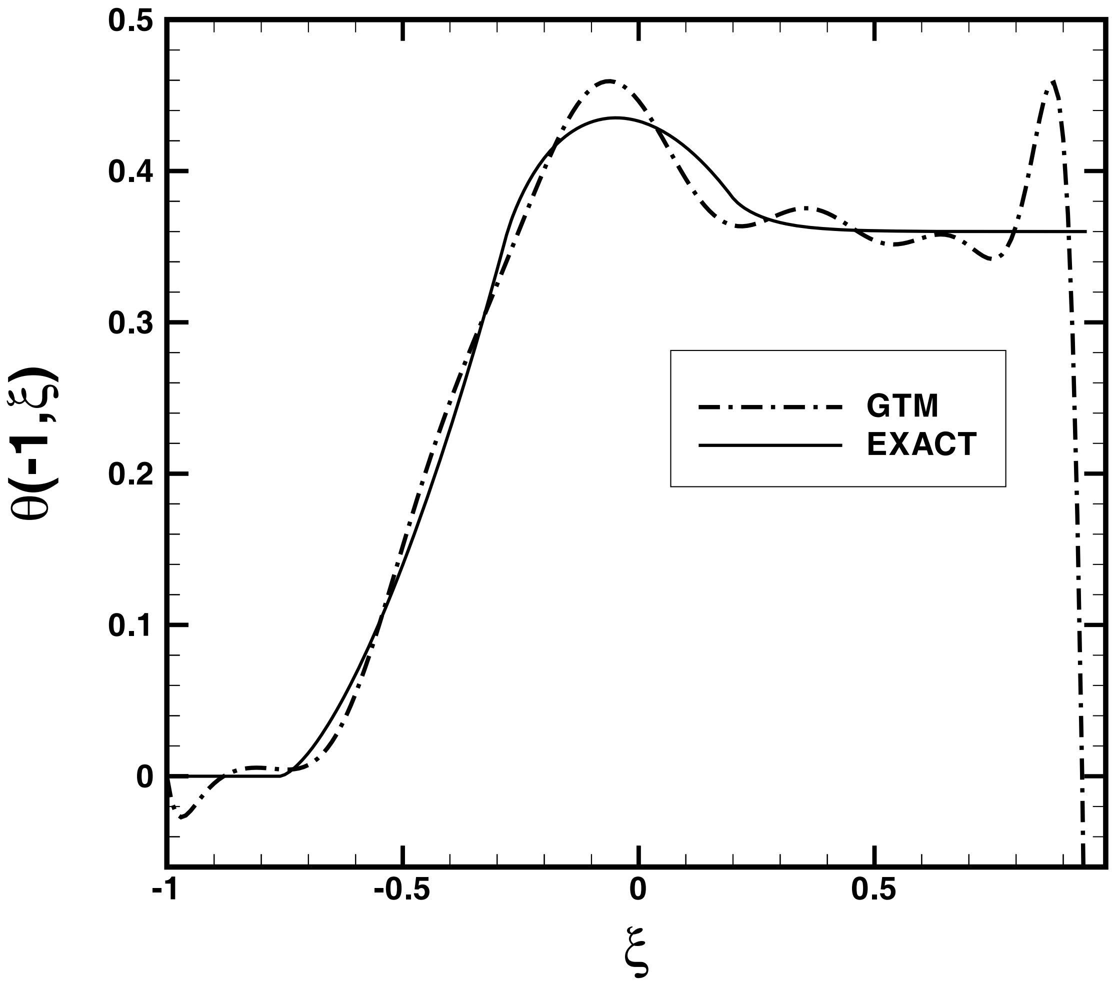

Figure 6.10: Predicted surface temperature at $\eta = -1$ using GTM with severe noise in the input data, $N = 10$, $P_m = 16$ and $\lambda = 1.25$.

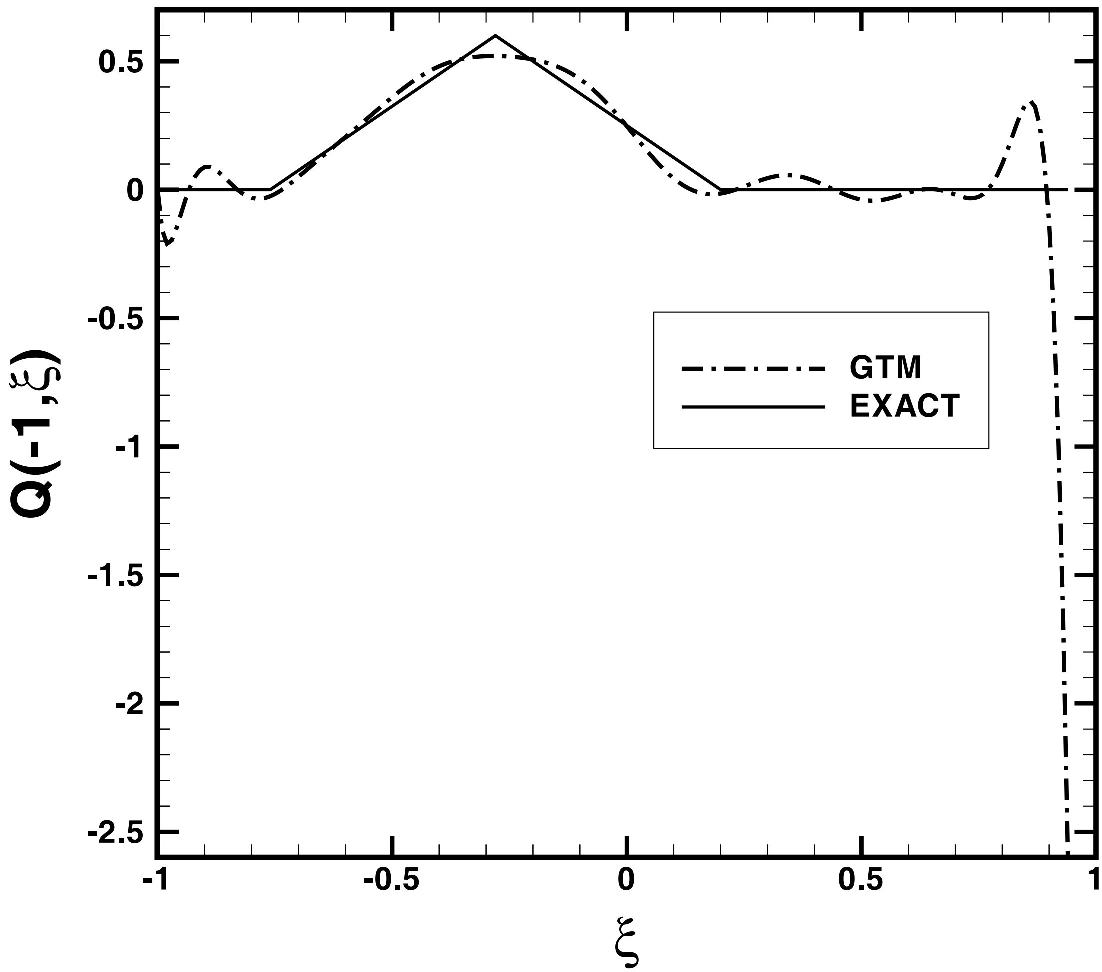

Figure 6.11: Predicted surface heat flux at $\eta = -1$ using GTM with severe noise in the input data, $N = 10$, $P_m = 16$ and $\lambda = 1.25$.

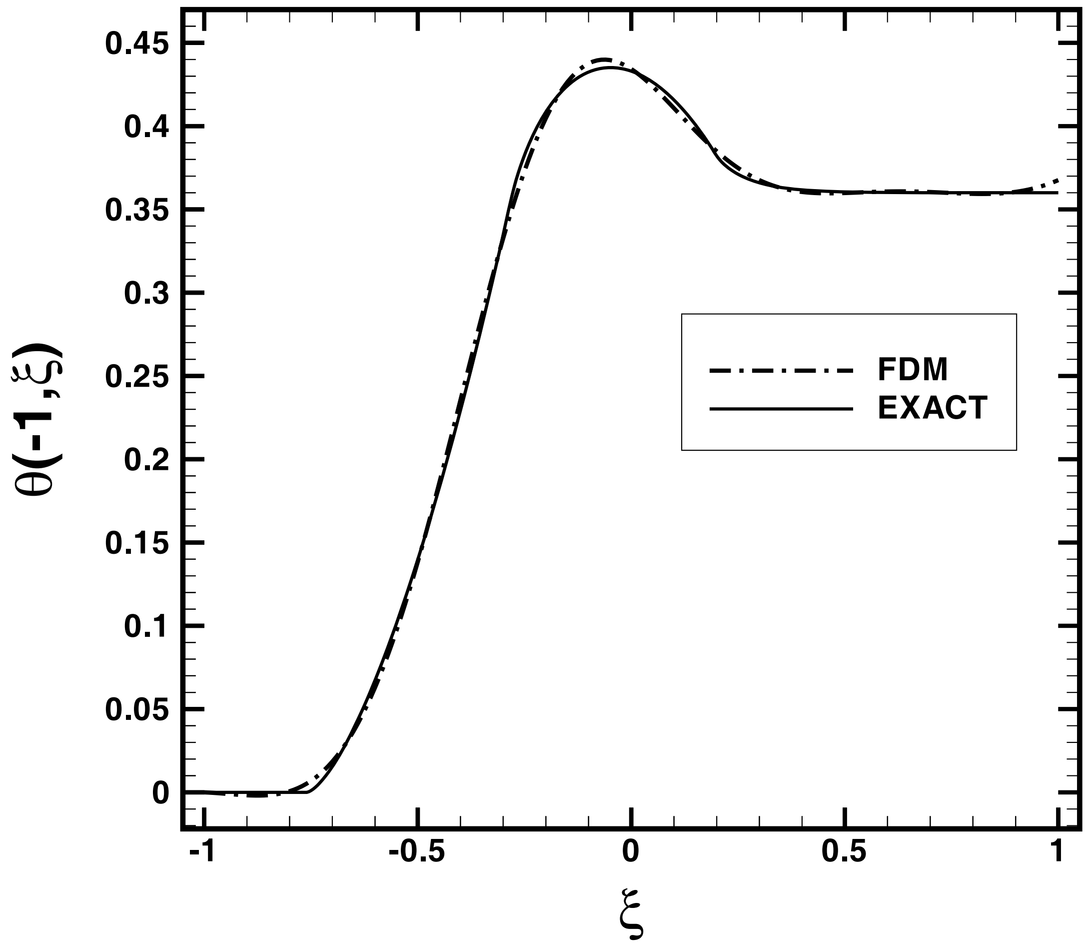

Figure 6.12: Predicted surface temperature at $\eta = -1$ using FDM with errorless data and $N = 6$, $P_N = 16$, and $P = 10$ for boundary variant $\gamma = I$ with $\beta = 1.0$ and $\lambda = 1.25$.

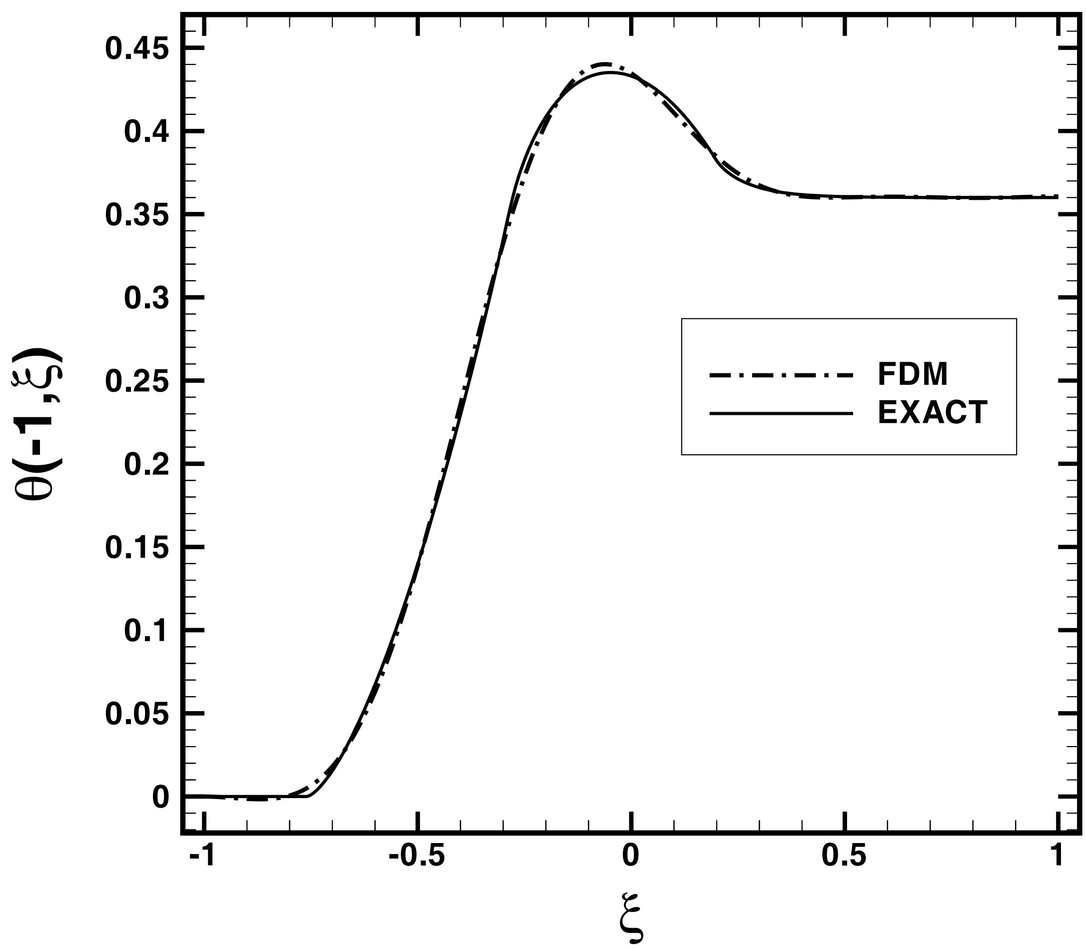

Figure 6.13: Predicted surface temperature at $\eta = -1$ using FDM with errorless data and $N = 6$, $P_N = 16$, and $P = 10$ for boundary variant $\gamma = II$ with $\beta = 1.0$ and $\lambda = 1.25$.

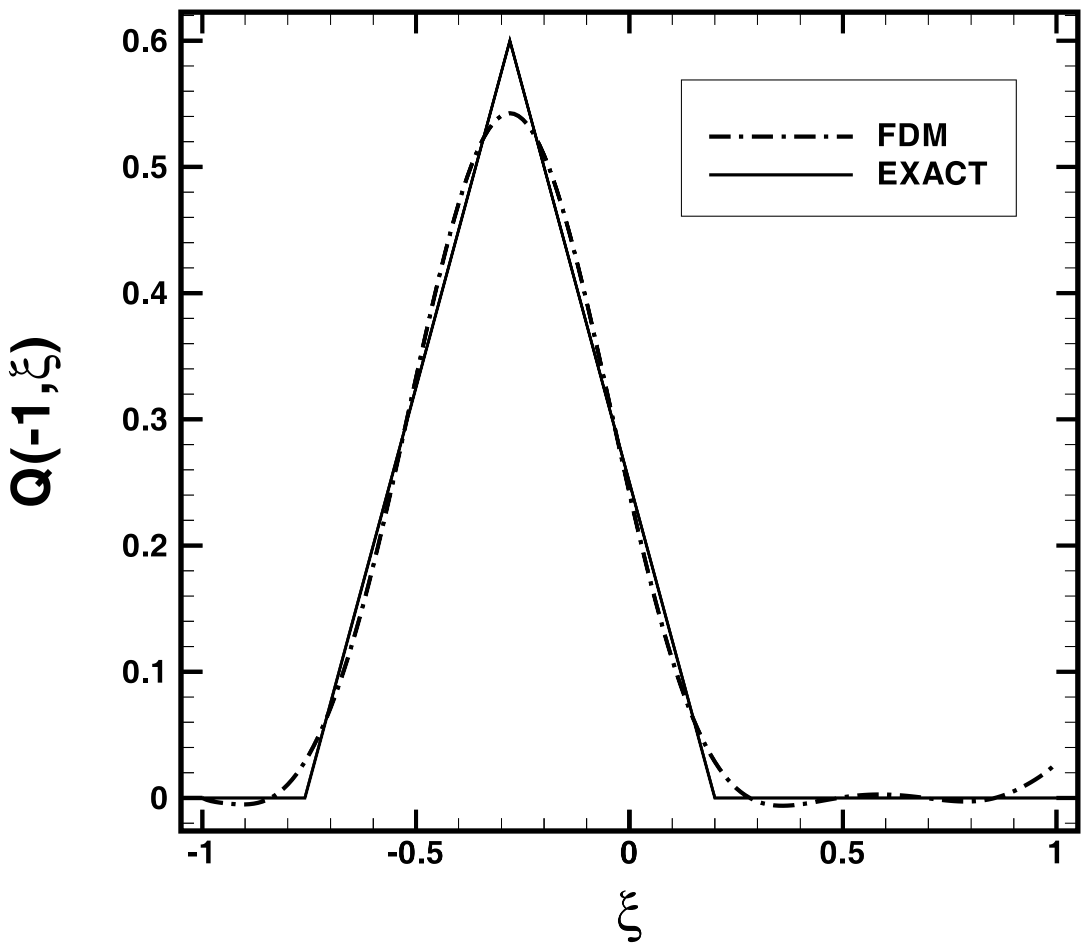

Figure 6.14: Predicted surface heat flux at $\eta = -1$ using FDM with errorless data and $N = 6$, $P_N = 16$, and $P = 10$ for boundary variant $\gamma = I$ with $\beta = 1.0$ and $\lambda = 1.25$.

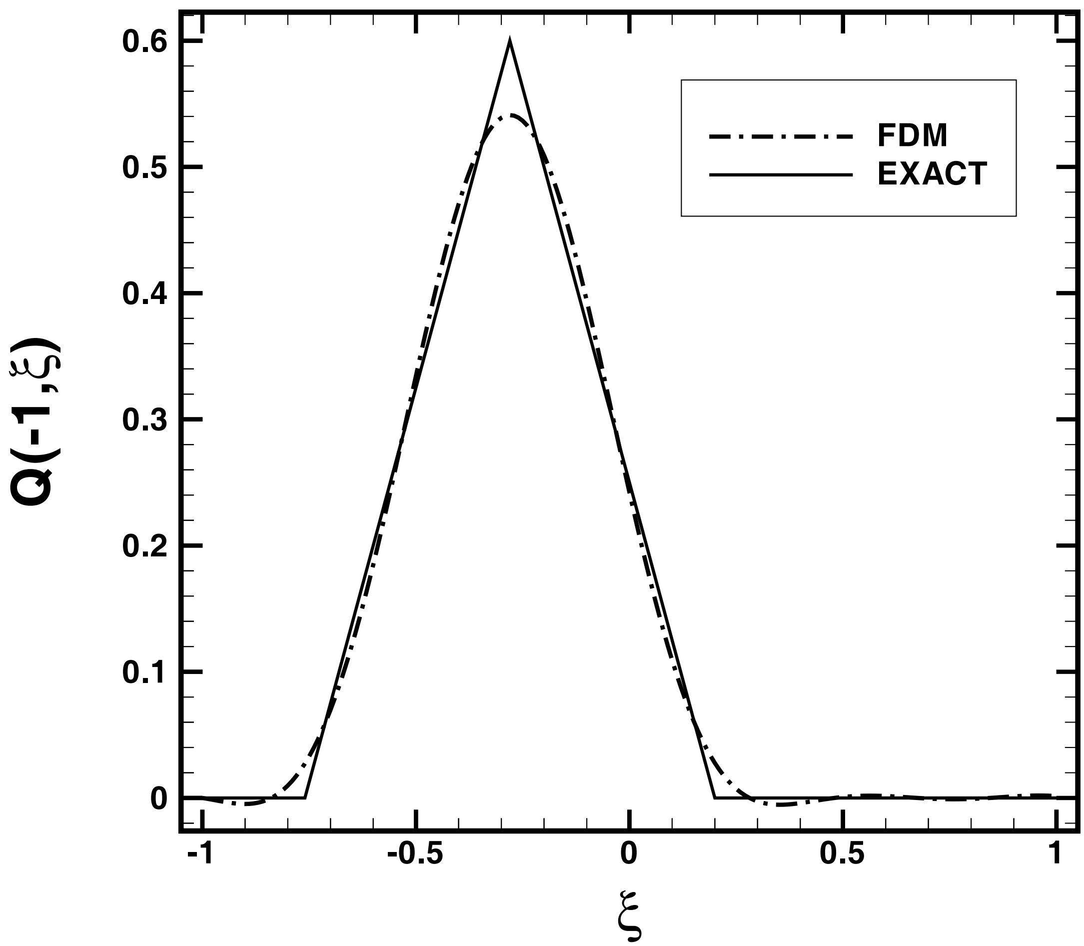

Figure 6.15: Predicted surface heat flux at $\eta = -1$ using FDM with errorless data and $N = 6$, $P_N = 16$, and $P = 10$ for boundary variant $\gamma = II$ with $\beta = 1.0$ and $\lambda = 1.25$.

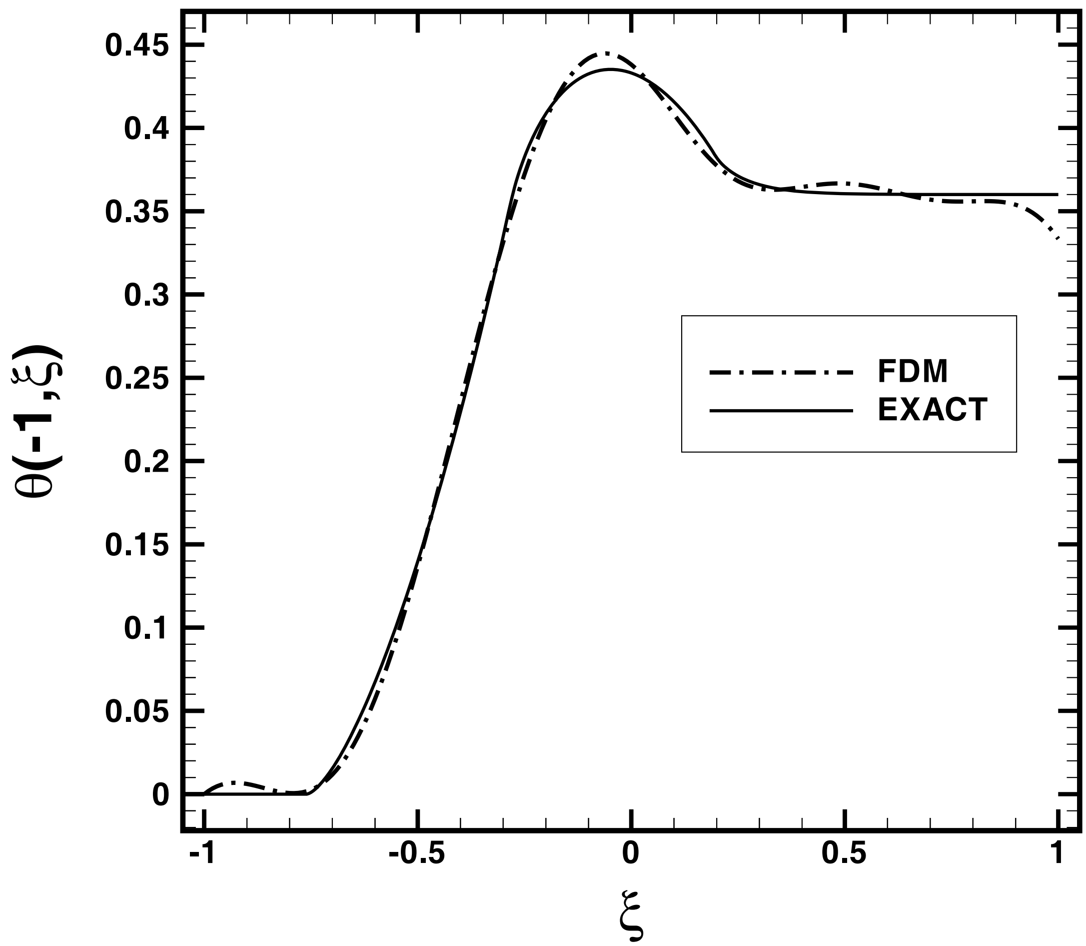

Figure 6.16: Predicted surface temperature at $\eta = -1$ using FDM with moderate noise in the input data ($\sigma = 0.015$) and $N = 8$, $P_N = 16$, and $P = 10$ for boundary variant $\gamma = I$ with $\beta = 1.0$ and $\lambda = 1.25$.

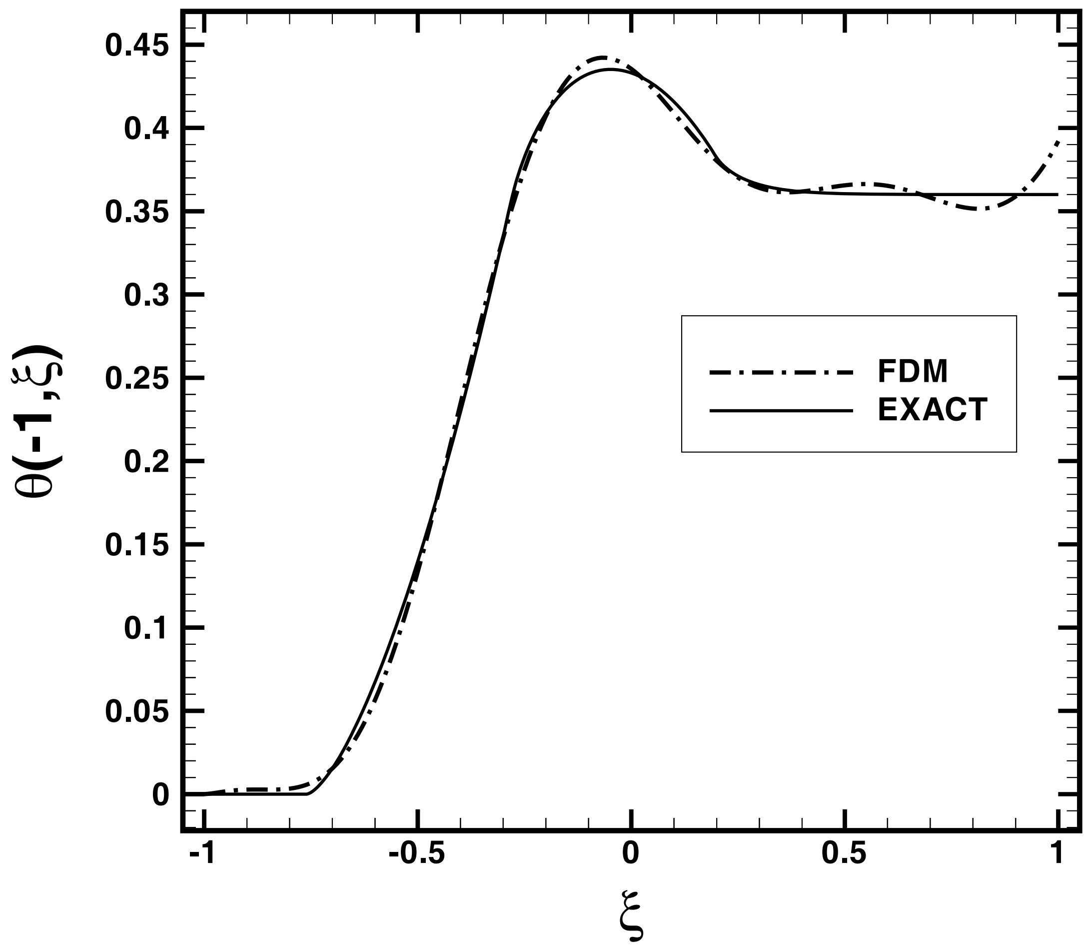

Figure 6.17: Predicted surface temperature at $\eta = -1$ using FDM with moderate noise in the input data ($\sigma = 0.015$) and $N = 6$, $P_N = 16$, and $P = 10$ for boundary variant $\gamma = II$ with $\beta = 1.0$ and $\lambda = 1.25$.

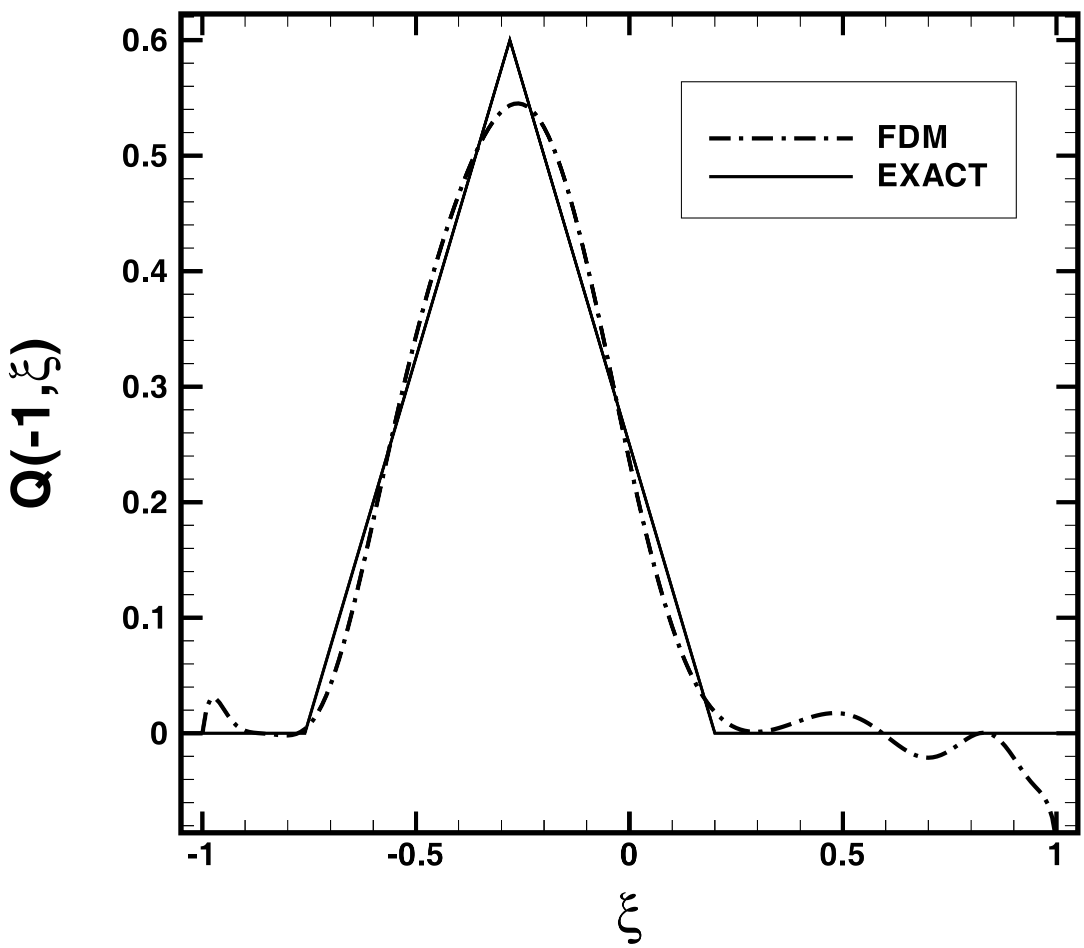

Figure 6.18: Predicted surface heat flux at $\eta = -1$ using FDM with moderate noise in the input data ($\sigma = 0.015$) and $N = 8$, $P_N = 16$, and $P = 10$ for boundary variant $\gamma = I$ with $\beta = 1.0$ and $\lambda = 1.25$.

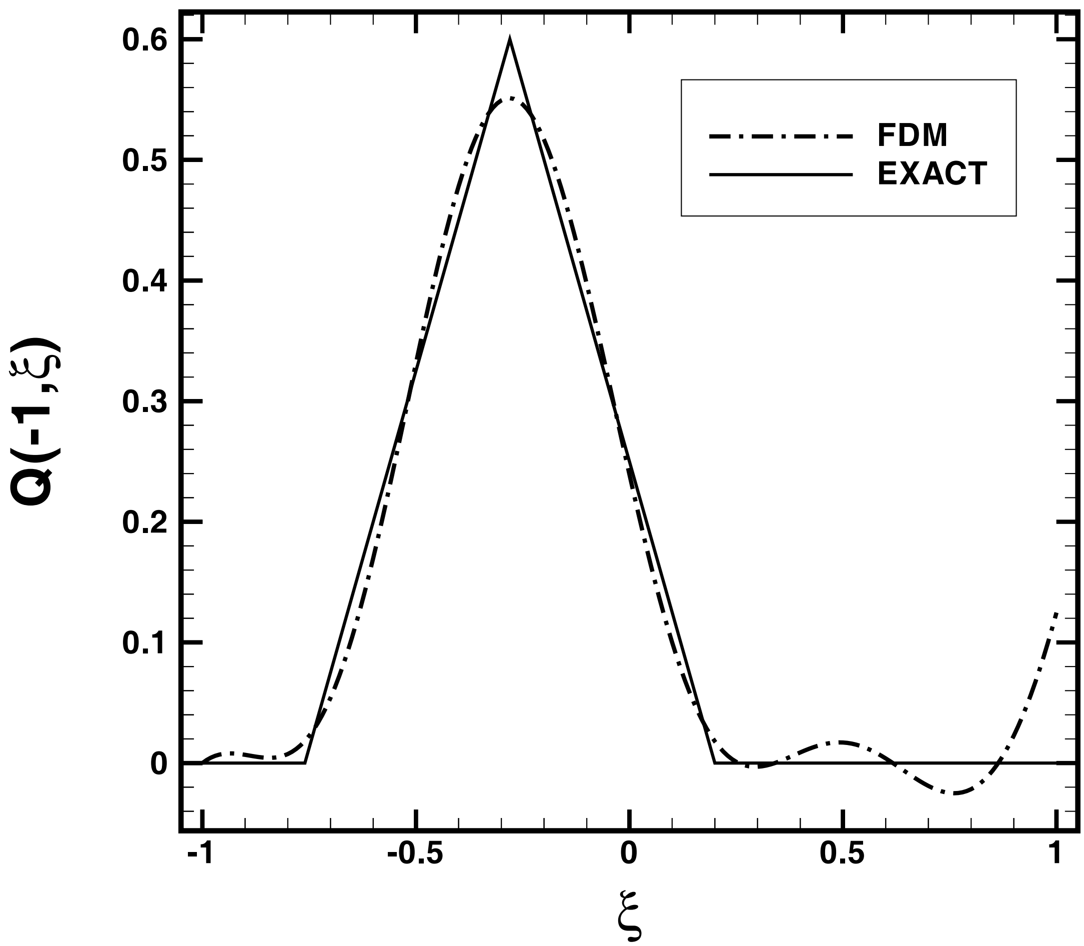

Figure 6.19: Predicted surface heat flux at $\eta = -1$ using FDM with moderate noise in the input data ($\sigma = 0.015$) and $N = 6$, $P_N = 16$, and $P = 10$ for boundary variant $\gamma = II$ with $\beta = 1.0$ and $\lambda = 1.25$.

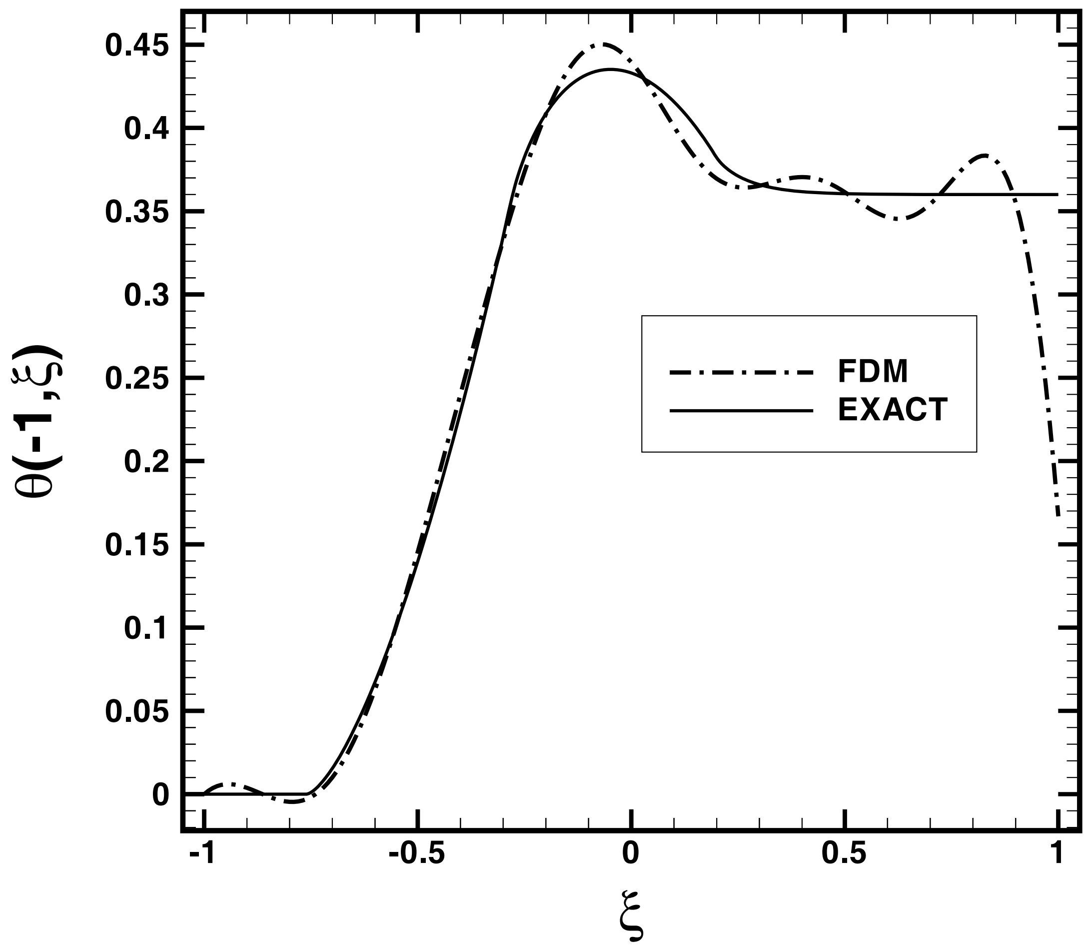

Figure 6.20: Predicted surface temperature at $\eta = -1$ using FDM with severe noise in the input data ($\sigma = 0.025$) and $N = 8$, $P_N = 16$, and $P = 10$ for boundary variant $\gamma = I$ with $\beta = 1.0$ and $\lambda = 1.25$.

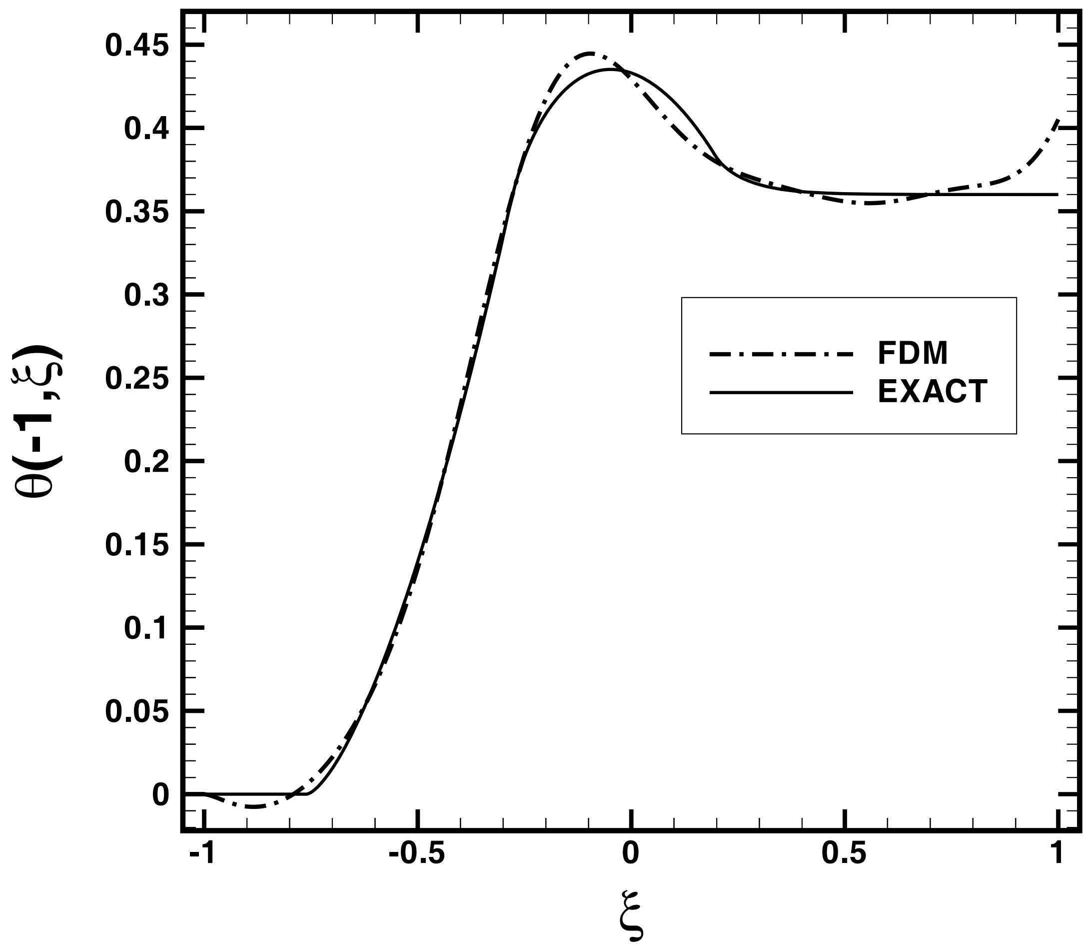

Figure 6.21: Predicted surface temperature at $\eta = -1$ using FDM with severe noise in the input data ($\sigma = 0.025$) and $N = 8$, $P_N = 16$, and $P = 10$ for boundary variant $\gamma = II$ with $\beta = 1.0$ and $\lambda = 1.25$.

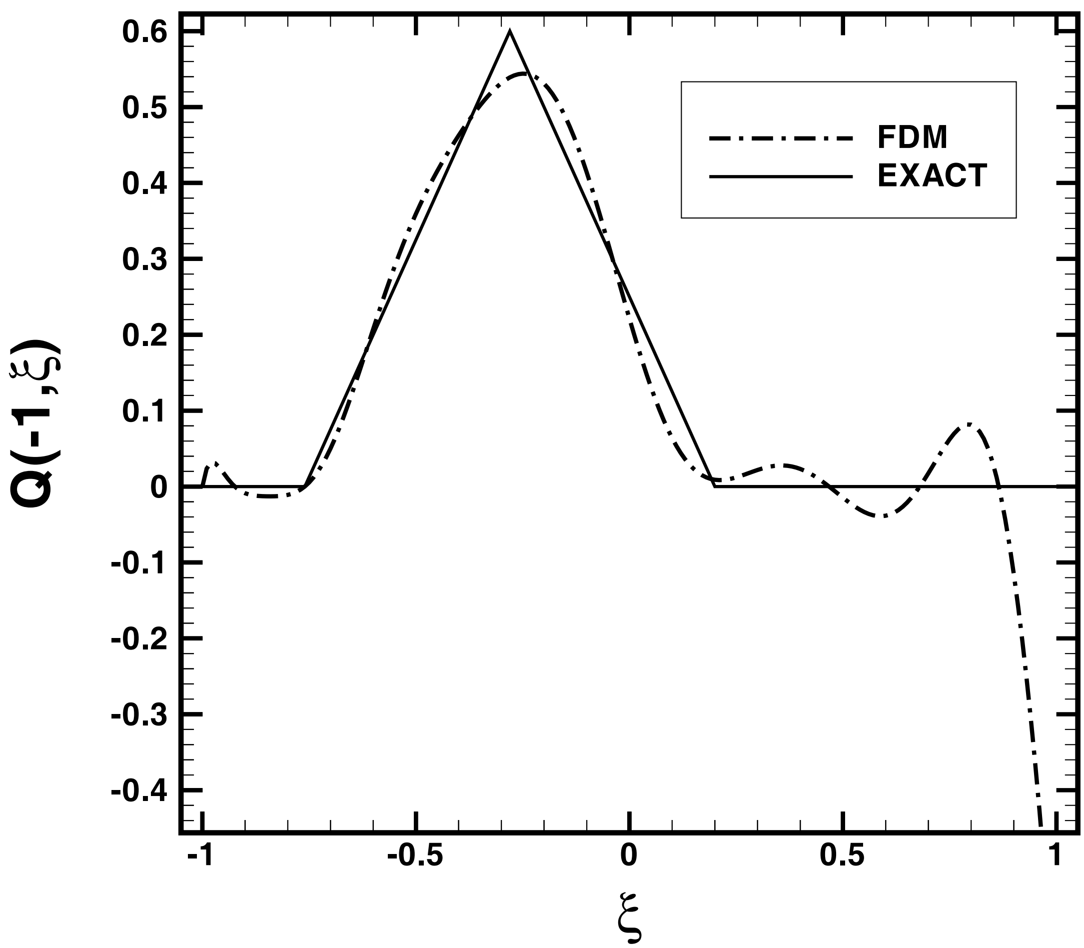

Figure 6.22: Predicted surface heat flux at $\eta = -1$ using FDM with severe noise in the input data ($\sigma = 0.025$) and $N = 8$, $P_N = 16$, and $P = 10$ for boundary variant $\gamma = I$ with $\beta = 1.0$ and $\lambda = 1.25$.

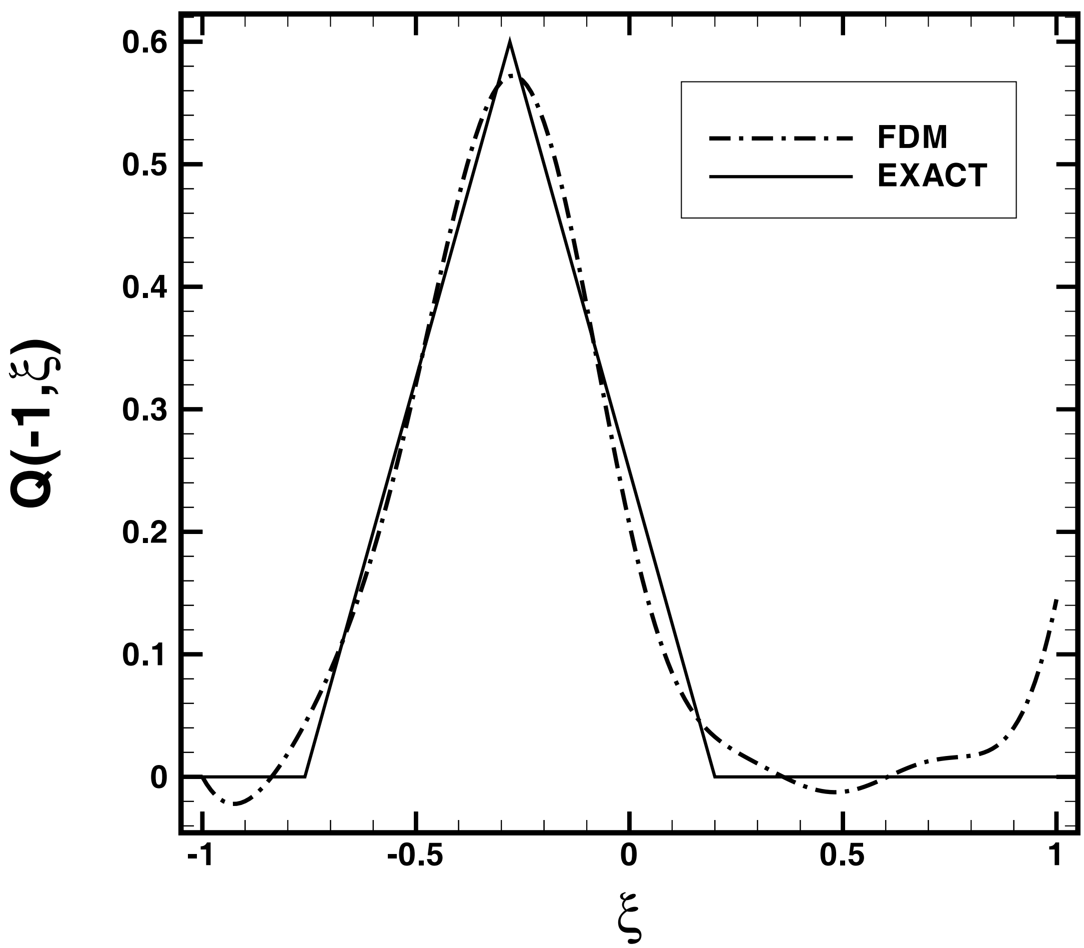

Figure 6.23: Predicted surface heat flux at $\eta = -1$ using FDM with severe noise in the input data ($\sigma = 0.025$) and $N = 8$, $P_N = 16$, and $P = 10$ for boundary variant $\gamma = II$ with $\beta = 1.0$ and $\lambda = 1.25$.

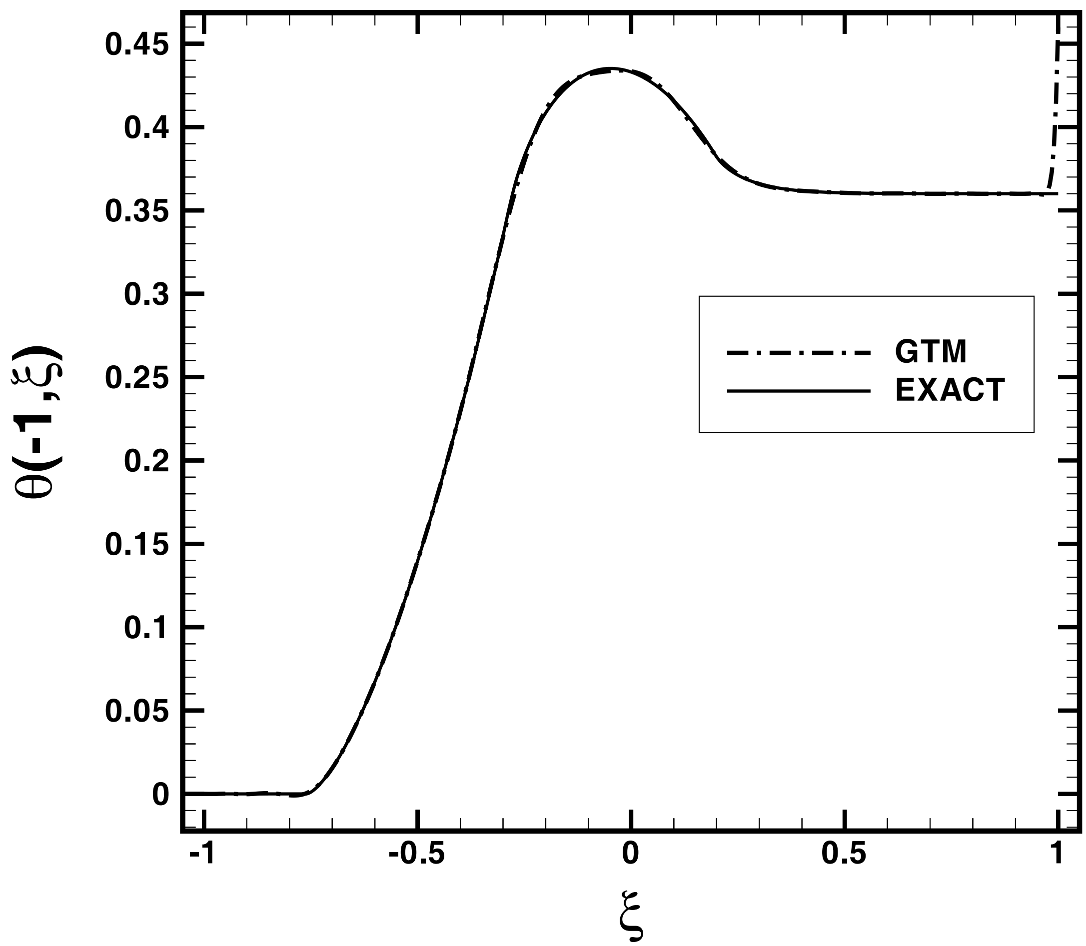

Figure 6.24: Predicted surface temperature at $\eta = -1$ for GTM with $N = 9$, $P_N = 30$ and $\lambda = 1.25$.

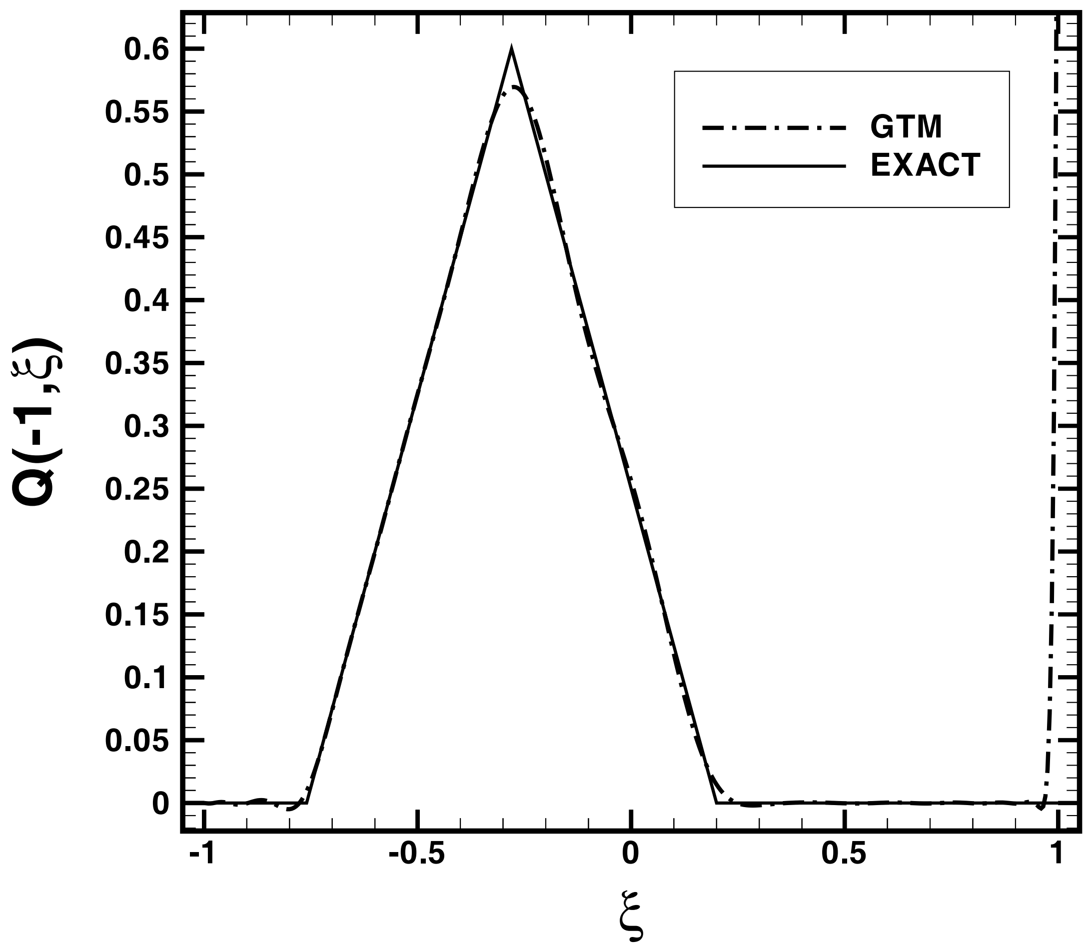

Figure 6.25: Predicted surface heat flux at $\eta = -1$ for GTM with $N = 9$, $P_N = 30$ and $\lambda = 1.25$.

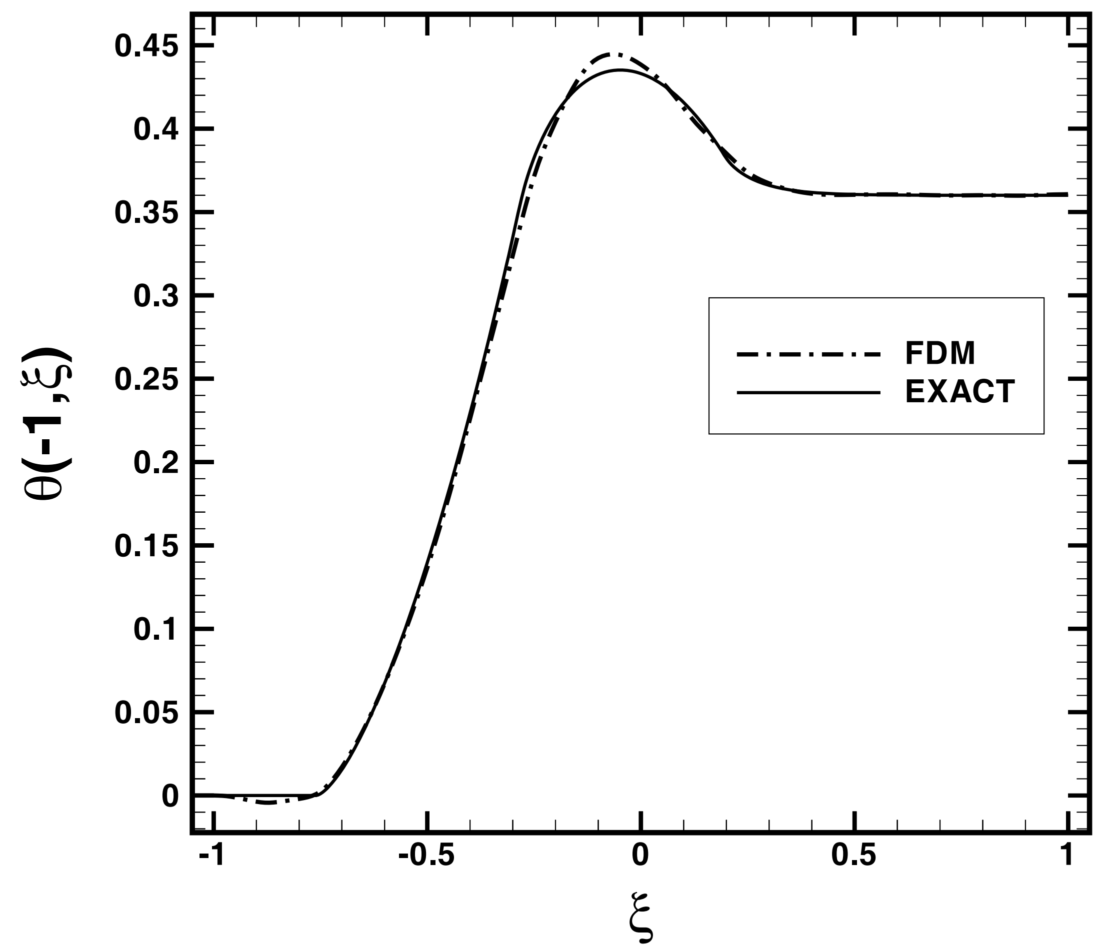

Figure 6.26: Predicted surface temperature at $\eta = -1$ for FDM using the least-squares method for determining sensitivity coefficients with $N = 8$, $P_N = 20$, $P = 16$ and with $\beta = 0.001$ and $\lambda = 1.25$.

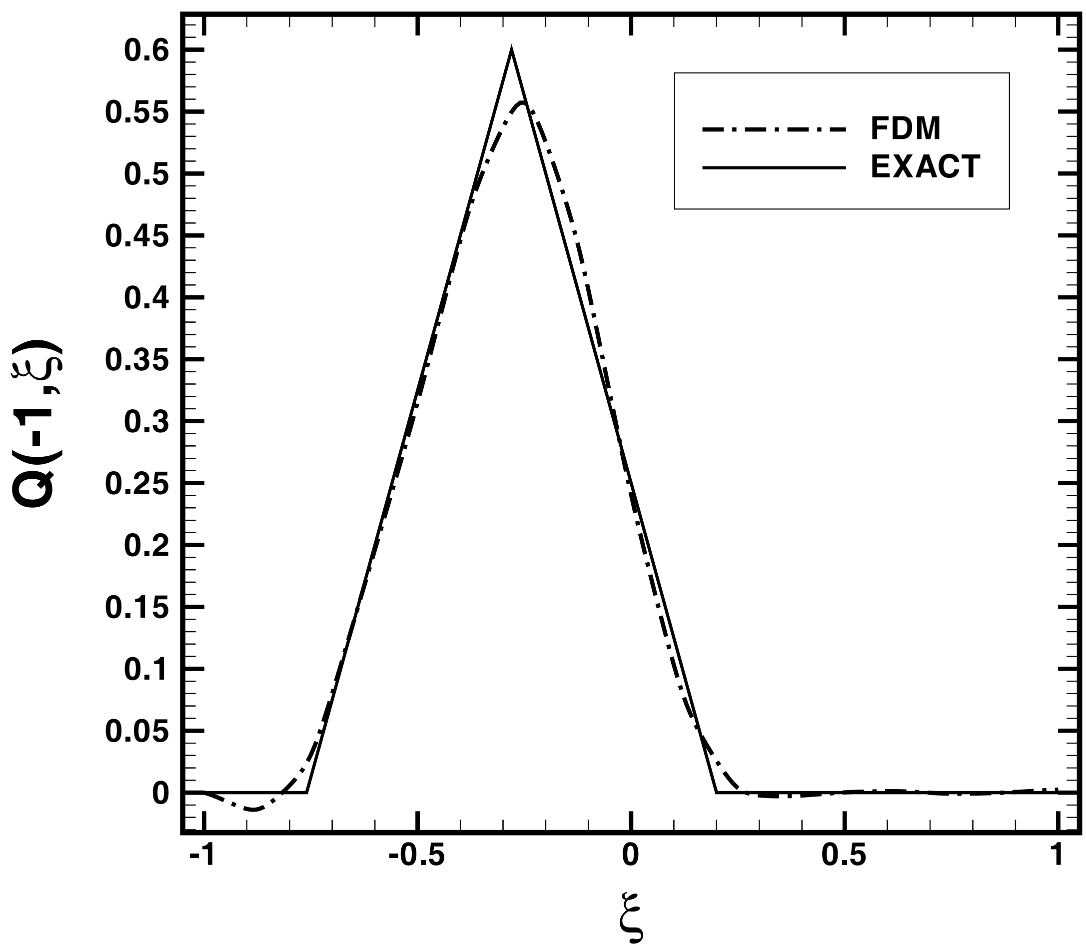

Figure 6.27: Predicted surface heat flux at $\eta = -1$ for FDM using the least-squares method for determining sensitivity coefficients with $N = 8$, $P_N = 20$, $P = 16$ and with $\beta = 0.001$ and $\lambda = 1.25$.

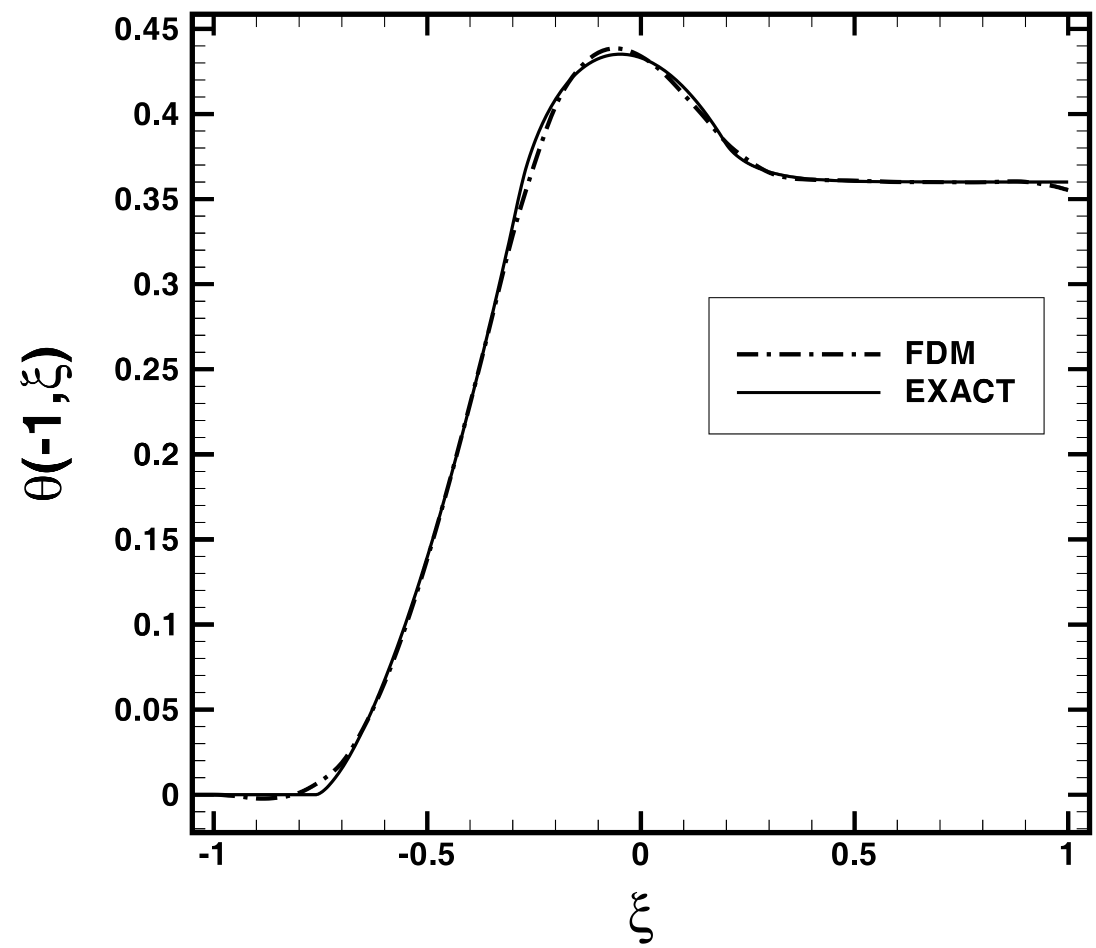

Figure 6.28: Predicted surface temperature at $\eta = -1$ for the FDM using the collocation method for determining sensitivity coefficients with $N = 8$, $P_N = 22$, $P = 20$ and with $\beta = 0.001$ and $\lambda = 1.25$.

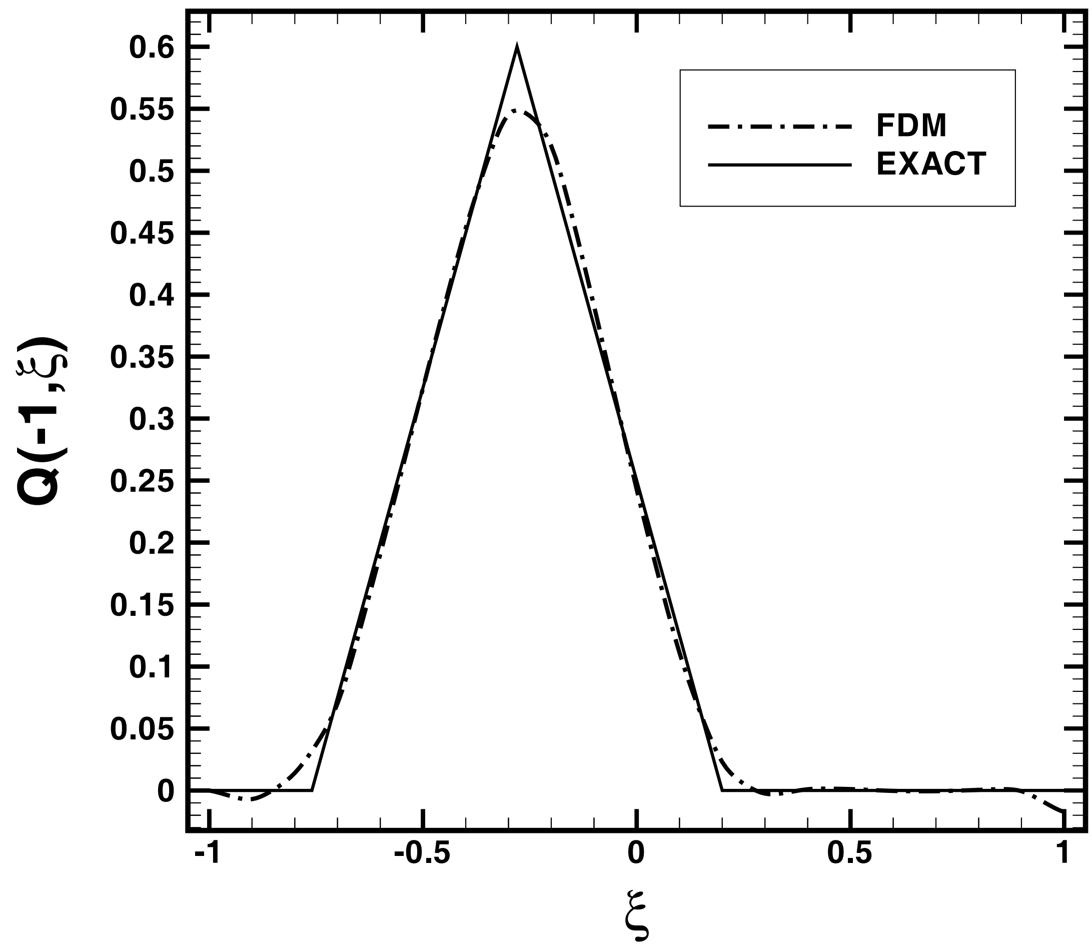

Figure 6.29: Predicted surface heat flux at $\eta = -1$ for the FDM using the collocation method for determining sensitivity coefficients with $N = 8$, $P_N = 22$, $P = 20$ and with $\beta = 0.001$ and $\lambda = 1.25$.

Appendix II

Tables

Table 4.1: Comparison of steady-state temperature distributions $\hat{f}_N^4(\eta)$ for the case of $L = 0.1$ with $N = 20$.

η	$\hat{f}_N^4(\eta)$ Prasad-Hering [115]	$\hat{f}_N^4(\eta)$ Heaslet-Warming [141]	$\hat{f}_N^4(\eta)$ Eq. (4.39b)
-1.000	0.571	0.571	0.5710
-0.800	0.554	0.556	0.5538
-0.600	0.539	0.541	0.5396
-0.400	0.526	0.525	0.5261
-0.200	0.512	0.513	0.5131
0.000	0.499	0.500	0.5000
0.200	0.486	0.487	0.4869
0.400	0.473	0.475	0.4738
0.600	0.460	0.459	0.4604
0.800	0.446	0.444	0.4461
1.000	0.428	0.429	0.4290

Table 4.2: Comparison of steady-state temperature distributions $\hat{f}_N^4(\eta)$ for the case of $L = 1$ with $N = 20$.

η	$\hat{f}_N^4(\eta)$ Prasad-Hering [115]	$\hat{f}_N^4(\eta)$ Heaslet-Warming [141]	$\hat{f}_N^4(\eta)$ Eq. (4.39b)
-1.000	0.760	0.756	0.7581
-0.800	0.692	0.698	0.6908
-0.600	0.642	0.646	0.6402
-0.400	0.594	0.590	0.5934
-0.200	0.545	0.551	0.5486
0.000	0.499	0.500	0.5000
0.200	0.452	0.449	0.4517
0.400	0.405	0.410	0.4064
0.600	0.355	0.354	0.3587
0.800	0.305	0.302	0.3073
1.000	0.240	0.244	0.2418

Table 4.3: Comparison of steady-state temperature distributions $\hat{f}_N^4(\eta)$ for the case of $L = 10$ with $N = 20$.

η	$\hat{f}_N^4(\eta)$ Prasad-Hering [115]	$\hat{f}_N^4(\eta)$ Heaslet-Warming [141]	$\hat{f}_N^4(\eta)$ Eq. (4.39b)
-1.000	0.949	0.956	0.9494
-0.800	0.851	0.854	0.8549
-0.600	0.763	0.765	0.7513
-0.400	0.675	0.678	0.6689
-0.200	0.587	0.590	0.5829
0.000	0.499	0.500	0.4967
0.200	0.412	0.410	0.4106
0.400	0.324	0.322	0.3241
0.600	0.236	0.235	0.2375
0.800	0.148	0.146	0.1480
1.000	0.050	0.044	0.0504

Table 5.1: Results of the parameter estimation algorithm for the case of errorless data with α corresponding to furnace temperature heating rates of 10 K/min, 20 K/min and 30 K/min.

Parameter	Exact Value	Initial Guess	Estimated Parameter Values (with iterations for convergence)		
			$\alpha \Rrightarrow$ 10 K/min (13 iterations)	$\alpha \Rrightarrow$ 20 K/min (16 iterations)	$\alpha \Rrightarrow$ 30 K/min (19 iterations)
τ_{c1}	3.330	2.000	3.330	3.330	3.330
τ_{c2}	4.166	2.000	4.166	4.166	4.166
τ_{c3}	3.330	10.00	3.330	3.330	3.330
τ_{c4}	3.330	10.00	3.330	3.330	3.330
τ_{r1}	80.000	120.00	80.000	80.000	80.000
τ_{r2}	800.00	1200.0	800.00	800.00	800.00
τ_{r3}	720.00	1200.0	720.00	720.00	720.00
τ_{r4}	256.00	170.00	256.00	256.00	256.00
τ_{r5}	800.00	400.00	800.00	800.00	800.00
τ_{r6}	3200.0	4000.0	3200.0	3200.0	3200.0
K_0	0.00130	0.00250	0.00130	0.00130	0.00130

Table 5.2: Results of the parameter estimation algorithm (no calibration sequence) for the case of data with increasing levels of noise and α corresponding to a furnace temperature heating rate of 20 K/min. N/C represents no achievable convergence.

Parameter	Exact Parameter Value	Estimated Parameter Values		
		$\epsilon = 0.001$ ($\pm$ 0.03 K)	$\epsilon = 0.002$ ($\pm$ 0.06 K)	$\epsilon = 0.005$ ($\pm$ 0.15 K)
τ_{c1}	3.330	2.562	1.943	N/C
τ_{c2}	4.166	3.174	2.419	N/C
τ_{c3}	3.330	3.597	4.325	N/C
τ_{c4}	3.330	3.664	4.491	N/C
τ_{r1}	80.000	89.380	101.61	N/C
τ_{r2}	800.00	779.48	750.44	N/C
τ_{r3}	720.00	758.80	826.50	N/C
τ_{r4}	256.00	286.29	368.44	N/C
τ_{r5}	800.00	765.20	712.25	N/C
τ_{r6}	3200.0	3369.4	3754.2	N/C
K_0	0.001300	0.001296	0.001254	N/C

Table 5.3: Results of the parameter estimation algorithm (two-step calibration sequence) for the case of data with increasing levels of noise and α corresponding to a furnace temperature heating rate of 20 K/min.

Parameter	Exact Parameter Value	Estimated Parameter Values		
		$\epsilon = 0.001$ ($\pm$ 0.03 K)	$\epsilon = 0.002$ ($\pm$ 0.06 K)	$\epsilon = 0.005$ ($\pm$ 0.15 K)
τ_{c1}^{a}	3.330	3.163	2.917	2.352
τ_{c2}^{a}	4.166	3.983	3.723	3.149
τ_{c3}	3.330	3.459	3.606	3.730
τ_{c4}	3.330	3.469	3.655	3.997
τ_{r1}	80.000	75.708	69.325	53.136
τ_{r2}^{a}	800.00	800.94	802.33	805.28
τ_{r3}	720.00	715.37	708.73	694.19
τ_{r4}	256.00	256.50	260.42	284.30
τ_{r5}^{a}	800.00	791.51	775.42	727.02
τ_{r6}^{a}	3200.0	3208.9	3237.8	3372.6
K_0	0.001300	0.001282	0.001251	0.001173

[a] Recovered from no pan model.

Vita

Gregory Evan Osborne was born in Kingsport, TN on March 26, 1964. After graduating from Dobyns-Bennett High School in 1982, he enrolled at Vanderbilt University where he was awarded a B.A. in Chemistry in 1986. Following his baccalaureate, he attended the University of New Orleans and received a Master of Science in Engineering in the discipline of Naval Architecture and Marine Engineering in 1990. He continued his studies in hydrodynamics at the Massachusetts Institute of Technology and earned the professional degree of Ocean Engineer in 1994. Shortly thereafter, he entered the Graduate School at the University of Tennessee in the fall of 1995 in order to pursue the degree of Doctor of Philosophy in the discipline of mechanical engineering.